SPIE PRESS | Field Guide

SPIE

Field Guide to

Nonlinear Optics

Peter E. Powers

Field Guide to

Nonlinear Optics

Peter E. Powers

SPIE Field Guides
Volume FG29

John E. Greivenkamp, Series Editor

SPIE PRESS
Bellingham, Washington USA

Library of Congress Cataloging-in-Publication Data

Powers, Peter E.
Field guide to nonlinear optics / Peter E. Powers.
pages cm. – (The field guide series; FG29)
Includes bibliographical references and index.
ISBN 978-0-8194-9635-5–ISBN 978-0-8194-9636-2–
ISBN 978-0-8194-9637-9 1. Nonlinear optics. I. Title.
QC446.2.P688 2013
621.36′94–dc23

2013014471

Published by

SPIE
P.O. Box 10
Bellingham, Washington 98227-0010 USA
Phone: +1.360.676.3290
Fax: +1.360.647.1445
Email: books@spie.org
www.spie.org

Printed in the United States of America.
First printing

Introduction to the Series

Welcome to the *SPIE Field Guides*—a series of publications written directly for the practicing engineer or scientist. Many textbooks and professional reference books cover optical principles and techniques in depth. The aim of the *SPIE Field Guides* is to distill this information, providing readers with a handy desk or briefcase reference that provides basic, essential information about optical principles, techniques, or phenomena, including definitions and descriptions, key equations, illustrations, application examples, design considerations, and additional resources. A significant effort will be made to provide a consistent notation and style between volumes in the series.

Each *SPIE Field Guide* addresses a major field of optical science and technology. The concept of these Field Guides is a format-intensive presentation based on figures and equations supplemented by concise explanations. In most cases, this modular approach places a single topic on a page, and provides full coverage of that topic on that page. Highlights, insights, and rules of thumb are displayed in sidebars to the main text. The appendices at the end of each Field Guide provide additional information such as related material outside the main scope of the volume, key mathematical relationships, and alternative methods. While complete in their coverage, the concise presentation may not be appropriate for those new to the field.

The *SPIE Field Guides* are intended to be living documents. The modular page-based presentation format allows them to be updated and expanded. We are interested in your suggestions for new Field Guide topics as well as what material should be added to an individual volume to make these Field Guides more useful to you. Please contact us at **fieldguides@SPIE.org.**

John E. Greivenkamp, *Series Editor*
College of Optical Sciences
The University of Arizona

The Field Guide Series

Keep information at your fingertips with all of the titles in the Field Guide Series:

Adaptive Optics, Second Edition, Robert Tyson & Benjamin Frazier

Atmospheric Optics, Larry Andrews

Binoculars and Scopes, Paul Yoder, Jr. & Daniel Vukobratovich

Diffractive Optics, Yakov Soskind

Geometrical Optics, John Greivenkamp

Illumination, Angelo Arecchi, Tahar Messadi, & John Koshel

Image Processing, Khan M. Iftekharuddin & Abdul Awwal

Infrared Systems, Detectors, and FPAs, 2nd Edition, Arnold Daniels

Interferometric Optical Testing, Eric Goodwin & Jim Wyant

Laser Pulse Generation, Rüdiger Paschotta

Lasers, Rüdiger Paschotta

Lens Design, Julie Bentley & Craig Olson

Microscopy, Tomasz Tkaczyk

Nonlinear Optics, Peter Powers

Optical Fabrication, Ray Williamson

Optical Fiber Technology, Rüdiger Paschotta

Optical Lithography, Chris Mack

Optical Thin Films, Ronald Willey

Optomechanical Design and Analysis, Katie Schwertz & James Burge

Physical Optics, Daniel Smith

Polarization, Edward Collett

Probability, Random Processes, and Random Data Analysis, Larry Andrews

Radiometry, Barbara Grant

Special Functions for Engineers, Larry Andrews

Spectroscopy, David Ball

Terahertz Sources, Detectors, and Optics, Créidhe O'Sullivan & J. Anthony Murphy

Visual and Ophthalmic Optics, Jim Schwiegerling

Field Guide to Nonlinear Optics

This Field Guide is designed for those looking for a condensed and concise source of key concepts, equations, and techniques for nonlinear optics. Topics covered include technologically important effects, recent developments in nonlinear optics, and linear optical properties central to nonlinear phenomena. The focus of each section is based on my research, my interactions with colleagues in the field, and my experiences teaching nonlinear optics.

Examples throughout this Field Guide illustrate fundamental concepts while demonstrating the application of key equations. Equations are presented without proof or derivation; however, the interested reader may refer to the bibliography for a list of resources that go into greater detail. In addition to the overview of nonlinear phenomena, this Field Guide includes an appendix of material properties for some commonly used nonlinear crystals.

This Field Guide features notations commonly encountered in nonlinear optics literature. All equations are written in SI units for convenience when comparing calculations to laboratory measurements. The formalism of writing equations using complex variable notation introduces ambiguity in defining the electric field's complex amplitude. Though one convention is used throughout this text, conventions and conversions are presented as part of the first topic. Equations in terms of experimentally measured quantities such as power, intensity, and energy, have no ambiguity.

Peter E. Powers
University of Dayton
March 2013

Table of Contents

Table of Contents

Table of Contents

Glossary of Terms and Acronyms

Constants

c	Speed of light in vacuum (299,792,458 m/sec)
e	Elementary charge (1.6022×10^{-19} C)
h	Planck's constant (6.6261×10^{-34} J · sec)
$\hbar$	$h/2\pi$ (1.0546×10^{-34} J · sec)
k_B	Boltzmann constant (1.3807×10^{-23} J/K)
m_e	Electron mass (9.1094×10^{-31} kg)
ε_0	Vacuum permittivity (8.8542×10^{-2} F/m)
μ_0	Vacuum permeability ($4\pi \times 10^{-7}$ N/A^2)

General

3PA	Three-photon absorption
A	Electric field's complex amplitude scalar
A	Electric field's complex amplitude vector
AC	Autocorrelation
AO	Acousto-optic
b	Confocal distance ($2z_R$)
B	Magnetic induction scalar
B	Magnetic induction vector
BBO	b-BaB_2O_4, b-barium borate
BIBO	BiB_3O_6, bismuth triborate
BPM	Birefringent phase matching
CARS	Coherent anti-Stokes Raman spectroscopy
c.c.	Complex conjugate
cgs	Centimeter-gram-second
D	Electric displacement vector
d_{eff}	Effective second-order nonlinearity
DFG	Difference-frequency generation
DFWM	Degenerate four-wave mixing
d_{ijk}	d tensor
DKDP	KD_2PO_4, deuterated potassium dihydrogen phosphate
DR-OPO	Doubly-resonant optical parametric oscillator
e	Extraordinary wave (e-wave)
E	Electric field scalar
E	Electric field vector
EO	Electro-optic

Glossary of Terms and Acronyms

E_{SC}	Space-charge electric field
f	Focal length of a lens
FROG	Frequency-resolved optical gating
fsec	Femtosecond (10^{-15} sec)
FWHM	Full-width at half-maximum
FWM	Four-wave mixing
GaAs	Gallium arsenide
GaP	Gallium phosphide
g_B	Brillouin intensity gain factor
g_R	Raman intensity gain factor
GVD	Group velocity dispersion
$\mathbf{H}$	Magnetic field
HHG	High harmonic generation
i	$\sqrt{-1}$
I	Light intensity
I_o	On-axis intensity
$\mathbf{j}_f$	Free current density
k	Wavevector magnitude
$\mathbf{k}$	Wavevector
$\mathbf{K}$	Acoustic wavevector
KDP	KH_2PO_4, potassium dihydrogen phosphate
KTP	$KTiOPO_4$, potassium titanyl phosphate
L	Interaction length
LBO	LiB_3O_5, lithium triborate
L_c	Coherence length
$LiNbO_3$	Lithium niobate
$LiTaO_3$	Lithium tantalite
LN	Lithium niobate
$\mathbf{M}$	Magnetization
MPA	Multi-photon absorption
n	Refractive index/index of refraction
$n_e(\theta)$	Extraordinary refractive index
n_2^I	Nonlinear index intensity coefficient
NL	Nonlinear
NLA	Nonlinear absorption
NLSE	Nonlinear Schrödinger equation
n_o	Ordinary refractive index
nsec	Nanosecond (10^{-9} sec)
n_X, n_Y, n_Z	Principal indices (or eigenindices)

Glossary of Terms and Acronyms

o	Ordinary wave (o-wave)
$\hat{\mathbf{o}}$	Ordinary wave unit vector
OPA	Optical parametric amplification
OPG	Optical parametric generation
OPO	Optical parametric oscillator
P	Optical power
$P^{(1)}$	Linear material polarization
$P^{(2)}$	Second-order nonlinear polarization
$P^{(3)}$	Third-order nonlinear polarization
PCM	Phase-conjugate mirror
pm	Picometer
$P^{(NL)}$	Nonlinear polarization
PPLN	Periodically poled lithium niobate
psec	Picosecond (10^{-12} sec)
P_{TH}	Threshold power
q	Gaussian beam parameter
QPM	Quasi-phase-matching
QWP	Quarter-wave plate
r	Electro-optic coefficient
R	Power reflectivity
$\mathbf{S}$	Poynting vector
SBS	Spontaneous Brillouin scattering
SESAM	Semiconductor saturable absorber mirror
SFG	Sum-frequency generation
SHG	Second-harmonic generation
sinc(x)	sin(x)/x
SPM	Self-phase modulation
SPS	Spontaneous parametric scattering
SR-OPO	Singly-resonant optical parametric oscillator
SVEA	Slowly varying envelope approximation
T	Temperature
THG	Third-harmonic generation
TPA	Two-photon absorption
U_p	Ponderomotive energy
v_g	Group velocity
w_o	Radius at the beam waist
$w(z)$	Beam radius
Z	Optic axis
ZGP	$ZnGeP_2$, zinc germanium phosphide

Glossary of Terms and Acronyms

ZnTe	Zinc telluride
z_R	Rayleigh range
α	Linear absorption coefficient
β	Waveguide propagation coefficient
β (TPA)	Two-photon absorption coefficient
Δ	Miller's delta
Δk	*k*-vector mismatch
ε_{ij}	Permittivity tensor
θ_{PM}	Phase matching angle (polar angle)
Λ	Quasi-phase-matching periodicity
λ	Vacuum wavelength
λ_I (λ_3)	Idler wavelength
λ_P (λ_1)	Pump wavelength
λ_S (λ_2)	Signal wavelength
ξ	Focusing parameter
ρ	Poynting vector walk-off angle
ρ_f	Free charge density
σ_R	Raman scattering cross-section
τ	Pulse duration
φ	Azimuthal angle
$\chi_{ij}^{(1)}$	Linear susceptibility tensor
$\chi_{eff}^{(2)}$	Effective nonlinear susceptibility
$\chi_{ijk}^{(2)}$	Second-order nonlinear susceptibility tensor
$\chi_{ijkl}^{(3)}$	Third-order nonlinear susceptibility tensor
$\chi_{B}^{(3)}$	Brillouin susceptibility
$\chi_{R}^{(3)}$	Raman susceptibility
ψ	Noncollinear angle
ω	Angular frequency
ω_{AS}	Anti-Stokes angular frequency
ω_S	Signal (parametric process) or Stokes frequency (Raman process)
Ω_B	Brillouin frequency

Conventions and Conversions

Nonlinear optics literature contains two **notation conventions** for the **electric field's** complex amplitude.

Real notation is $E = E_o \cos(kz - \omega t + \phi)$

Complex notation is

a) $E = {}^1\!/\!_2 A e^{i(kz-\omega t)}$ + **complex conjugate (*c.c.*)***

$A = E_o e^{i\phi}$ is the **complex amplitude**

b) $E = A' e^{i(kz-\omega t)} + c.c.$

*Convention used for this Field Guide.

In the complex expressions, the addition of the *c.c.* ensures that the overall expression is real. It is important to know which definition of complex amplitude is being used. For example, the **intensity** (equivalent to **irradiance** when used in nonlinear optics) is given by

$$I = \frac{1}{2} n\varepsilon_0 c|A|^2 \quad \text{or} \quad I = 2n\varepsilon_0 c|A'|^2$$

depending on the particular convention we choose for the complex amplitude. Another example is

$$P^{(2)} = \varepsilon_0 \chi^{(2)}_{eff} A_1 A_2 \quad \text{or} \quad P^{(2)\prime} = 2\varepsilon_0 \chi^{(2)}_{eff} A'_1 A'_2$$

To convert from one convention to the other, we add a factor of two in the complex amplitude—for example:

$$A_1 \to 2A'_1, \quad A_2 \to 2A'_2, \quad \text{and} \quad P^{(2)} \to 2P^{(2)\prime}$$

Different systems of units are encountered in nonlinear optics—SI or Gaussian cgs units are common.

To convert from cgs to SI units:

$$E(\text{SI}) = E(\text{cgs}) \times c \times 10^{-4}$$

$$\chi^{(2)}(\text{SI}) = \chi^{(2)}(\text{cgs}) \times \frac{4\pi}{c \times 10^{-4}}$$

$$\chi^{(3)}(\text{SI}) = \chi^{(3)}(\text{cgs}) \times \frac{4\pi}{(c \times 10^{-4})^2}$$

where c is the speed of light in SI units

Maxwell's Equations and the Wave Equation

The foundation of optics, **Maxwell's equations** are written here in terms of macroscopic field variables:

$$\nabla \cdot \mathbf{D} = \rho_f \quad \nabla \times \mathbf{E} = -\frac{\partial \mathbf{B}}{\partial t} \quad \nabla \cdot \mathbf{B} = 0 \quad \nabla \times \mathbf{H} = \mathbf{j}_f + \frac{\partial \mathbf{D}}{\partial t}$$

where **E** is the **electric field**, **B** is the **magnetic induction**, **D** is the **electric displacement**, and **H** is the **magnetic field**. ρ_f and $\mathbf{j}_f$ are the free charge density and free current density, respectively. **D** and **H** are obtained through the **constitutive relationships**:

$$\mathbf{D} = \varepsilon_0 \mathbf{E} + \mathbf{P} \qquad \mathbf{H} = \frac{\mathbf{B}}{\mu_0} - \mathbf{M}$$

where **P** is the **polarization**, **M** is the **magnetization**, and ε_0 and μ_0 are the permittivity and permeability of free space, respectively. The media are usually nonmagnetic, and we may take $\mathbf{B} = \mu_0 \mathbf{H}$. The polarization can be split into linear and nonlinear parts:

$$\mathbf{P} = \mathbf{P}^{(L)} + \mathbf{P}^{(NL)}$$

The **wave equation** is obtained by starting with

$$\nabla \times (\nabla \times \mathbf{E}) = -\frac{\partial}{\partial t}(\nabla \times \mathbf{B})$$

For linearly polarized plane-wave fields, the field may be represented as a scalar quantity:

$$E = \frac{1}{2} A e^{i(kz - \omega t)} + c.c.$$

where A is the complex amplitude of the field, ω is the angular frequency, and k is the wavevector magnitude ($k = n\omega/c = 2\pi n/\lambda_{vacuum}$). In lossless and nonmagnetic media, and for a weak interaction where the field envelope changes slowly, the wave equation simplifies to an expression relating the complex amplitude of the field and nonlinear polarization:

$$\frac{dA(\omega)}{dz} = i \frac{\omega}{2n\varepsilon_0 c} P^{(NL)}(\omega) e^{-ikz}$$

The particular form of the nonlinear polarization depends on the type of interaction, such as $\chi^{(2)}$, $\chi^{(3)}$, Raman, Brillouin, etc.

Uniaxial Crystals

A **birefringent crystal** is characterized by three **principal indices**: n_X, n_Y, and n_Z. These indices are sometimes termed **eigenindices**. For **uniaxial crystals**, $n_X = n_Y \neq n_Z$, and the optic axis is along the Z axis associated with the principal index, n_Z. The other two principal indices n_X, n_Y are equal, with a value of n_o, known as the **ordinary index**.

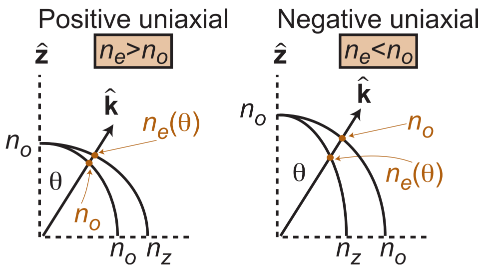

A laser traveling through a uniaxial crystal is decomposed into two orthogonal, linearly polarized eigenpolarizations called ordinary and extraordinary waves (**o-waves** and **e-waves**). The e-wave has an associated **extraordinary index** $n_e(\theta)$ that is dependent on propagation direction. The angle θ is conventionally taken to be the angle between the k vector and the uniaxial optic axis Z.

The index n_o associated with the o-wave does not change with propagation direction. When $n_e > n_o$, the crystal is called **positive uniaxial**, and when $n_e < n_o$, the crystal is called **negative uniaxial**. Two equivalent formulae for the extraordinary index, valid for both positive and negative uniaxial crystals, are

$$\frac{1}{n_e^2(\theta)} = \frac{\cos^2\theta}{n_o^2} + \frac{\sin^2\theta}{n_Z^2} \quad \text{or} \quad n_e(\theta) = n_o\sqrt{\frac{1+\tan^2\theta}{1+\frac{n_o^2}{n_Z^2}\tan^2\theta}}$$

The e and o polarization directions are perpendicular to the k vector. e-waves are polarized in the plane containing the k vector and the optic Z axis, whereas o-waves are polarized perpendicular to the plane.

Biaxial Crystals

Biaxial crystals have three principal indices: $n_X \neq n_Y \neq n_Z$. Depending on the particular crystal, $n_Z > n_Y > n_X$ or $n_Z < n_Y < n_X$. In many applications, the interaction is restricted to one of the three principal planes *XY*, *YZ*, or *XZ*. In these cases, uniaxial terminology of e- and o-waves and indices is used. A wave polarized in a given principal plane is called an e-wave, whereas a wave polarized perpendicular to a given plane is called an o-wave.

Visualizing the indices for e- and o-waves:

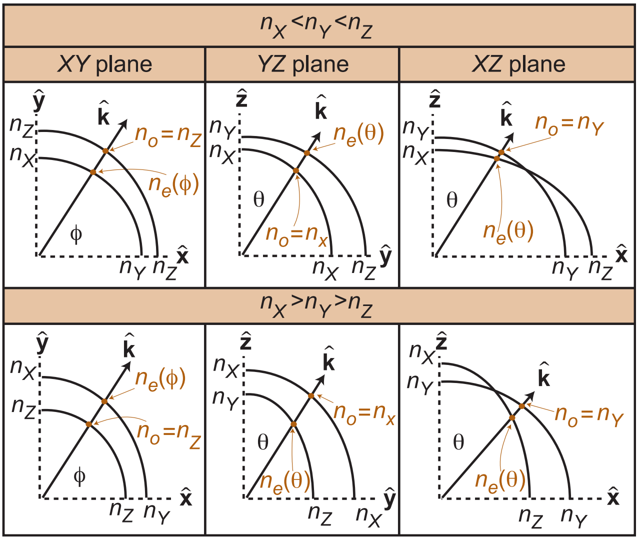

Formulae for the extraordinary index:

XY plane	*YZ* plane	*XZ* plane
$\frac{1}{n_e^2(\phi)} = \frac{\cos^2\phi}{n_Y^2} + \frac{\sin^2\phi}{n_X^2}$	$\frac{1}{n_e^2(\theta)} = \frac{\cos^2\theta}{n_Y^2} + \frac{\sin^2\theta}{n_Z^2}$	$\frac{1}{n_e^2(\theta)} = \frac{\cos^2\theta}{n_X^2} + \frac{\sin^2\theta}{n_Z^2}$

A biaxial crystal has two **optic axes** that lie in the *XZ* plane corresponding to the intersection of the n_e and n_o curves (see figure above). The optic axis angle V_z measured with respect to the Z axis is given by

$$\tan V_z = \pm(n_Z/n_X)\sqrt{|n_X^2 - n_Y^2|/|n_Y^2 - n_Z^2|}$$

Nonlinear Polarization for Parametric Interactions

For a sufficiently weak nonlinearity, the polarization can be separated into linear and nonlinear parts: $\mathbf{P} = \mathbf{P}^{(L)} + \mathbf{P}^{(NL)}$. For **parametric interactions** where the total photon energy is conserved, the **nonlinear polarization** results from a nonlinear material response to an incident electric field. For example, the scalar polarization is expanded in a power series in the electric field:

$$P = \varepsilon_0 \chi^{(1)} E + \varepsilon_0 \chi^{(2)} E^2 + \varepsilon_0 \chi^{(3)} E^3 + \cdots$$

where $\chi^{(1)}$, $\chi^{(2)}$, and $\chi^{(3)}$ denote the expansion orders of the susceptibility. Typically, nonlinear effects are classified according to their expansion order as **$\chi^{(2)}$ effects**, **$\chi^{(3)}$ effects**, and so on. $\chi^{(2)}$ effects result from squaring the electric field. For example, consider a scalar electric field given by $E_{incident} = E_2 \cos(k_2 z - \omega_2 t) + E_3 \cos(k_3 z - \omega_3 t)$, where k is the wavevector magnitude. The resulting second-order polarization gives rise to **second-harmonic generation (SHG)**, **optical rectification**, **difference-frequency generation (DFG)**, and **sum-frequency generation (SFG)**.

Second harmonics

$$\begin{aligned} P^{(2)} = {} & \frac{1}{2} E_2^2 \cos[2k_2 z - 2\omega_2 t] + \frac{1}{2} E_3^2 \cos[2k_3 z - 2\omega_3 t] \\ & + \frac{1}{2}\left(E_2^2 + E_3^2\right) \leftarrow \text{Optical rectification} \\ & + E_2 E_3 \cos[(k_2 - k_3) z - (\omega_2 - \omega_3) t] \leftarrow \text{DFG} \\ & + E_2 E_3 \cos[(k_2 + k_3) z - (\omega_2 + \omega_3) t] \leftarrow \text{SFG} \end{aligned}$$

DFG is equivalent to **optical parametric amplification (OPA)**.

$\chi^{(3)}$ effects arise from cubing the incident field, and a similar expression for $P^{(3)}$ is obtained, except that it has many more sum- and difference-frequency combinations.

Although the nonlinear polarization has new frequency components, an efficient output is typically restricted to one process dictated by phase matching.

Classical Expressions for Nonlinear Susceptibility

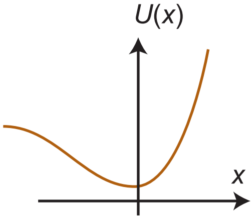

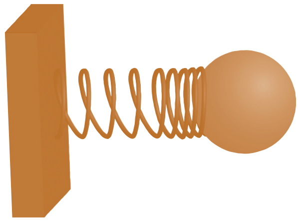

The electronic nonlinearity of a material has a classical origin described as an electron in an anharmonic potential well *U(x)*, modeled above as a mass on a nonlinear spring. The classical solution to this problem uses a perturbation expansion and leads to **classical expressions** for **nonlinear susceptibility**. This procedure gives qualitative information about the dispersion of the nonlinearity that is used to compare the nonlinearities of different crystals. **Miller's rule** is a useful result based on this classical model and is given by

$$\begin{aligned}\chi^{(2)}(\omega_1;\omega_2,\omega_3) &= \chi^{(1)}(\omega_1)\chi^{(1)}(\omega_2)\chi^{(1)}(\omega_3)\Delta \\ &= [n^2(\omega_1)-1][n^2(\omega_2)-1][n^2(\omega_3)-1]\Delta\end{aligned}$$

where n is the index of refraction, and Δ is **Miller's delta** and is roughly constant and independent of the medium. Miller's rule has a qualitative result in which the larger the index of refraction, the larger the nonlinearity.

Knowing $\chi^{(2)}$ for an SHG process allows us to calculate $\chi^{(2)}$ for other processes, provided we also know the indices. For SHG, Δ is given by

$$\Delta = \frac{\chi^{(2)}(2\omega_o;\omega_o,\omega_o)}{[n^2(\omega_o)-1]^3}$$

Note that $n(\omega) = n(2\omega)$ for SHG. To find $\chi^{(2)}$ for a DFG process we substitute in Δ into the DFG expression and rearrange to obtain

$$\frac{\chi^{(2)}(\omega_3;\omega_1,-\omega_2)}{\chi^{(2)}(2\omega_o;\omega_o,\omega_o)} = \frac{[n^2(\omega_1)-1][n^2(\omega_2)-1][n^2(\omega_3)-1]}{[n^2(\omega_o)-1]^3}$$

The ratio of $\chi^{(2)}$ susceptibilities for any two processes in the same material is calculated in a similar fashion.

Nonlinear Susceptibilities

In a nonlinear medium, an incident field may couple to fields with different frequencies and different polarization directions. A **nonlinear susceptibility tensor** combines frequency and polarization direction information:

$$\chi^{(2)}_{ijk}(\omega_m + \omega_n; \omega_m, \omega_n) \quad \chi^{(3)}_{ijkl}(\omega_m + \omega_n + \omega_p; \omega_m, \omega_n, \omega_p)$$

where $\omega_m + \omega_n$ and $\omega_m + \omega_n + \omega_p$ correspond to sum- and difference-frequency combinations of the frequencies ω_m, ω_n, and ω_p present in the incident field. For difference-frequency combinations, one of the corresponding frequencies is negative. The subscripted indices correspond to the **Cartesian coordinates**, x, y, and z (equivalently labeled 1, 2, and 3 so that $\chi_{xyz} = \chi_{123}$, etc.). A tensor element connects specific field directions with a nonlinear polarization direction. For example, $\chi^{(2)}_{xyz}$ couples E_y and E_z to P_x, which for DFG is given by

$$P^{(2)}_x(\omega_3 = \omega_1 - \omega_2) = 2\varepsilon_0 \chi^{(2)}_{xyz}(\omega_1 - \omega_2; \omega_1, -\omega_2) E_y(\omega_1) E^*_z(\omega_2)$$

In many cases, the frequency dependence in the nonlinear susceptibility (termed **Kleinman symmetry**) is ignored. Another notation for $\chi^{(2)}$ is the ***d* coefficient**, where

$$d_{ijk} \equiv \frac{1}{2}\chi^{(2)}_{ijk}$$

Under the Kleinman symmetry condition, susceptibilities with permuted indices are equal (e.g., $d_{123} = d_{213}$). When Kleinman symmetry is valid, expressions for the nonlinear polarization are unaltered by exchanging the second two indices, allowing a **contracted notation** $d_{ijk} = d_{im}$, where m is the contracted index given below:

j,k	Contracted index
xx	1
yy	2
zz	3
yz, zy	4
xz, zx	5
xy, yx	6

Contracted notation examples

$d_{123} = d_{14}$

$d_{233} = d_{23}$

$d_{321} = d_{36}$

Kleinman symmetry examples

$d_{14} = d_{123} = d_{213} = d_{25}$

$d_{14} = d_{123} = d_{312} = d_{36}$

$d_{23} = d_{233} = d_{323} = d_{34}$

d Matrices

The nonlinear polarization for $\chi^{(2)}$ interactions under Kleinman symmetry simplifies to matrix multiplication between a ***d* matrix** and a column vector. The d matrix is the same for **SHG**, **DFG**, and **SFG**, but the column vector is different. For an incident field with frequencies ω_1 and ω_2, the field is given by

$$\mathbf{E}_{incident} = \frac{1}{2}\mathbf{A}(\omega_1)e^{i(k_1 z - \omega_1 t)} + \frac{1}{2}\mathbf{A}(\omega_2)e^{i(k_2 z - \omega_2 t)} + c.c.$$

The expression for the nonlinear polarization at the difference frequency $\omega_1 - \omega_2$ is

$$\mathbf{P}^{(2)}(\omega_1 - \omega_2) = 2\varepsilon_0 \times$$

$$\begin{pmatrix} d_{11} & d_{12} & d_{13} & d_{14} & d_{15} & d_{16} \\ d_{21} & d_{22} & d_{23} & d_{24} & d_{25} & d_{26} \\ d_{31} & d_{32} & d_{33} & d_{34} & d_{35} & d_{36} \end{pmatrix} \begin{pmatrix} A_x(\omega_1)A_x^*(\omega_2) \\ A_y(\omega_1)A_y^*(\omega_2) \\ A_z(\omega_1)A_z^*(\omega_2) \\ A_y(\omega_1)A_z^*(\omega_2) + A_z(\omega_1)A_y^*(\omega_2) \\ A_x(\omega_1)A_z^*(\omega_2) + A_z(\omega_1)A_x^*(\omega_2) \\ A_x(\omega_1)A_y^*(\omega_2) + A_y(\omega_1)A_x^*(\omega_2) \end{pmatrix}$$

The expression for the sum frequency at $\omega_1 + \omega_2$ is

$$\mathbf{P}^{(2)}(\omega_1 + \omega_2) = 2\varepsilon_0 \times$$

$$\begin{pmatrix} d_{11} & d_{12} & d_{13} & d_{14} & d_{15} & d_{16} \\ d_{21} & d_{22} & d_{23} & d_{24} & d_{25} & d_{26} \\ d_{31} & d_{32} & d_{33} & d_{34} & d_{35} & d_{36} \end{pmatrix} \begin{pmatrix} A_x(\omega_1)A_x(\omega_2) \\ A_y(\omega_1)A_y(\omega_2) \\ A_z(\omega_1)A_z(\omega_2) \\ A_y(\omega_1)A_z(\omega_2) + A_z(\omega_1)A_y(\omega_2) \\ A_x(\omega_1)A_z(\omega_2) + A_z(\omega_1)A_x(\omega_2) \\ A_x(\omega_1)A_y(\omega_2) + A_y(\omega_1)A_x(\omega_2) \end{pmatrix}$$

The column vector for a DFG interaction for the field given below is shown at the right.

$$\mathbf{E}_{incident} = \frac{1}{2}A(\omega_1)e^{i(k_1 z - \omega_1 t)}\left(\frac{\hat{\mathbf{x}} + \hat{\mathbf{y}}}{\sqrt{2}}\right) + \frac{1}{2}A(\omega_2)e^{i(k_2 z - \omega_2 t)}\left(\frac{\hat{\mathbf{x}} - \hat{\mathbf{y}}}{\sqrt{2}}\right) + c.c.$$

$$\begin{pmatrix} \dfrac{A(\omega_1)A^*(\omega_2)}{2} \\ -\dfrac{A(\omega_1)A^*(\omega_2)}{2} \\ 0 \\ 0 \\ 0 \\ 0 \end{pmatrix}$$

Working with *d* Matrices and SHG

The expression for **SHG** when the incident field is given by

$$\mathbf{E}_{incident} = \frac{1}{2}\mathbf{A}(\omega)e^{i(kz-\omega t)} + c.c. \text{ is}$$

$$\mathbf{P}^{(2)}(2\omega) = \varepsilon_o \begin{pmatrix} d_{11} & d_{12} & d_{13} & d_{14} & d_{15} & d_{16} \\ d_{21} & d_{22} & d_{23} & d_{24} & d_{25} & d_{26} \\ d_{31} & d_{32} & d_{33} & d_{34} & d_{35} & d_{36} \end{pmatrix} \begin{pmatrix} A_x^2(\omega) \\ A_y^2(\omega) \\ A_z^2(\omega) \\ 2A_y(\omega)A_z(\omega) \\ 2A_x(\omega)A_z(\omega) \\ 2A_x(\omega)A_y(\omega) \end{pmatrix}$$

The resultant expression for the nonlinear polarization may be used to calculate an **effective nonlinearity** d_{eff} by projecting $\mathbf{P}^{(2)}$ onto the e and o directions.

d_{eff} for an $o + o \rightarrow e$ SHG interaction in class-4 crystals:

The e and o directions are

$$\hat{\mathbf{e}} = -\cos\theta\cos\phi\,\hat{\mathbf{x}} - \cos\theta\sin\phi\,\hat{\mathbf{y}} + \sin\theta\,\hat{\mathbf{z}}$$

$$\hat{\mathbf{o}} = \sin\phi\,\hat{\mathbf{x}} - \cos\phi\,\hat{\mathbf{y}}$$

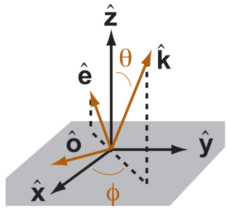

For an $o + o \rightarrow e$ interaction, the incident fundamental field is given by

$$\mathbf{E}_F = \frac{1}{2}A_F e^{(i\mathbf{k}\cdot\mathbf{r}-\omega_F t)}\hat{\mathbf{o}} + c.c.$$

The corresponding field amplitude is $A_F\hat{\mathbf{o}}$; therefore, $A_x(\omega_F) = A_F\sin\phi$, $A_y(\omega_F) = -A_F\cos\phi$, and $A_z(\omega_F) = 0$

$$\mathbf{P}^{(2)}(2\omega) = \varepsilon_0 \begin{pmatrix} 0 & 0 & 0 & 0 & d_{15} & 0 \\ 0 & 0 & 0 & d_{15} & 0 & 0 \\ d_{15} & d_{15} & d_{33} & 0 & 0 & 0 \end{pmatrix} \begin{pmatrix} \sin^2\phi \\ \cos^2\phi \\ 0 \\ 0 \\ 0 \\ -\sin 2\phi \end{pmatrix} A_F^2 = \varepsilon_0 A_F^2 \begin{pmatrix} 0 \\ 0 \\ d_{15} \end{pmatrix}$$

The component of $\mathbf{P}^{(2)}$ that couples to the e direction is $\mathbf{P}^{(2)}(2\omega)\cdot\hat{\mathbf{e}} = \varepsilon_0 A_F^2 d_{15}\sin\theta$. Hence, $d_{eff} = d_{15}\sin\theta$.

Effective Nonlinearities

Point group		Two o-waves and one e-wave	Two e-waves and one o-wave
Uniaxial principal planes			
$\bar{4}2m$		$-d_{36}\sin\theta\sin 2\phi$	$d_{36}\sin 2\theta\cos 2\phi$
3m		$d_{15}\sin\theta - d_{22}\cos\theta\sin 3\phi$	$d_{22}\cos^2\theta\cos 3\phi$
4, 4mm, 6, 6mm		$d_{15}\sin\theta$	0
$\bar{4}$		$-\begin{pmatrix} d_{14}\sin 2\phi \\ +d_{15}\cos 2\phi \end{pmatrix}\sin\theta$	$\begin{pmatrix} d_{14}\cos 2\phi \\ -d_{15}\sin 2\phi \end{pmatrix}\sin 2\theta$
3		$\begin{pmatrix} d_{11}\cos 3\phi \\ -d_{22}\sin 3\phi \end{pmatrix}\cos\theta + d_{15}\sin\theta$	$\begin{pmatrix} d_{11}\sin 3\phi \\ +d_{22}\cos 3\phi \end{pmatrix}\cos^2\theta$
32		$d_{11}\cos\theta\cos 3\phi$	$d_{11}\cos^2\theta\sin 3\phi$
$\bar{6}$		$\begin{pmatrix} d_{11}\cos 3\phi \\ -d_{22}\sin 3\phi \end{pmatrix}\cos\theta$	$\begin{pmatrix} d_{11}\sin 3\phi \\ +d_{22}\cos 3\phi \end{pmatrix}\cos^2\theta$
$\bar{6}m2$		$-d_{22}\cos\theta\sin 3\phi$	$d_{22}\cos^2\theta\cos 3\phi$
Biaxial principal planes			
2	XY	$d_{23}\cos\phi$	$-d_{36}\sin 2\phi$
	YZ	$-d_{16}\cos\theta$	$-d_{14}\sin 2\theta$
	XZ	0	$-d_{14}\sin 2\theta + d_{21}\cos^2\theta + d_{23}\sin^2\theta$
m	XY	$-d_{13}\sin\phi$	$d_{15}\sin^2\phi + d_{24}\cos^2\phi$
	YZ	$d_{15}\sin\theta$	$d_{12}\cos^2\theta + d_{13}\sin^2\theta$
	XZ	$-d_{12}\cos\theta + d_{24}\sin\theta$	0
mm2	XY	0	$d_{15}\sin^2\phi + d_{24}\cos^2\phi$
	YZ	$d_{15}\sin\theta$	0
	XZ	$d_{24}\sin\theta$	0
222	XY	0	$-d_{14}\sin 2\phi$
	YZ	0	$-d_{14}\sin 2\theta$
	XZ	0	$-d_{14}\sin 2\theta$

Kleinman symmetry is assumed for the table above.

Tabulation of *d* Matrices

Point group	***d*** **matrix**
1	$\begin{pmatrix} d_{11} & d_{12} & d_{13} & d_{14} & d_{15} & d_{16} \\ d_{21} & d_{22} & d_{23} & d_{24} & d_{25} & d_{26} \\ d_{31} & d_{32} & d_{33} & d_{34} & d_{35} & d_{36} \end{pmatrix}$
2	$\begin{pmatrix} 0 & 0 & 0 & d_{14} & 0 & d_{16} \\ d_{21} & d_{22} & d_{23} & 0 & d_{25} & 0 \\ 0 & 0 & 0 & d_{34} & 0 & d_{36} \end{pmatrix}$
m	$\begin{pmatrix} d_{11} & d_{12} & d_{13} & 0 & d_{15} & 0 \\ 0 & 0 & 0 & d_{24} & 0 & d_{26} \\ d_{31} & d_{32} & d_{33} & 0 & d_{35} & 0 \end{pmatrix}$
222	$\begin{pmatrix} 0 & 0 & 0 & d_{14} & 0 & 0 \\ 0 & 0 & 0 & 0 & d_{25} & 0 \\ 0 & 0 & 0 & 0 & 0 & d_{36} \end{pmatrix}$
mm2	$\begin{pmatrix} 0 & 0 & 0 & 0 & d_{15} & 0 \\ 0 & 0 & 0 & d_{24} & 0 & 0 \\ d_{31} & d_{32} & d_{33} & 0 & 0 & 0 \end{pmatrix}$
3	$\begin{pmatrix} d_{11} & -d_{11} & 0 & d_{14} & d_{15} & -d_{22} \\ -d_{22} & d_{22} & 0 & d_{15} & -d_{14} & -d_{11} \\ d_{15} & d_{15} & d_{33} & 0 & 0 & 0 \end{pmatrix}$
3m	$\begin{pmatrix} 0 & 0 & 0 & 0 & d_{15} & -d_{22} \\ -d_{22} & d_{22} & 0 & d_{15} & 0 & 0 \\ d_{31} & d_{31} & d_{33} & 0 & 0 & 0 \end{pmatrix}$
$\overline{6}$	$\begin{pmatrix} d_{11} & -d_{11} & 0 & 0 & 0 & -d_{22} \\ -d_{22} & d_{22} & 0 & 0 & 0 & -d_{11} \\ 0 & 0 & 0 & 0 & 0 & 0 \end{pmatrix}$
$\overline{6}$m2	$\begin{pmatrix} 0 & 0 & 0 & 0 & 0 & -d_{22} \\ -d_{22} & d_{22} & 0 & 0 & 0 & 0 \\ 0 & 0 & 0 & 0 & 0 & 0 \end{pmatrix}$
6,4	$\begin{pmatrix} 0 & 0 & 0 & d_{14} & d_{15} & 0 \\ 0 & 0 & 0 & d_{15} & -d_{14} & 0 \\ d_{31} & d_{31} & d_{33} & 0 & 0 & 0 \end{pmatrix}$

Tabulation of *d* Matrices (cont.)

Point group	*d* matrix
6mm,4mm	$\begin{pmatrix} 0 & 0 & 0 & 0 & d_{15} & 0 \\ 0 & 0 & 0 & d_{15} & 0 & 0 \\ d_{31} & d_{31} & d_{33} & 0 & 0 & 0 \end{pmatrix}$
$\overline{4}$	$\begin{pmatrix} 0 & 0 & 0 & d_{14} & d_{15} & 0 \\ 0 & 0 & 0 & -d_{15} & d_{14} & 0 \\ d_{15} & -d_{15} & 0 & 0 & 0 & d_{14} \end{pmatrix}$
32	$\begin{pmatrix} d_{11} & -d_{11} & 0 & d_{14} & 0 & 0 \\ 0 & 0 & 0 & 0 & -d_{14} & -d_{11} \\ 0 & 0 & 0 & 0 & 0 & 0 \end{pmatrix}$
$\overline{4}$2m	$\begin{pmatrix} 0 & 0 & 0 & d_{14} & 0 & 0 \\ 0 & 0 & 0 & 0 & d_{14} & 0 \\ 0 & 0 & 0 & 0 & 0 & d_{36} \end{pmatrix}$
$\overline{4}$3m, 23	$\begin{pmatrix} 0 & 0 & 0 & d_{14} & 0 & 0 \\ 0 & 0 & 0 & 0 & d_{14} & 0 \\ 0 & 0 & 0 & 0 & 0 & d_{14} \end{pmatrix}$

Zeros and the equality of certain elements result from crystal symmetry considerations. Consider crystals that are invariant under an inversion of the coordinate system (**centrosymmetric**). For any crystal under inversion of the coordinate system, $d'_{ijk} = -d_{ijk}$. If the crystal is also centrosymmetric, then the symmetry dictates that $d'_{ijk} = +d_{ijk}$, which leads to $d_{ijk} = -d_{ijk}$, and hence all $d_{ijk} = 0$ for centrosymmetric crystals.

Further simplifications of the above ***d* matrices** are possible when Kleinman symmetry is valid:

$d_{12} = d_{26}$ $\quad d_{15} = d_{31}$ $\quad d_{24} = d_{32}$

$d_{13} = d_{35}$ $\quad d_{16} = d_{21}$

$d_{14} = d_{25} = d_{36}$ $\quad d_{23} = d_{34}$

Electro-optic Effect

The linear **electro-optic effect** (or **Pockels effect**) is due to an electric-field-induced change in the permittivity tensor ε_{ij}. The **impermeability tensor** **B** is typically used to calculate the changes. Unperturbed, this tensor is written in matrix form:

$$\mathbf{B} = \begin{pmatrix} 1/\varepsilon_{xx} & 0 & 0 \\ 0 & 1/\varepsilon_{xx} & 0 \\ 0 & 0 & 1/\varepsilon_{xx} \end{pmatrix} = \begin{pmatrix} 1/n_x^2 & 0 & 0 \\ 0 & 1/n_y^2 & 0 \\ 0 & 0 & 1/n_z^2 \end{pmatrix}$$

When an electric field is applied to the crystal, the impermeability matrix is modified:

$$\mathbf{B}' = \begin{pmatrix} 1/n_x^2 & 0 & 0 \\ 0 & 1/n_y^2 & 0 \\ 0 & 0 & 1/n_z^2 \end{pmatrix} + \begin{pmatrix} \Delta B_1 & \Delta B_6 & \Delta B_5 \\ \Delta B_6 & \Delta B_2 & \Delta B_4 \\ \Delta B_5 & \Delta B_4 & \Delta B_3 \end{pmatrix}$$

where ΔB_m ($m = 1$ through 6) is obtained from

$$\begin{pmatrix} \Delta B_1 \\ \Delta B_2 \\ \Delta B_3 \\ \Delta B_4 \\ \Delta B_5 \\ \Delta B_6 \end{pmatrix} = \begin{pmatrix} r_{11} & r_{12} & r_{13} \\ r_{21} & r_{22} & r_{23} \\ r_{31} & r_{32} & r_{33} \\ r_{41} & r_{42} & r_{43} \\ r_{51} & r_{52} & r_{53} \\ r_{61} & r_{62} & r_{63} \end{pmatrix} \begin{pmatrix} E_x \\ E_y \\ E_z \end{pmatrix}$$

where the r matrix is tabulated for each crystal class. The new principal indices and axes are found by diagonalizing $\mathbf{B}'$.

An electric field E_z applied to the z axis of a $\overline{4}2$m crystal leads to $\Delta B_m = 0$, except $\Delta B_6 = r_{63}E_z$. Hence, $\mathbf{B}'$ is:

$$\begin{pmatrix} 1/n_o^2 & r_{63}E_z & 0 \\ r_{63}E_z & 1/n_o^2 & 0 \\ 0 & 0 & 1/n_z^2 \end{pmatrix} \text{ with eigenvalues: } \begin{array}{l} \lambda_{1,2} = \dfrac{1}{n_o^2} \pm r_{63}E_z \\ \lambda_3 = \dfrac{1}{n_2^2} \end{array}$$

Therefore, $n_3 = n_z$ and $n_{1,2} = n_o(1 \pm n_o^2 r_{63}E_z)^{-1/2}$, which for small $r_{63}E_z$ is approximately $n_{1,2} = n_o \mp n_o^3 r_{63}E_z/2$. The new principal axes (eigenvectors) are $\hat{\mathbf{z}}$ and $(\hat{\mathbf{x}} \pm \hat{\mathbf{y}})/\sqrt{2}$.

r Matrices

Point group	r matrix	Point group	r matrix
1	$\begin{pmatrix} r_{11} & r_{12} & r_{13} \\ r_{21} & r_{22} & r_{23} \\ r_{31} & r_{32} & r_{33} \\ r_{41} & r_{42} & r_{43} \\ r_{51} & r_{52} & r_{53} \\ r_{61} & r_{62} & r_{63} \end{pmatrix}$	3m	$\begin{pmatrix} 0 & -r_{22} & r_{13} \\ 0 & r_{22} & r_{13} \\ 0 & 0 & r_{33} \\ 0 & r_{51} & 0 \\ r_{51} & 0 & 0 \\ -r_{22} & 0 & 0 \end{pmatrix}$
2	$\begin{pmatrix} 0 & r_{12} & 0 \\ 0 & r_{22} & 0 \\ 0 & r_{32} & 0 \\ r_{41} & 0 & r_{43} \\ 0 & r_{52} & 0 \\ r_{61} & 0 & r_{63} \end{pmatrix}$	$\overline{6}$	$\begin{pmatrix} r_{11} & -r_{22} & 0 \\ -r_{11} & r_{22} & 0 \\ 0 & 0 & 0 \\ 0 & 0 & 0 \\ 0 & 0 & 0 \\ -r_{22} & -r_{11} & 0 \end{pmatrix}$
m	$\begin{pmatrix} r_{11} & 0 & r_{13} \\ r_{21} & 0 & r_{23} \\ r_{31} & 0 & r_{33} \\ 0 & r_{42} & 0 \\ r_{51} & 0 & r_{53} \\ 0 & r_{62} & 0 \end{pmatrix}$	$\overline{6}$m2	$\begin{pmatrix} 0 & -r_{22} & 0 \\ 0 & r_{22} & 0 \\ 0 & 0 & 0 \\ 0 & 0 & 0 \\ 0 & 0 & 0 \\ -r_{22} & 0 & 0 \end{pmatrix}$
222	$\begin{pmatrix} 0 & 0 & 0 \\ 0 & 0 & 0 \\ 0 & 0 & 0 \\ r_{41} & 0 & 0 \\ 0 & r_{52} & 0 \\ 0 & 0 & r_{63} \end{pmatrix}$	6,4	$\begin{pmatrix} 0 & 0 & r_{13} \\ 0 & 0 & r_{13} \\ 0 & 0 & r_{33} \\ r_{41} & r_{51} & 0 \\ r_{51} & -r_{41} & 0 \\ 0 & 0 & 0 \end{pmatrix}$
mm2	$\begin{pmatrix} 0 & 0 & r_{13} \\ 0 & 0 & r_{23} \\ 0 & 0 & r_{33} \\ 0 & r_{42} & 0 \\ r_{51} & 0 & 0 \\ 0 & 0 & 0 \end{pmatrix}$	$\overline{4}$	$\begin{pmatrix} 0 & 0 & r_{13} \\ 0 & 0 & -r_{13} \\ 0 & 0 & 0 \\ r_{41} & -r_{51} & 0 \\ r_{51} & r_{41} & 0 \\ 0 & 0 & r_{63} \end{pmatrix}$

r Matrices (cont.)

Point group	*r* matrix	Point group	*r* matrix
3	$\begin{pmatrix} r_{11} & -r_{22} & r_{13} \\ -r_{11} & r_{22} & r_{13} \\ 0 & 0 & r_{33} \\ r_{41} & r_{51} & 0 \\ r_{51} & -r_{41} & 0 \\ -r_{22} & -r_{11} & 0 \end{pmatrix}$	32	$\begin{pmatrix} r_{11} & 0 & 0 \\ -r_{11} & 0 & 0 \\ 0 & 0 & 0 \\ r_{41} & 0 & 0 \\ 0 & -r_{41} & 0 \\ 0 & -r_{11} & 0 \end{pmatrix}$
$\bar{4}$2m	$\begin{pmatrix} 0 & 0 & 0 \\ 0 & 0 & 0 \\ 0 & 0 & 0 \\ r_{41} & 0 & 0 \\ 0 & r_{41} & 0 \\ 0 & 0 & r_{63} \end{pmatrix}$	$\bar{4}$3m,23	$\begin{pmatrix} 0 & 0 & 0 \\ 0 & 0 & 0 \\ 0 & 0 & 0 \\ r_{41} & 0 & 0 \\ 0 & r_{41} & 0 \\ 0 & 0 & r_{41} \end{pmatrix}$
		6mm 4mm	$\begin{pmatrix} 0 & 0 & r_{13} \\ 0 & 0 & r_{13} \\ 0 & 0 & r_{33} \\ 0 & r_{51} & 0 \\ r_{51} & 0 & 0 \\ 0 & 0 & 0 \end{pmatrix}$

***r* matrices** use the same contraction convention as *d* matrices. For individual *r* matrix elements given by r_{mi} use the table on the right to identify the contraction. Note that the Cartesian indices, *x*, *y*, and *z* are also interchangeable with 1, 2, and 3.

j,k	m
xx	1
yy	2
zz	3
yz, *zy*	4
xz, *zx*	5
xy, *yx*	6

The electro-optic effect is a $\chi^{(2)}$ effect; therefore, the *r* matrix coefficients are related to the nonlinear susceptibility:

$$r_{mi} = -4\frac{d_{im}}{n_m^4}, \quad \text{where} \quad n_m^4 = n_j^2 n_k^2$$

and where *m* is the contracted index.

Electro-optic Waveplates

An application of the electro-optic effect is a voltage-controlled **waveplate**. In one design, a voltage is applied to a uniaxial crystal using a ring electrode.

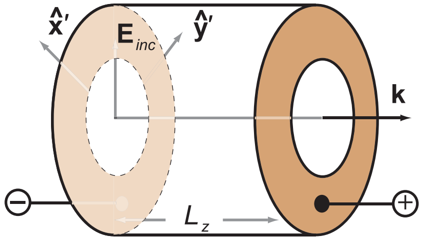

Such a configuration in which the applied field is parallel to $\hat{\mathbf{k}}$ is called the **longitudinal electro-optic effect**. The incident linearly polarized beam is 45 deg to $\hat{\mathbf{x}}'$ and $\hat{\mathbf{y}}'$, exciting a linear superposition of two modes polarized along these axes. The two modes travel at different phase velocities, inducing a polarization change. The phase difference of the two modes is

$$\Delta\phi = 2\pi(n'_x - n'_y)L_z/\lambda$$

KD*P is a uniaxial, class-$\bar{4}$2m crystal. Applying an electric field along the Z axis gives $n'_{x,y} = n_o \pm n_o^3 r_{63} E_z/2$. Therefore, $\Delta\phi = 2\pi n_o^3 r_{63} V/\lambda$ ($E_z = V/L_z$). The **quarter-wave voltage** (written as $V_{\pi/2}$) is the voltage required to induce a quarter-wave phase shift ($\Delta\phi = \pi/2$). Similarly, the **half-wave voltage** V_π corresponds to $\Delta\phi = \pi$. In KD*P, $n_o \approx 1.5$, $r_{63} = 26.4$ pm/V, and for $\lambda = 1.064$ μm, $V_{\pi/2} = 2985V$.

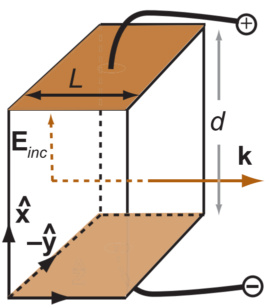

The **transverse electro-optic effect** has the benefit of an open aperture, usually with lower voltages. Typical electro-optic (EO) crystals are KD*P, BBO, and lithium niobate (LN). In this configuration, for LN (class 3m), $V_{\pi/2} = \lambda d/(4Ln_o^3 r_{22})$, and a small contribution from r_{51} is negligible. For lithium niobate, $r_{22} = 6.8$ pm/V (low frequencies).

Q Switches

An **electro-optic Q switch** is based on the **electro-optic effect**. Unpolarized light, incident from the left, is first polarized. When the Pockels cell is unbiased, the polarization state remains unchanged, hence a linear polarization is incident on the **quarter-wave plate (QWP)**.

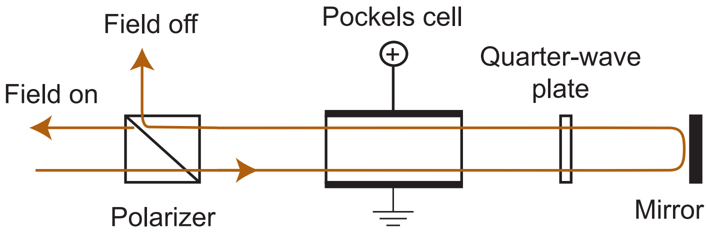

The linear polarization becomes circularly polarized and, after reflection from the mirror, the sense of rotation changes (right circular becomes left circular). After passing through the QWP again, the light becomes linearly polarized, but rotated 90 deg to the incident beam so that it is rejected by the polarizer. When a voltage of $V_{\pi/2}$ is applied to the Pockels cell, it becomes a QWP. The two QWPs in series act as a half-wave plate, leaving the outgoing polarization the same as the ingoing one.

An **acousto-optic Q switch** is based on the acousto-optic (AO) effect. A laser beam diffracts from an acoustically induced index grating. By turning the acoustic wave on and off, one is able to momentarily deflect the beam. In the setup shown below, the AO cell acts as a fast shutter when placed in a laser cavity.

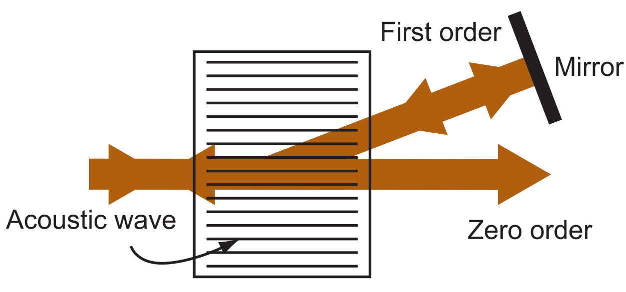

Amplitude and Phase Modulators

The ability of an EO waveplate to change the polarization state of a laser translates to a voltage-controlled **amplitude modulator**. The waveplate induces a phase shift Γ between the two orthogonally polarized modes. For example, for KD*P with a longitudinal EO setup $\Gamma = 2\pi n_o^3 r_{63} V/\lambda$. The intensities transmitted through the second polarizer's two ports are $I_1/I_o = \sin^2(\Gamma/2)$ and $I_2/I_o = \cos^2(\Gamma/2)$. Typically, the electro-optic voltage is set so that small voltages about this bias lead to a linear amplitude modulation for small voltage changes.

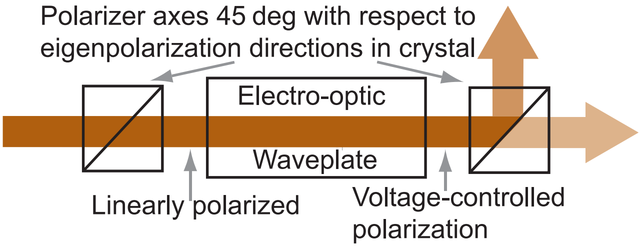

In an **electro-optic phase modulator**, a linearly polarized laser is aligned to excite either an e- or o-wave, accumulating a voltage-induced phase shift:

$$\phi_{out} = \omega_o t - kL = \omega_o t - 2\pi(n_o + \Delta n)L/\lambda$$

where Δn is the EO index change (directly proportional to the voltage). For $V = V_o \sin \Omega_m t$, the transmitted field is

$$E_{out} = E_o \cos(\omega_o t + \delta \sin \Omega_m t)$$

where δ is the **phase modulation index**, and its magnitude is determined by the EO effect. For example, in KD*P, for a longitudinal configuration, $\delta = \pi n_o^3 r_{63} V_o/\lambda_o$. The phase-modulated field is expanded in a **Bessel series**:

$$E_{out} = E_o J_0(\delta)\cos(\omega_o t) + E_o \sum_{k=1}^{\infty} \left\{ J_k(\delta) \left[\cos(\omega_o + k\Omega_m)t + (-1)^k \cos(\omega_o - k\Omega_m)t \right] \right\}$$

For a low-modulation index, the field is well approximated by a carrier at ω_o and two sidebands (keeping only $k = 1$ in the summation).

Electro-optic Sampling for Terahertz Detection

Short bursts of **terahertz** radiation may be generated by **optical rectification** of ultrashort laser pulses in $\chi^{(2)}$ media. This process is also understood in terms of difference-frequency generation between the frequency components present in the ultrashort pulse's bandwidth. Pulses with bandwidths of several terahertz are common.

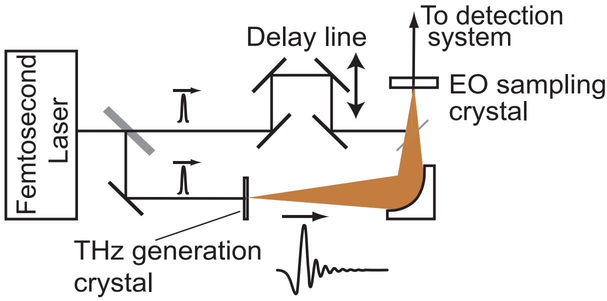

Terahertz time-domain waveforms can be measured using **electro-optic sampling**. The key is overlapping an ultrashort pulse with a portion of the terahertz field, E_{THz}, in an EO crystal. As the terahertz field propagates through a $\chi^{(2)}$ material, its field modifies the crystal birefringence through the **EO** effect. The probe-pulse polarization state changes due to this birefringence change. The relative phase-shift Γ, induced between the x and y components of the probe field, depends on the **EO sampling crystal**. For example, in ZnTe (class $\overline{4}3$m) with the THz field aligned with the Z axis [001],

$$\Gamma = \pi n_o^3 r_{14} E_{\mathrm{THz}} L/\lambda$$

where r_{14} is the EO coefficient, n_o is the index, L is the interaction length, and λ is the vacuum wavelength.

By measuring the change in polarization, one obtains a signal directly proportional to E_{THz}. By changing the relative delay between the probe and terahertz field, one can map out $E_{\mathrm{THz}}(t)$. This timing is possible by using the same femtosecond laser to generate the terahertz field and provide probe pulses.

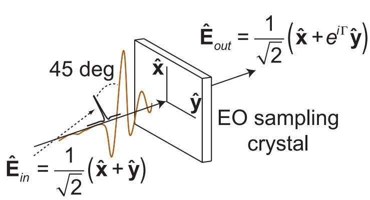

Photorefraction

The **photorefractive effect** occurs in transparent media when a laser photo-excites impurity states, generating free carriers. These charges diffuse out of the laser beam, leading to a space-charge field. This field induces an index change to the medium via the electro-optic effect. In some crystals, the photo-excited charges are ejected in a preferred direction, giving the **photogalvanic** current in addition to the diffusion of charges.

The induced change in index may have a complicated structure that can lead to severe beam distortion. In some cases, photorefraction can be mitigated by heating the crystal. In lithium niobate, doping with MgO can increase photoconductivity and decrease the photogalvanic current, resulting in a reduced-space charge field.

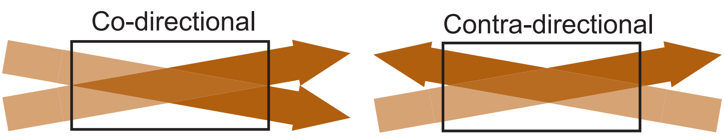

When two beams are present in the medium, photorefractive effects lead to applications in **two-beam coupling**. This process transfers energy from one beam to the other, in some cases allowing for beam clean-up. In two-beam coupling, the two beams diffract off of a photorefractive-induced grating such that one beam is amplified and the other is attenuated. In a lossless medium where the two beams are co-directional

$$I_1(L) = I_{10}\frac{I_{10}+I_{20}}{I_{10}+I_{20}e^{\gamma L}},\quad I_2(L) = I_{20}\frac{I_{10}+I_{20}}{I_{20}+I_{10}e^{-\gamma L}},\quad \gamma = \frac{2\pi}{\lambda}n^3 r_{eff}E_{SC}$$

where I_{10} and I_{20} are the input intensities, n is the index, E_{SC} is the space-charged electric field, and λ is the vacuum wavelength. r_{eff} is an effective electro-optic r coefficient that depends on the crystal and its orientation relative to the input beams. For contra-directional beams

$$I_1(L) = I_{10}\frac{I_{10}+I_{2L}}{I_{10}+I_{2L}e^{\gamma L}}\quad I_2(0) = I_{2L}\frac{I_{10}+I_{2L}}{I_{2L}+I_{10}e^{-\gamma L}}$$

where I_{10} and $I_{2\mathrm{L}}$ are the inputs at $z = 0$ and L, respectively.

$\chi^{(2)}$ Coupled Amplitude Equations

Understanding many nonlinear phenomena starts with a wave equation derived from Maxwell's equations. The simplest case assumes a collinear monochromatic plane-wave interaction and a field envelope that changes slowly with propagation distance, known as the **slowly varying envelope approximation (SVEA)**. For a field of the form $E = \frac{1}{2}A(z)e^{ikz} + c.c.$, the SVEA allows for the following approximation:

$$\left|\frac{d^2A}{dz^2}\right| \ll \left|2k\frac{dA}{dz}\right|$$

In this regime, a general three-wave collinear plane-wave interaction defined by $\omega_1 = \omega_2 + \omega_3$ with complex amplitudes A_1, A_2, and A_3, an effective nonlinearity of d_{eff}, absorption coefficients of α_1 through α_3, and where $\Delta k = k_1 - k_2 - k_3$, yields three **coupled amplitude equations**:

$$\frac{dA_1}{dz} + \frac{\alpha_1}{2}A_1 = i\frac{\omega_1}{n_1 c}d_{eff}A_3A_2e^{-i\Delta kz}$$
$$\frac{dA_2}{dz} + \frac{\alpha_2}{2}A_2 = i\frac{\omega_2}{n_2 c}d_{eff}A_1A_3^*e^{i\Delta kz}$$
$$\frac{dA_3}{dz} + \frac{\alpha_3}{2}A_3 = i\frac{\omega_3}{n_3 c}d_{eff}A_1A_2^*e^{i\Delta kz}$$

In the case of second-harmonic generation, where only two fields are present at the fundamental ω_F and second harmonic $\omega_{SHG} = 2\omega_F$, only two equations result:

$$\frac{dA_{SHG}}{dz} + \frac{\alpha_{SHG}}{2}A_{SHG} = i\frac{\omega_{SHG}}{2n_{SHG}c}d_{eff}A_F^2e^{-i\Delta kz}$$

$$\frac{dA_F}{dz} + \frac{\alpha_F}{2}A_F = i\frac{\omega_F}{n_F c}d_{eff}A_{SHG}A_F^*e^{i\Delta kz}$$

Note that when authors use the convention $E = Ae^{ikz} + c.c.$, $A_1 \rightarrow 2A_1$, $A_2 \rightarrow 2A_2$, $A_3 \rightarrow 2A_3$, etc. The three coupled equations reduce in number in the small signal limit where one or more of the fields remain approximately constant. For these **undepleted fields**, $dA/dz \approx 0$.

$\chi^{(2)}$ Processes with Focused Gaussian Beams

When working with **focused Gaussian beams**, it is appropriate to use plane-wave equations with a **gain reduction factor** that accounts for imperfect overlap of differently sized beams. This approach works best for crystal lengths of less than $2z_R$. For an interaction defined by $\omega_1 = \omega_2 + \omega_3$, with beam sizes (1/*e* field radius) of w_1, w_2, and w_3, the gain reduction factors g_i are

$$g_1 = \frac{2\overline{w}_1^2}{\overline{w}_1^2 + w_1^2} \qquad g_2 = \frac{2\overline{w}_2^2}{\overline{w}_2^2 + w_2^2} \qquad g_3 = \frac{2\overline{w}_3^2}{\overline{w}_3^2 + w_3^2}$$

$$\frac{1}{\overline{w}_3^2} \equiv \frac{1}{w_1^2} + \frac{1}{w_2^2} \qquad \frac{1}{\overline{w}_2^2} \equiv \frac{1}{w_1^2} + \frac{1}{w_3^2} \qquad \frac{1}{\overline{w}_1^2} \equiv \frac{1}{w_2^2} + \frac{1}{w_3^2}$$

Typically, two of the w's in a three-wave process are constrained by the focusing conditions of a setup. The third w is unconstrained and is given by $w = \overline{w}$, which then results in $g = 1$ for that beam. When resonators are involved, the resonator w's are determined by the cavity mode, usually yielding $g \neq 1$. The coupled amplitude equations for loosely focused Gaussian beams are

$$\frac{dA_{10}}{dz} + \frac{\alpha_1}{2}A_{10} = ig_1\frac{\omega_1}{n_1 c}d_{eff}A_{30}A_{20}e^{-i\Delta kz}$$
$$\frac{dA_{20}}{dz} + \frac{\alpha_2}{2}A_{20} = ig_2\frac{\omega_2}{n_2 c}d_{eff}A_{10}A_{30}^{*}e^{i\Delta kz}$$
$$\frac{dA_{30}}{dz} + \frac{\alpha_3}{2}A_{30} = ig_3\frac{\omega_3}{n_3 c}d_{eff}A_{10}A_{20}^{*}e^{i\Delta kz}$$

where A_{10}, A_{20}, and A_{30} are the on-axis field amplitudes.

A useful relationship for a Gaussian beam with a beam size of w_o is the on-axis intensity's relationship to the total power:

$$I_o = \frac{2P}{\pi w_o^2}$$

When the beam is confocally focused into a crystal, the above relationship becomes

$$I_o = \frac{4n}{\lambda L}P$$

DFG and OPA

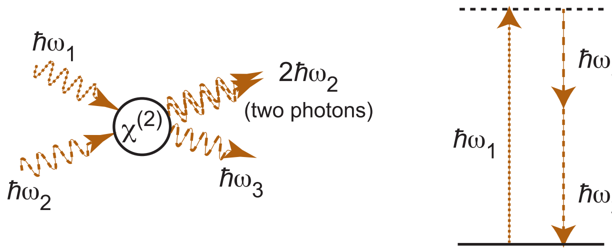

Difference-frequency generation (DFG) is defined by the energy relationship $\hbar\omega_{DFG} = \hbar\omega_1 - \hbar\omega_2$, where $\hbar$ is Planck's constant divided by 2π. Below, $\omega_3 = \omega_{DFG}$. In a DFG process, the high-energy photon at ω_1 splits into two lower-energy photons—one at the difference frequency and one at the same frequency as the second input ω_2. Therefore, the DFG process amplifies the second input, referred to as **optical parametric amplification (OPA)**. Hence, an OPA output may be found from DFG:

$$P_2(L) = P_2(0) + \frac{\lambda_3}{\lambda_2} P_3(L)$$

In the small signal limit for a plane-wave DFG interaction

$$I_3 = \frac{8\pi^2 L^2}{n_1 n_2 n_3 \varepsilon_0 c \lambda_3^2} d_{eff}^2 I_1 I_2 \,\mathrm{sinc}^2(\Delta k L/2), \quad \mathrm{sinc}(x) \equiv \frac{\sin(x)}{x}$$

In the **undepleted pump approximation**, where the pump at ω_1 remains approximately constant, the DFG and OPA outputs may be written in terms of photon numbers $N(z)$, as

$$N_3(z) = N_{20}\sinh^2(\Gamma z) + N_{30}\cosh^2(\Gamma z)$$
$$N_2(z) = N_{30}\sinh^2(\Gamma z) + N_{20}\cosh^2(\Gamma z)$$

where N_{20} and N_{30} are $N_2(0)$ and $N_3(0)$, and where

$$\Gamma^2 = \frac{2\omega_2\omega_3 d_{eff}^2}{n_1 n_2 n_3 \varepsilon_0 c^3} I_1 = \frac{8\pi^2 d_{eff}^2}{n_1 n_2 n_3 \varepsilon_0 c \lambda_2 \lambda_3} I_1$$

For Gaussian beams confocally focused in a crystal, the phase-matched ($\Delta k = 0$) power for DFG is

$$P_3(L) = \frac{32\pi^2 d^2 L}{n_3 \varepsilon_0 c \lambda_3^2 (n_2\lambda_1 + n_1\lambda_2)} P_1(0) P_2(0)$$

Sum-Frequency Generation

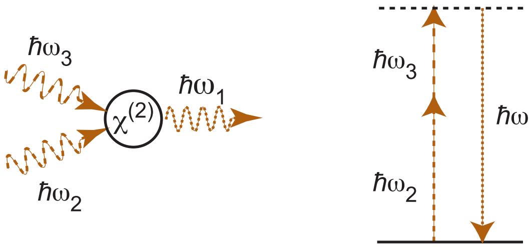

Sum-frequency generation (SFG) is defined by the energy relationship $\hbar\omega_{SFG} = \hbar\omega_2 + \hbar\omega_3$. In an SFG process, two low-energy photons at ω_2 and ω_3 merge to generate one photon of higher energy at ω_1. In the small signal limit, where the two input fields remain approximately constant

$$I_1 = \frac{8\pi^2 L^2}{\varepsilon_0 c n_1 n_2 n_3 \lambda_1^2} d_{eff}^2 I_2 I_3 \, \mathrm{sinc}^2(\Delta k L/2)$$

For Gaussian beams confocally focused in a crystal, and for $\Delta k = 0$, the SFG in terms of beam powers is

$$P_{SFG} = \frac{32\pi^2 L}{n_1 \varepsilon_0 \lambda_1^2 c(n_2\lambda_3 + n_3\lambda_2)} d^2 P_2 P_3$$

SFG calculation	Input parameters
To calculate the SFG output, first find the sum-frequency wavelength using energy conservation: $1/\lambda_{SFG} = 1/1064 + 1/1320 \rightarrow \lambda_{SFG} = 589.1$ nm Calculate the SFG-output power (assuming confocal focus) using the equation above, yielding an output SFG power of $P_1 = 119$ mW. To perform the experiment with a confocal geometry, $z_R = L/2$. This relationship allows us to calculate the required beam radii, $w_2 = \sqrt{\frac{\lambda_2 L}{2\pi n_2}} = 28$ μm; similarly, $w_3 = 31$ μm.	$\lambda_2 = 1064$ nm $\lambda_3 = 1320$ nm $P_2 = 10$ W $P_3 = 10$ W $L_{crystal} = 1$ cm n~2.2 $d_{eff} = 2$ pm/V

Second-Harmonic Generation

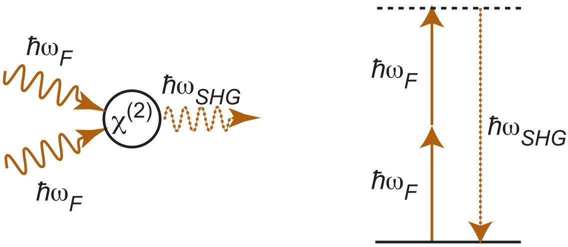

Second-harmonic generation (SHG) is defined by the energy relationship $\hbar\omega_{SFG} = 2\hbar\omega_F$, where ω_F refers to the input, or **fundamental frequency**. In an SHG process, two photons at ω_F combine to generate one photon of twice the energy at ω_{SHG}. In the small signal limit

$$I_{SHG} = \frac{8\pi^2 L^2}{n_{SHG} n_F^2 \varepsilon_0 c \lambda_F^2} d_{eff}^2 I_F^2 \,\mathrm{sinc}^2(\Delta k L/2)$$

For confocally focused Gaussian beams, $\Delta k = 0$, and no Poynting vector walk-off:

$$P_{SHG} = \frac{16\pi^2 d^2 L}{\varepsilon_o c n_F^2 \lambda_F^3} P_F^2$$

Optimum focusing for a Type-I phase-matching interaction in birefringent media may be numerically calculated.

$h(B,\xi)$ is an optimization function where $\xi = L/b$, $b = 2z_R$, $B = \frac{\rho}{2}\sqrt{\frac{2\pi L n_F}{\lambda_F}}$, and ρ is the walk-off angle. When $B = 0$, optimum focusing occurs for $\xi = 2.84$.

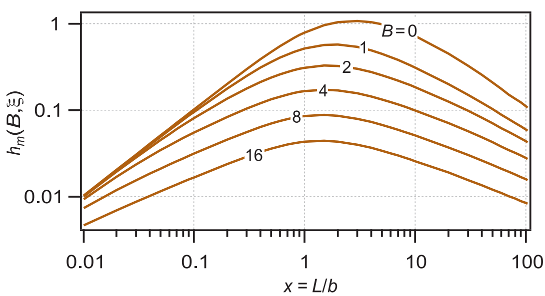

Three-Wave Mixing Processes with Depletion

In cases of high conversion efficiency, formulae for mixing processes must include the effects of **depletion**. In this regime, the power at the desired output frequency becomes large enough that it **back-converts**—to the pump in the case of DFG, and to the signal and idler in the case of SFG. Energy periodically flows from the inputs to the output and back again. Formulae for plane-wave interactions, assuming $\Delta k = 0$, are

SFG, $\omega_{SFG} = \omega_2 + \omega_3$:

$$I_{SFG}(z) = I_3(0)\frac{\lambda_3}{\lambda_{SFG}}\mathrm{sn}^2[(z/L_{NL}),\gamma_{SFG}] \qquad \gamma_{SFG} = \frac{\lambda_3 I_{30}}{\lambda_2 I_{20}}$$

$$L_{NL} = \frac{1}{4\pi d_{eff}}\sqrt{\frac{2\varepsilon_0 n_{SFG} n_2 n_3 c \lambda_3 \lambda_{SFG}}{I_2(0)}}$$

DFG, $\omega_{DFG} = \omega_1 - \omega_2$:

$$I_{DFG} = \frac{\lambda_2}{\lambda_{DFG}}\mathrm{sn}^2(iL/L_{NL}, i\gamma_{DFG}) \quad \gamma_{DFG} = \frac{\lambda_2 I_{20}}{\lambda_1 I_{10}}$$

$$L_{NL} = \frac{1}{4\pi d_{eff}}\sqrt{\frac{2\varepsilon_0 n_1 n_2 n_{DFG} c \lambda_2 \lambda_{DFG}}{I_1(0)}}$$

OPA:

$$I_2(L) = I_2(0) + \frac{\lambda_3}{\lambda_2} I_3(L)$$

where sn is a **Jacobi elliptic sine function** that has tabulated values and is a built-in function for many mathematical packages. Initially, the process of depletion starts as DFG, but after the pump depletes to zero, the signal and idler back-convert to regenerate the pump in an SFG process.

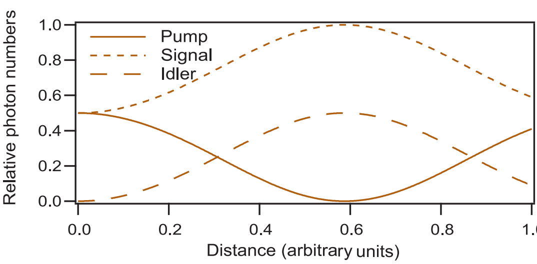

Optical Parametric Generation

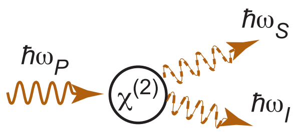

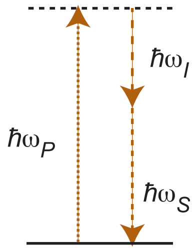

Spontaneous parametric down-conversion occurs when a pump photon at ω_P spontaneously splits into two photons—called the **signal** at ω_S, and the **idler** at ω_I (by convention, the signal frequency is higher than the idler frequency, but the convention may be reversed in some contexts). The process is also called **spontaneous parametric scattering (SPS)** and **optical parametric generation (OPG)**. OPG occurs in $\chi^{(2)}$ crystals and is defined by the energy conservation statement $\hbar\omega_P = \hbar\omega_S + \hbar\omega_I$. The signal and idler central frequencies and the bandwidth are dictated by phase matching.

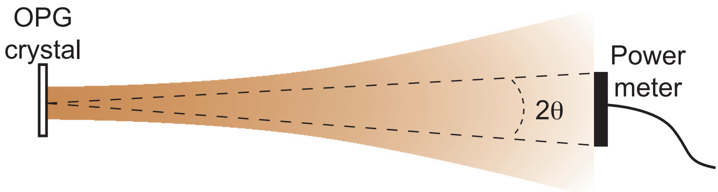

In the small signal regime, the power collected by a detector of a finite size is given by

$$dP_s(z) = \frac{\hbar n_S \omega_S^4 \omega_I d_{eff}^2}{2\pi^2 \varepsilon_0 c^5 n_p n_i} \frac{\sinh^2(gz)}{g^2} P_p \theta d\theta d\omega_s$$

where $$g = \sqrt{\Gamma^2 - \left(\frac{\Delta k}{2}\right)^2} \quad \text{and} \quad \Gamma^2 = \frac{2\omega_S \omega_I d_{eff}^2}{n_P n_S n_I \varepsilon_0 c^3} I_P$$

I_P and P_P are the intensity and power of the incident pump beam, respectively. Although typically weak, the OPG process can deplete the incident pump beam for high-peak-power pump beams.

Optical Parametric Oscillator

In an **optical parametric oscillator (OPO)**, a pump beam spontaneously down-converts into a signal-and-idler beam where the signal and/or idler are resonated. If the roundtrip losses are less than the parametric gain, an oscillation occurs, yielding relatively high conversion from the incident pump beam to the signal and idler. The threshold power P_{TH} for a plane-wave OPO is given by

$$P_{TH} = A\frac{n_p n_S n_I \varepsilon_0 c \lambda_S \lambda_I}{4\pi^2 d_{eff}^2 L^2}\frac{(1-\rho_S)(1-\rho_I)}{\rho_S+\rho_I}$$

where A is the cross-section of the plane-wave beam, and L is the crystal length. The cavity losses are lumped together in terms ρ_S and ρ_I, given by

$$\rho_S = \sqrt{R_{aS}R_{bS}}e^{-2\alpha_S L} \quad \text{and} \quad \rho_I = \sqrt{R_{aI}R_{bI}}e^{-2\alpha_I L}$$

R_{aS} and R_{bS} correspond to the reflectivities of the two cavity mirrors, and α_S is the crystal absorption for the signal wavelength; a similar notation is used for idler variables. For an SR-OPO, $R_I = 0$.

An OPO where only the signal is resonated is a **singly resonant OPO (SR-OPO)**. An OPO where both the signal and idler are resonated is a **doubly resonant OPO (DR-OPO)**.

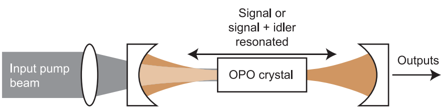

The OPO threshold with loosely focused Gaussian beams is given by

$$P_{TH} = \frac{n_P n_S n_I \varepsilon_0 c \lambda_S \lambda_I W^2}{32\pi L^2 d_{eff}^2}\frac{(1-\rho_S)(1-\rho_I)}{\rho_S+\rho_I}$$

$$\frac{1}{W^2} = \left(\frac{w_P w_S w_I}{w_P^2 w_S^2 + w_P^2 w_I^2 + w_S^2 w_I^2}\right)^2$$

where w_P, w_S, and w_I are the beam radii for the pump, signal, and idler, respectively. For a DR-OPO, w_S and w_I are determined by the cavity. For an SR-OPO

$$1/w_I^2 = 1/w_P^2 + 1/w_S^2$$

Singly Resonant Optical Parametric Oscillator

For continuous-wave OPOs, a stable resonator and tight focusing are used to minimize the OPO threshold. The optimum focusing condition depends on the particular phase-matching interaction. Calculations of the threshold, including the effects of diffraction and walk-off, show that a focusing parameter near $\xi = 1$ (where $\xi = L_{crystal}/2z_R$) is optimum. In this region, the Gaussian-beam threshold equation gives a reasonable estimate for the **SR-OPO** threshold.

Optimum focusing for the pump laser is achieved using external optics. However, the mode size for the signal is determined by the resonator. For a symmetric linear cavity, the cavity beam waist is

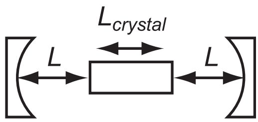

$$w_o^2 = \frac{\lambda}{\pi}\sqrt{L_{eff}(R - L_{eff})}; \quad L_{eff} = L + \frac{L_{crystal}}{2n}$$

where R is the radius of curvature for the mirrors, n is the crystal index, and L is the crystal-to-mirror distance.

SR-OPO threshold calculation	Parameters
Assuming that the pump is confocally focused, $2z_R = L_{crystal}$, we calculate $w_{oP} = 62\ \mu m$. Find w_{oS} using the cavity equation given above, yielding $w_{oS} = 80\ \mu m$, which gives a focusing parameter $\xi_S = 0.88$. The idler beam size is determined by the pump and signal: $1/w_I^2 = 1/w_P^2 + 1/w_S^2$, which gives $w_I = 49\ \mu m$. These beam sizes let us calculate $W = 202\ \mu m$. From the mirror reflectivities, and assuming no crystal losses, $\rho_S = 0.95$ and $\rho_I = 0$. Placing all of the parameters into the threshold equation gives $P_{TH} = 1.1$ W.	$\lambda_P = 1.064\ \mu m$ $\lambda_S = 1.55\ \mu m$ $\alpha = 0$ (no loss) $d_{eff} = 17$ pm/V $L_{crystal} = 5$ cm $L = 3.5$ cm $n = 2.2$ Left mirror: $R_S = 100\%$ $R_I = 0$ Right mirror: $R_S = 97.5\%$ $R_I = 0$ Mirror radius of curvature = 5 cm

Birefringent Phase Matching

Phase matching occurs when the nonlinear polarization is in phase with the field it is driving. Phase matching for a three-wave interaction defined by the energy conservation statement $\hbar\omega_1 = \hbar\omega_2 + \hbar\omega_3$ is expressed by

$$\Delta \mathbf{k} = \mathbf{k}_1 - \mathbf{k}_2 - \mathbf{k}_3 = 0$$

where $\mathbf{k}_1$, $\mathbf{k}_2$, and $\mathbf{k}_3$ are the ***k* vectors** corresponding to the frequencies ω_1, ω_2, and ω_3, respectively. The magnitude of a k vector is $n\omega/c = 2\pi n/\lambda$, and its direction is parallel to the propagation direction. For linearly polarized fields, the index is either *o* or *e* polarized.

Phase matching occurs for $\Delta \mathbf{k} = 0$.

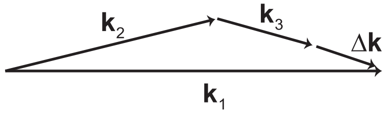

Collinear phase matching occurs when all k vectors are parallel, and **noncollinear phase matching** occurs when the k vectors are nonparallel. A noncollinear situation is shown above. If all three fields have the same polarization, and for materials with normal dispersion, perfect phase matching is not possible. Note that an absorption band lying between two of the frequencies may invalidate the normal dispersion condition. **Birefringent phase matching** uses a mixture of *e* and *o* polarizations to make $\Delta \mathbf{k} = 0$, making phase matching possible but not guaranteed. Different birefringent phase-matching types are characterized by their particular polarization combinations, most commonly categorized into **Type-I** and **Type-II phase matching**.

	ω_1	ω_2	ω_3	$\omega_1 > \omega_2 \geq \omega_3$
Type I	*o*	*e*	*e*	Positive uniaxial
	e	*o*	*o*	Negative uniaxial
Type II	*o*	*e*	*o*	Positive uniaxial
	o	*o*	*e*	
	e	*e*	*o*	Negative uniaxial
	e	*o*	*e*	

e- and o-Wave Phase Matching

A large class of nonlinear interactions require orienting the crystal for phase matching. In *uniaxial* crystals, the phase-matching angle depends only on the angle between the Z axis and the k vector of the laser beam. This **polar angle** is usually called the **phase-matching angle**. The **crystal cut** is chosen to allow rotation of the phase-matching angle, while keeping the **azimuthal angle** (angle between X axis and k vector) fixed. For interactions confined to the principal planes of a biaxial crystal, the phase-matching angle is defined to be between one of the principal axes and the laser k vector. The mapping of an external polarization state to an e- or o-wave depends on the specific crystal orientation, as shown below:

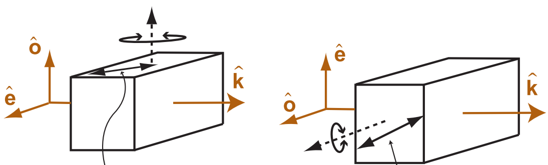

Another important consideration when working with a mixture of e- and o-waves is **Poynting vector walk-off** ρ. In many cases, walk-off limits the effective crystal length since the interacting beams physically separate.

$$\rho = \tan^{-1}\left(\frac{n_o^2}{n_z^2}\tan\theta\right) - \theta$$

θ is the phase-matching angle.

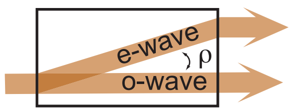

Finding **uniaxial e- and o-waves**:

- Draw Z axis (optic axis, OA),
- Draw laser k vector,
- e-waves are polarized in the plane of OA/k-vector,
- o-waves are polarized perpendicular to this plane.

Finding **biaxial e- and o-waves**:

In the principal planes of a biaxial crystal, e-waves are polarized in the principal plane, and o-waves are polarized perpendicular to this plane.

DFG and SFG Phase Matching for Uniaxial Crystals

The table uses the notation: $n_{o1} = n_o(\lambda_1)$, $n_{o2} = n_o(\lambda_2)$, etc.; $n_{z1} = n_z(\lambda_1)$, $n_{z2} = n_z(\lambda_2)$, etc. θ is the phase-matching angle (between k and OA in figure). Only two input wavelengths are required—the third is obtained from $1/\lambda_1 = 1/\lambda_2 + 1/\lambda_3$, where $\lambda_1 < \lambda_2 \leq \lambda_3$. The notation for e and o polarizations in this guide assumes a wavelength ordering from low to high, going left to right:

$e \leftrightarrow o + o$ (negative uniaxial)

$$\tan^2\theta = \frac{\dfrac{\lambda_1^2}{n_{o1}^2}\left(\dfrac{n_{o2}}{\lambda_2} + \dfrac{n_{o3}}{\lambda_3}\right)^2 - 1}{1 - \dfrac{\lambda_1^2}{n_{z1}^2}\left(\dfrac{n_{o2}}{\lambda_2} + \dfrac{n_{o3}}{\lambda_3}\right)^2}$$

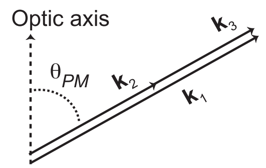

$o \leftrightarrow o + e$ (positive uniaxial)

$$\tan^2\theta = \frac{\dfrac{\lambda_3^2}{n_{o3}^2}\left(\dfrac{n_{o1}}{\lambda_1} - \dfrac{n_{o2}}{\lambda_2}\right)^2 - 1}{1 - \dfrac{\lambda_3^2}{n_{z3}^2}\left(\dfrac{n_{o1}}{\lambda_1} - \dfrac{n_{o2}}{\lambda_2}\right)^2}$$

$o \leftrightarrow e + o$ (positive uniaxial)

$$\tan^2\theta = \frac{\dfrac{\lambda_2^2}{n_{o2}^2}\left(\dfrac{n_{o1}}{\lambda_1} - \dfrac{n_{o3}}{\lambda_3}\right)^2 - 1}{1 - \dfrac{\lambda_2^2}{n_{z2}^2}\left(\dfrac{n_{o1}}{\lambda_1} - \dfrac{n_{o3}}{\lambda_3}\right)^2}$$

$o \leftrightarrow e + e$ (positive uniaxial)†

$$\frac{n_{o1}}{\lambda_1} = \frac{n_{o2}}{\lambda_2\sqrt{1 - \left(1 - \dfrac{n_{o2}^2}{n_{z2}^2}\right)\sin^2\theta}} + \frac{n_{o3}}{\lambda_3\sqrt{1 - \left(1 - \dfrac{n_{o3}^2}{n_{z3}^2}\right)\sin^2\theta}}$$

$e \leftrightarrow o + e$ (negative uniaxial)†

$$\frac{n_{o1}}{\lambda_1\sqrt{1 - \left(1 - \dfrac{n_{o1}^2}{n_{z1}^2}\right)\sin^2\theta}} = \frac{n_{o2}}{\lambda_2} + \frac{n_{o3}}{\lambda_3\sqrt{1 - \left(1 - \dfrac{n_{o3}^2}{n_{z3}^2}\right)\sin^2\theta}}$$

$e \leftrightarrow e + o$ (negative uniaxial)†

$$\frac{n_{o1}}{\lambda_1\sqrt{1 - \left(1 - \dfrac{n_{o1}^2}{n_{z1}^2}\right)\sin^2\theta}} = \frac{n_{o2}}{\lambda_2\sqrt{1 - \left(1 - \dfrac{n_{o2}^2}{n_{z2}^2}\right)\sin^2\theta}} + \frac{n_{o3}}{\lambda_3}$$

†Solved graphically or by using a root-finding algorithm.

SHG Phase Matching for Uniaxial Crystals

Phase-matching expressions for **SHG** simplify due to the relationship between the SHG and fundamental wavelengths: $\lambda_{SHG} = \lambda_F/2$.

Further simplification occurs for SHG Type-I interactions, which reduce to $n_e(\theta,\lambda_{SHG}) = n_o(\lambda_F)$ for $o + o \to e$ and $n_o(\lambda_{SHG}) = n_e(\theta,\lambda_F)$ for $e + e \to o$.

The phase-matching equations for SHG given below use the notation: $n_{oF} = n_o(\lambda_F)$, $n_{oSHG} = n_o(\lambda_{SHG})$, etc. θ is the phase-matching angle (angle between k and the OA).

$e \to o + o$ **(negative uniaxial)**	$o \to e + e$ **(positive uniaxial)**
$\tan^2\theta = \dfrac{n_{zSHG}^2(n_{oF}^2 - n_{oSHG}^2)}{n_{oSHG}^2(n_{zSHG}^2 - n_{oF}^2)}$	$\tan^2\theta = \dfrac{n_{zF}^2(n_{oSHG}^2 - n_{oF}^2)}{n_{oF}^2(n_{zF}^2 - n_{oSHG}^2)}$
$o \to o + e$ **(positive uniaxial)**	
$\tan^2\theta = \dfrac{n_{zF}^2[(2n_{oSHG} - n_{oF})^2 - n_{oF}^2]}{n_{oF}^2[n_{zF}^2 - (2n_{oSHG} - n_{oF})^2]}$	
$e \to o + e$ **(negative uniaxial)**†	
$2n_{oSHG}\sqrt{\dfrac{1+\tan^2\theta}{1+\dfrac{n_{oSHG}^2}{n_{ZSHG}^2}\tan^2\theta}} = n_{oF} + n_{oF}\sqrt{\dfrac{1+\tan^2\theta}{1+\dfrac{n_{oF}^2}{n_{ZF}^2}\tan^2\theta}}$	

†Solved graphically or by using a root-finding algorithm.

Doubling 532 nm to 266 nm in β-BaB_2O_4 (BBO):

We apply the appropriate formulae from the table above (negative uniaxial) and use the Sellmeier equations for BBO to find $\theta = 47.6$ deg for $o + o \to e$.

We plot the function for the $o + e \to e$ interaction:

$$f(\theta) = 2n_{oSHG}\sqrt{\frac{1+\tan^2\theta}{1+\frac{n_{oSHG}^2}{n_{ZSHG}^2}\tan^2\theta}} - n_{oF}\sqrt{\frac{1+\tan^2\theta}{1+\frac{n_{oF}^2}{n_{ZF}^2}\tan^2\theta}} - n_{oF}$$

The zero of this function corresponds to the phase-matching angle, which, for this example, yields $\theta = 81$ deg. Although both interactions will phase-match, d_{eff} for the $o + o \to e$ interaction is larger.

Biaxial Crystals in the *XY* Plane

For k vectors restricted to propagate in one of the principal planes, a wave polarized in that plane is e polarized, and one perpendicular to the plane is o polarized. The phase-matching angle ϕ is the angle between the k vector and the x axis. (Wavelength and index notation conventions are the same as for uniaxial crystals.) ***XY* plane** $n_X < n_Y < n_Z$:

$e \rightarrow o + o$

$$\tan^2\phi = \frac{\dfrac{\lambda_1^2}{n_{Y1}^2}\left(\dfrac{n_{Z2}}{\lambda_2}+\dfrac{n_{Z3}}{\lambda_3}\right)^2 - 1}{1-\dfrac{\lambda_1^2}{n_{X1}^2}\left(\dfrac{n_{Z2}}{\lambda_2}+\dfrac{n_{Z3}}{\lambda_3}\right)^2}$$

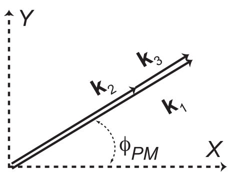

$e \rightarrow o + e$†

$$\frac{n_{Y1}}{\lambda_1\sqrt{1-\left(1-\dfrac{n_{Y1}^2}{n_{X1}^2}\right)\sin^2\phi}} = \frac{n_{Z2}}{\lambda_2} + \frac{n_{Y3}}{\lambda_3\sqrt{1-\left(1-\dfrac{n_{Y3}^2}{n_{X3}^2}\right)\sin^2\phi}}$$

$e \rightarrow e + o$†

$$\frac{n_{Y1}}{\lambda_1\sqrt{1-\left(1-\dfrac{n_{Y1}^2}{n_{X1}^2}\right)\sin^2\phi}} = \frac{n_{Y2}}{\lambda_2\sqrt{1-\left(1-\dfrac{n_{Y2}^2}{n_{X2}^2}\right)\sin^2\phi}} + \frac{n_{Z3}}{\lambda_3}$$

$o \rightarrow e + o$

$$\tan^2\phi = \frac{\dfrac{\lambda_2^2}{n_{Y2}^2}\left(\dfrac{n_{Z1}}{\lambda_1}-\dfrac{n_{Z3}}{\lambda_3}\right)^2 - 1}{1-\dfrac{\lambda_2^2}{n_{X2}^2}\left(\dfrac{n_{Z1}}{\lambda_1}-\dfrac{n_{Z3}}{\lambda_3}\right)^2}$$

$o \rightarrow o + e$

$$\tan^2\phi = \frac{\dfrac{\lambda_3^2}{n_{Y3}^2}\left(\dfrac{n_{Z1}}{\lambda_1}-\dfrac{n_{Z2}}{\lambda_2}\right)^2 - 1}{1-\dfrac{\lambda_3^2}{n_{X3}^2}\left(\dfrac{n_{Z1}}{\lambda_1}-\dfrac{n_{Z2}}{\lambda_2}\right)^2}$$

$o \rightarrow e + e$†

$$\frac{n_{Z1}}{\lambda_1} = \frac{n_{Y2}}{\lambda_2\sqrt{1-\left(1-\dfrac{n_{Y2}^2}{n_{X2}^2}\right)\sin^2\phi}} + \frac{n_{Y3}}{\lambda_3\sqrt{1-\left(1-\dfrac{n_{Y3}^2}{n_{X3}^2}\right)\sin^2\phi}}$$

†Solved graphically or by using a root-finding algorithm.

Biaxial Crystals in the *YZ* Plane

For k vectors restricted to propagate in one of the principal planes, a wave polarized in that plane is e polarized, and one perpendicular to the plane is o polarized. The phase-matching angle θ is defined as the angle between the k vector and the z axis. Polarization and λ conventions are the same as for uniaxial crystals. For SHG, $\lambda_2 = \lambda_3$.

***YZ* plane**, $n_X < n_Y < n_Z$:

$e \rightarrow o + o$

$$\tan^2\theta = \frac{\dfrac{\lambda_1^2}{n_{Y1}^2}\left(\dfrac{n_{X2}}{\lambda_2} + \dfrac{n_{X3}}{\lambda_3}\right)^2 - 1}{1 - \dfrac{\lambda_1^2}{n_{Z1}^2}\left(\dfrac{n_{X2}}{\lambda_2} + \dfrac{n_{X3}}{\lambda_3}\right)^2}$$

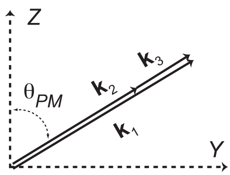

$e \rightarrow o + e$†

$$\frac{n_{Y1}}{\lambda_1\sqrt{1 - \left(1 - \dfrac{n_{Y1}^2}{n_{Z1}^2}\right)\sin^2\theta}} = \frac{n_{X2}}{\lambda_2} + \frac{n_{Y3}}{\lambda_3\sqrt{1 - \left(1 - \dfrac{n_{Y3}^2}{n_{Z3}^2}\right)\sin^2\theta}}$$

$e \rightarrow e + o$†

$$\frac{n_{Y1}}{\lambda_1\sqrt{1 - \left(1 - \dfrac{n_{Y1}^2}{n_{Z1}^2}\right)\sin^2\theta}} = \frac{n_{Y2}}{\lambda_2\sqrt{1 - \left(1 - \dfrac{n_{Y2}^2}{n_{Z2}^2}\right)\sin^2\theta}} + \frac{n_{X3}}{\lambda_3}$$

$o \rightarrow e + o$

$$\tan^2\theta = \frac{\dfrac{\lambda_2^2}{n_{Y2}^2}\left(\dfrac{n_{X1}}{\lambda_1} - \dfrac{n_{X3}}{\lambda_3}\right)^2 - 1}{1 - \dfrac{\lambda_2^2}{n_{Z2}^2}\left(\dfrac{n_{X1}}{\lambda_1} - \dfrac{n_{X3}}{\lambda_3}\right)^2}$$

$o \rightarrow o + e$

$$\tan^2\theta = \frac{\dfrac{\lambda_3^2}{n_{Y3}^2}\left(\dfrac{n_{X1}}{\lambda_1} - \dfrac{n_{X2}}{\lambda_2}\right)^2 - 1}{1 - \dfrac{\lambda_3^2}{n_{Z3}^2}\left(\dfrac{n_{X1}}{\lambda_1} - \dfrac{n_{X2}}{\lambda_2}\right)^2}$$

$o \rightarrow e + e$†

$$\frac{n_{X1}}{\lambda_1} = \frac{n_{Y2}}{\lambda_2\sqrt{1 - \left(1 - \dfrac{n_{Y2}^2}{n_{Z2}^2}\right)\sin^2\theta}} + \frac{n_{Y3}}{\lambda_3\sqrt{1 - \left(1 - \dfrac{n_{Y3}^2}{n_{Z3}^2}\right)\sin^2\theta}}$$

†Solved graphically or by using a root-finding algorithm.

Biaxial Crystals in the *XZ* Plane

A biaxial crystal has two **optic axes** that lie in the *XZ* plane, with an angle V_z with respect to the *Z* axis.

$$\tan V_z = \pm \frac{n_Z}{n_X}\sqrt{\left|\frac{n_X^2 - n_Y^2}{n_Y^2 - n_Z^2}\right|}$$

***XZ* plane**, $\theta < V_Z, \quad n_X < n_Y < n_Z$
or $\quad \theta > V_Z, \quad n_X > n_Y > n_Z$:

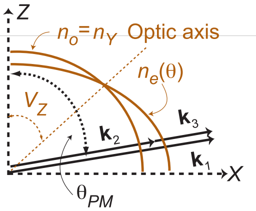

$e \rightarrow o + o$

$$\tan^2\theta = \frac{\dfrac{\lambda_1^2}{n_{X1}^2}\left(\dfrac{n_{Y2}}{\lambda_2}+\dfrac{n_{Y3}}{\lambda_3}\right)^2 - 1}{1-\dfrac{\lambda_1^2}{n_{Z1}^2}\left(\dfrac{n_{Y2}}{\lambda_2}+\dfrac{n_{Y3}}{\lambda_3}\right)^2}$$

$e \rightarrow o + e^{\dagger}$

$$\frac{n_{X1}}{\lambda_1\sqrt{1-\left(1-\dfrac{n_{X1}^2}{n_{Z1}^2}\right)\sin^2\theta}} = \frac{n_{Y2}}{\lambda_2} + \frac{n_{X3}}{\lambda_3\sqrt{1-\left(1-\dfrac{n_{X3}^2}{n_{Z3}^2}\right)\sin^2\theta}}$$

$e \rightarrow e + o^{\dagger}$

$$\frac{n_{X1}}{\lambda_1\sqrt{1-\left(1-\dfrac{n_{X1}^2}{n_{Z1}^2}\right)\sin^2\theta}} = \frac{n_{X2}}{\lambda_2\sqrt{1-\left(1-\dfrac{n_{X2}^2}{n_{Z2}^2}\right)\sin^2\theta}} + \frac{n_{Y3}}{\lambda_3}$$

XZ Plane, $\theta < V_Z, \quad n_X > n_Y > n_Z \quad$ or $\quad \theta > V_Z, \quad n_X < n_Y < n_Z$:

$o \rightarrow e + o$

$$\tan^2\theta = \frac{\dfrac{\lambda_2^2}{n_{X2}^2}\left(\dfrac{n_{Y1}}{\lambda_1}-\dfrac{n_{Y3}}{\lambda_3}\right)^2 - 1}{1-\dfrac{\lambda_2^2}{n_{Z2}^2}\left(\dfrac{n_{Y1}}{\lambda_1}-\dfrac{n_{Y3}}{\lambda_3}\right)^2}$$

$o \rightarrow o + e$

$$\tan^2\theta = \frac{\dfrac{\lambda_3^2}{n_{X3}^2}\left(\dfrac{n_{Y1}}{\lambda_1}-\dfrac{n_{Y2}}{\lambda_2}\right)^2 - 1}{1-\dfrac{\lambda_3^2}{n_{Z3}^2}\left(\dfrac{n_{Y1}}{\lambda_1}-\dfrac{n_{Y2}}{\lambda_2}\right)^2}$$

$o \rightarrow e + e^{\dagger}$

$$\frac{n_{Y1}}{\lambda_1} = \frac{n_{X2}}{\lambda_2\sqrt{1-\left(1-\dfrac{n_{X2}^2}{n_{Z2}^2}\right)\sin^2\theta}} + \frac{n_{X3}}{\lambda_3\sqrt{1-\left(1-\dfrac{n_{X3}^2}{n_{Z3}^2}\right)\sin^2\theta}}$$

† Solved graphically or by using a root-finding algorithm.

Quasi-phase-matching

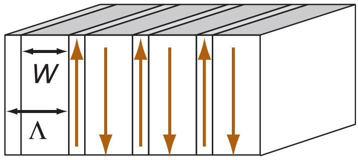

Quasi-phase-matching (QPM) periodically resets the nonlinear polarization to keep the induced polarization and the field it drives in phase. Most QPM realizations are achieved by periodically reorienting a crystal, changing the nonlinearity, as illustrated by the sign of the arrows in the figure above. Such crystals are fabricated using a variety of techniques including stacking and bonding crystal wafers, electric field poling of ferroelectric crystals, and regrowth over a pre-oriented template. In principle, any three-wave process can be quasi-phase-matched, provided the appropriate periodic structure can be engineered into the crystal. The effective nonlinearity for a QPM structure is given by

$$d_{eff} = \frac{2}{m\pi} d_o \sin\left(m\pi \frac{W}{\Lambda} \right)$$

where d_o is the bulk nonlinearity, m is the **QPM order**, Λ is the periodicity, and W is the distance shown in the figure. Quasi-phase-matching is achieved when

$$\Delta k_m = k_1 - k_2 - k_3 - \frac{2\pi}{\Lambda} m = 0$$

In **first-order QPM** ($m = 1$), the nonlinearity is changed every **coherence length** (the distance over which the energy flows from the polarization to the generated field). For **higher-order QPM** ($m \neq 1$), the nonlinearity is flipped after a multiple m of the coherence length. In most cases, the structure is fabricated with $W = \Lambda/2$, resulting in $d_{eff} = 0$ for even-order QPM processes. The phase mismatch of a nonlinear mixing process with Δk is compensated, provided the QPM periodicity is engineered to be

$$\Lambda_m = \frac{2\pi}{\Delta k} m$$

Although higher-order QPM processes have a lower d_{eff}, the periodicity is larger and is simpler to fabricate.

Birefringent versus Quasi-phase-matching

Consider a parametric amplifier for 1.55 μm (λ_S) pumped by a Nd:YAG laser, operating at 1.064 μm (λ_P) in lithium niobate. In the process of amplifying 1.55 μm, another output (λ_I) is generated at the difference frequency, satisfying photon energy conservation:

$$1/\lambda_P = 1/\lambda_S + 1/\lambda_I$$

We solve for $\lambda_I = 3.39$ μm. Note that lithium niobate is transparent well beyond 3.39 μm.

In **birefringent phase matching (BPM)**, lithium niobate is negative uniaxial, therefore we consider $e \rightarrow o + o$, $e \rightarrow o + e$, and $e \rightarrow e + o$ interactions and use the phase-matching formulae to obtain

λ_P 1.064 μm	λ_S 1.550 μm	λ_I 3.39 μm	Phase-matching angle
e	*o*	*o*	46.9 deg
e	*o*	*e*	58.4 deg
e	*e*	*o*	no phase matching

Comparing d_{eff}, the $e \rightarrow o + o$ interaction is favorable:

$$d_{eff,\, e \rightarrow o+o} = d_{15} \sin\theta - d_{22} \cos\theta \sin 3\phi = -4.6 \text{ pm/V}$$
$$d_{eff,\, e \rightarrow o+e} = d_{22} \cos^2\theta \cos 3\phi = 0.58 \text{ pm/V}$$

When looking up d_{15}, use Kleinman symmetry $d_{15} = d_{31}$.

In **quasi-phase-matching (QPM)**, we choose an interaction that couples to the largest nonlinearity of lithium niobate, d_{33} (d_{zzz}). The indices *zzz* correspond to the three fields that couple to this coefficient, so the interaction has all fields pointing in the *z* direction ($e \rightarrow e + e$) with $\hat{\mathbf{k}}$ at 90 deg to the *z* axis.

$$\Delta k = 2\pi[n_z(\lambda_P)/\lambda_P - n_z(\lambda_S)/\lambda_S - n_z(\lambda_I)/\lambda_I] = 0.2042 \text{ μm}^{-1}$$

The first-order QPM periodicity and d_{eff} are

$$\Lambda = \frac{2\pi}{\Delta k} = 30.8 \text{ μm} \quad \text{and} \quad d_{eff} = \frac{2}{\pi} d_{33} = -17 \text{ pm/V}$$

The QPM interaction has a much larger d_{eff} than the BPM interaction has, and it has the advantage of $\hat{\mathbf{k}}$ being 90 deg to the *z* axis so that there is no Poynting vector walk-off.

Noncollinear Phase Matching

Noncollinear SFG ($\omega_1 = \omega_2 + \omega_3$) and DFG ($\omega_3 = \omega_1 - \omega_2$) interactions in a uniaxial crystal are illustrated below. Noncollinear SHG may also be considered as a special case of SFG by letting $\omega_2 = \omega_3$. Phase matching with noncollinear k vectors is called **noncollinear phase matching**, or **vector phase matching**. The two inputs ($\mathbf{k}_2$ and $\mathbf{k}_3$ for SFG; $\mathbf{k}_1$ and $\mathbf{k}_2$ for DFG) to the process have experimentally set angles with respect to the Z axis in an uniaxial crystal, where the difference in angle is called the **noncollinear angle** ψ. For interactions in a principal plane of a biaxial crystal, the angles are referenced to one of the principal axes.

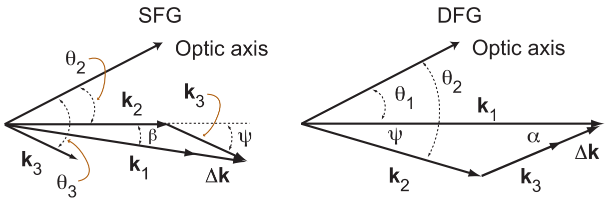

$$\Delta k_{SFG} = \sqrt{k_2^2 + k_3^2 + 2k_2k_3\cos\psi} - k_1$$

$$\Delta k_{DFG} = \sqrt{k_1^2 + k_2^2 - 2k_1k_2\cos\psi} - k_3$$

where $\Delta k = |\Delta\mathbf{k}|$, $k_1 = |\mathbf{k}_1|$, etc.

The magnitude of a given k vector depends on its polarization; that is, $k_o = 2\pi n_o(\lambda)/\lambda$, and $k_e = 2\pi n_e(\lambda,\theta)/\lambda$. For e-waves, we need the angle with respect to the optic axis. This angle is known for the two inputs, but it must be calculated for the SFG or DFG output: for SFG, $\theta_{SFG} = \theta_2 + \beta$, and for DFG, $\theta_{DFG} = \theta_1 - \alpha$. Equations for α and β in terms of input parameters are

$$\tan\beta = \frac{(k_3/k_2)\sin\psi}{1 + (k_3/k_2)\cos\psi} \qquad \tan\alpha = \frac{(k_2/k_1)\sin\psi}{1 - (k_2/k_1)\cos\psi}$$

Substituting the k vector magnitudes into the appropriate Δk expression and solving for the angle where $\Delta k = 0$ yields the phase-matching angle. Finding $\Delta k = 0$ is accomplished graphically or with a zero-finding algorithm.

Tuning Curves

A **tuning curve** plots the changes in phase-matching conditions with different parameter variations. For example, the figure below shows the phase-matching angle versus the signal wavelength in $KTiOPO_4$ (KTP) for a DFG process, while holding the pump wavelength and temperature fixed. The tuning curve is calculated using a phase-matching formula, or by solving for $\Delta k = 0$ using a root-finding algorithm (typically built into a mathematics package). Note that when one curve is calculated, the other may be inferred from energy conservation.

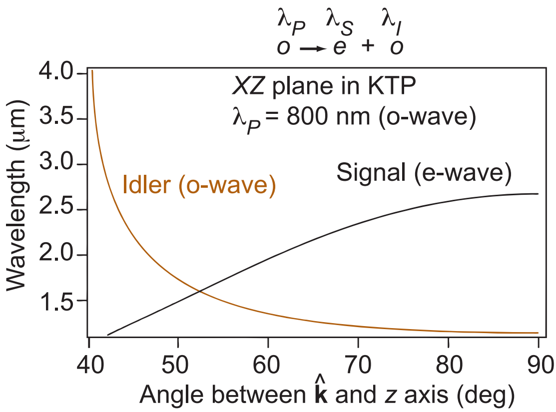

An example of a QPM tuning curve is QPM periodicity versus wavelength. The periodicity is given by $\Lambda = 2\pi/\Delta k$, and for an $e \rightarrow e + e$ interaction:

$$\Delta k = 2\pi\left[\frac{n_Z(\lambda_1,T)}{\lambda_1} - \frac{n_Z(\lambda_2,T)}{\lambda_2} - \frac{n_Z(\lambda_3,T)}{\lambda_3}\right]$$

Δk is calculated using the appropriate Sellmeier equation and wavelengths. From Δk we obtain Λ_{QPM}. The figure at the right illustrates the QPM periodicity for an SHG interaction ($\lambda_2 = \lambda_3 = 2\lambda_1$) in lithium niobate.

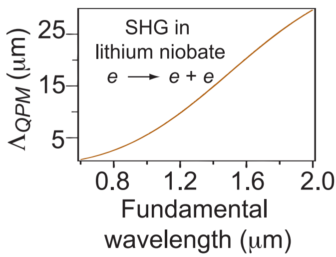

Bandwidths for DFG and SFG

The efficiency of three-wave mixing processes strongly depends on phase matching. In the small signal limit, the output intensity's dependence on phase matching is through the expression $I_{out} \propto \mathrm{sinc}^2(\Delta k L/2)$, where L is the crystal length, $\mathrm{sinc}(x) \equiv \sin(x)/x$, and

$$\Delta k = 2\pi\left[n(\lambda_1,T,\theta)/\lambda_1 - n(\lambda_2,T,\theta)/\lambda_2 - n(\lambda_3,T,\theta)/\lambda_3\right]$$

Bandwidths may be determined by plotting $\mathrm{sinc}^2(\Delta kL/2)$ as a function of the variable of interest, or one may expand Δk in a **Taylor series** to obtain an approximate analytic expression for the **full-width at half-maximum (FWHM)** for frequency, angle, or temperature:

$$\Delta\omega = \pm\frac{0.886\pi}{L|\partial\Delta k/\partial\omega|} \quad \Delta\theta = \pm\frac{0.886\pi}{L|\partial\Delta k/\partial\theta|} \quad \Delta T = \pm\frac{0.886\pi}{L|\partial\Delta k/\partial T|}$$

For biaxial crystals, we assume an interaction in one of the principal planes so that we may use e and o terminology for the interaction type. QPM interaction types ($e \leftrightarrow e + e$ and $o \leftrightarrow o + o$) are included in the tables on pages 43–47.

Three-wave interactions are defined by energy conservation $\hbar\omega_1 = \hbar\omega_2 + \hbar\omega_3$ $(1/\lambda_1 = 1/\lambda_2 + 1/\lambda_3)$, where our convention is $\lambda_1 < \lambda_2 \leq \lambda_3$. For **DFG** and **SFG bandwidth calculations**, we assume that one of the frequencies is held fixed (monochromatic) and energy conservation dictates the relationship between the two other frequencies. The notation for e and o polarizations assumes a wavelength ordering from low to high, going left to right:

$$\begin{array}{ccccc} e & \leftrightarrow & e & + & o \\ \lambda_1 & & \lambda_2 & & \lambda_3 \end{array}$$

Notation for partial derivatives, such as

$$\left.\frac{\partial n_e}{\partial\lambda}\right|_{\lambda_1,\theta_{PM}}$$

should be interpreted as the derivative of n_e as a function of λ about the set point λ_1 at a fixed angle θ_{PM}.

Bandwidth Calculation Aids

The bulk of the work in calculating **bandwidths** involves evaluating the index of refraction and its derivatives from Sellmeier equations. Since the Sellmeier equations are written in terms of n^2, derivatives are usually evaluated with the help of the chain rule for differentiation. For example, a typical Sellmeier equation for a principal index is written as

$$n^2(\lambda) = A + \frac{B}{\lambda^2 - C} + D\lambda^2$$

where A, B, C, and D are constants specific to the crystal. Derivatives of the principal indices are evaluated as

$$\frac{dn^2}{d\lambda} = 2n\frac{dn}{d\lambda}; \quad \text{therefore,} \quad \frac{dn}{d\lambda} = \frac{1}{2n}\frac{dn^2}{d\lambda}$$

For the particular Sellmeier form given above, we obtain an analytic expression:

$$\frac{dn}{d\lambda} = \frac{\lambda}{n}\left[D - \frac{B}{(\lambda^2 - C)^2}\right]$$

Alternatively, one may evaluate the derivative using numerical differentiation.

When evaluating derivatives of the extraordinary index, we use a similar approach. Since $n_e(\theta)$ is written as

$$\frac{1}{n_e^2(\theta)} = \frac{\cos^2\theta}{n_o^2} + \frac{\sin^2\theta}{n_Z^2}$$

derivatives in terms of n_e^{-2} are convenient. For example, $\frac{dn_e^{-2}}{d\theta} = -\frac{2}{n_e^3}\frac{dn_e}{d\theta}$ and hence, $\frac{dn_e}{d\theta} = -\frac{n_e^3}{2}\frac{dn_e^{-2}}{d\theta} = \frac{\sin 2\theta}{2} n_e^3\left(\frac{1}{n_o^2} - \frac{1}{n_Z^2}\right)$ Similarly, other derivatives required for calculating bandwidths are

$$\frac{\partial n_e}{\partial\lambda} = -\frac{n_e^3}{2}\frac{dn_e^{-2}}{d\lambda} = n_e^3\left(\frac{\cos^2\theta}{n_o^3}\frac{\partial n_o}{\partial\lambda} + \frac{\sin^2\theta}{n_Z^3}\frac{\partial n_Z}{\partial\lambda}\right)$$

$$\frac{\partial n_e}{\partial T} = -\frac{n_e^3}{2}\frac{dn_e^{-2}}{dT} = n_e^3\left(\frac{\cos^2\theta}{n_o^3}\frac{\partial n_o}{\partial T} + \frac{\sin^2\theta}{n_Z^3}\frac{\partial n_Z}{\partial T}\right)$$

SFG and DFG Bandwidth Formulae

Temperature bandwidth:

$o \leftrightarrow o + o$ QPM	$\Delta T = \pm \frac{0.443}{L}\left(\frac{1}{\lambda_1}\frac{\partial n_o}{\partial T}\Big\vert_{\lambda_1} - \frac{1}{\lambda_2}\frac{\partial n_o}{\partial T}\Big\vert_{\lambda_2} - \frac{1}{\lambda_3}\frac{\partial n_o}{\partial T}\Big\vert_{\lambda_3}\right)^{-1}$
$o \leftrightarrow o + e$	$\Delta T = \pm \frac{0.443}{L}\left(\frac{1}{\lambda_1}\frac{\partial n_o}{\partial T}\Big\vert_{\lambda_1} - \frac{1}{\lambda_2}\frac{\partial n_o}{\partial T}\Big\vert_{\lambda_2} - \frac{1}{\lambda_3}\frac{\partial n_e}{\partial T}\Big\vert_{\lambda_3,\theta_{PM}}\right)^{-1}$
$o \leftrightarrow e + o$	$\Delta T = \pm \frac{0.443}{L}\left(\frac{1}{\lambda_1}\frac{\partial n_o}{\partial T}\Big\vert_{\lambda_1} - \frac{1}{\lambda_2}\frac{\partial n_e}{\partial T}\Big\vert_{\lambda_2,\theta_{PM}} - \frac{1}{\lambda_3}\frac{\partial n_o}{\partial T}\Big\vert_{\lambda_3}\right)^{-1}$
$o \leftrightarrow e + e$	$\Delta T = \pm \frac{0.443}{L}\left(\frac{1}{\lambda_1}\frac{\partial n_o}{\partial T}\Big\vert_{\lambda_1} - \frac{1}{\lambda_2}\frac{\partial n_e}{\partial T}\Big\vert_{\lambda_2,\theta_{PM}} - \frac{1}{\lambda_3}\frac{\partial n_e}{\partial T}\Big\vert_{\lambda_3,\theta_{PM}}\right)^{-1}$
$e \leftrightarrow o + o$	$\Delta T = \pm \frac{0.443}{L}\left(\frac{1}{\lambda_1}\frac{\partial n_e}{\partial T}\Big\vert_{\lambda_1,\theta_{PM}} - \frac{1}{\lambda_2}\frac{\partial n_o}{\partial T}\Big\vert_{\lambda_2} - \frac{1}{\lambda_3}\frac{\partial n_o}{\partial T}\Big\vert_{\lambda_3}\right)^{-1}$
$e \leftrightarrow o + e$	$\Delta T = \pm \frac{0.443}{L}\left(\frac{1}{\lambda_1}\frac{\partial n_e}{\partial T}\Big\vert_{\lambda_1,\theta_{PM}} - \frac{1}{\lambda_2}\frac{\partial n_o}{\partial T}\Big\vert_{\lambda_2} - \frac{1}{\lambda_3}\frac{\partial n_e}{\partial T}\Big\vert_{\lambda_3,\theta_{PM}}\right)^{-1}$
$e \leftrightarrow e + o$	$\Delta T = \pm \frac{0.443}{L}\left(\frac{1}{\lambda_1}\frac{\partial n_e}{\partial T}\Big\vert_{\lambda_1,\theta_{PM}} - \frac{1}{\lambda_2}\frac{\partial n_e}{\partial T}\Big\vert_{\lambda_2,\theta_{PM}} - \frac{1}{\lambda_3}\frac{\partial n_o}{\partial T}\Big\vert_{\lambda_3}\right)^{-1}$
$e \leftrightarrow e + e$ QPM	$\Delta T = \pm \frac{0.443}{L}\left(\frac{1}{\lambda_1}\frac{\partial n_e}{\partial T}\Big\vert_{\lambda_1,\theta_{PM}} - \frac{1}{\lambda_2}\frac{\partial n_e}{\partial T}\Big\vert_{\lambda_2,\theta_{PM}} - \frac{1}{\lambda_3}\frac{\partial n_e}{\partial T}\Big\vert_{\lambda_3,\theta_{PM}}\right)^{-1}$

where $$\frac{\partial n_e(\lambda,\theta,T)}{\partial T}\Big\vert_{\lambda,\theta} = n_e^3(\lambda,\theta,T)\left(\frac{\cos^2\theta}{n_o^3}\frac{\partial n_o}{\partial T} + \frac{\sin^2\theta}{n_Z^3}\frac{\partial n_Z}{\partial T}\right)$$

Angular acceptance (measured internal to crystal):

$o \leftrightarrow o + e$	$\Delta\theta = \pm \frac{0.443}{L}\left(\frac{1}{\lambda_3}\frac{\partial n_e}{\partial\theta}\Big\vert_{\lambda_3,T}\right)^{-1}$
$o \leftrightarrow e + o$	$\Delta\theta = \pm \frac{0.443}{L}\left(\frac{1}{\lambda_2}\frac{\partial n_e}{\partial\theta}\Big\vert_{\lambda_2,T}\right)^{-1}$
$o \leftrightarrow e + e$	$\Delta\theta = \pm \frac{0.443}{L}\left(\frac{1}{\lambda_2}\frac{\partial n_e}{\partial\theta}\Big\vert_{\lambda_2,T} + \frac{1}{\lambda_3}\frac{\partial n_e}{\partial\theta}\Big\vert_{\lambda_3,T}\right)^{-1}$

SFG and DFG Bandwidth Formulae (cont.)

Angular acceptance (measured internal to crystal):

$e \leftrightarrow o + o$	$\Delta\theta = \pm\frac{0.443}{L}\left(\frac{1}{\lambda_1}\frac{\partial n_e}{\partial\theta}\bigg\vert_{\lambda_1,T}\right)^{-1}$
$e \leftrightarrow e + o$	$\Delta\theta = \pm\frac{0.443}{L}\left(\frac{1}{\lambda_1}\frac{\partial n_e}{\partial\theta}\bigg\vert_{\lambda_1,T} - \frac{1}{\lambda_2}\frac{\partial n_e}{\partial\theta}\bigg\vert_{\lambda_2,T}\right)^{-1}$
$e \leftrightarrow o + e$	$\Delta\theta = \pm\frac{0.443}{L}\left(\frac{1}{\lambda_1}\frac{\partial n_e}{\partial\theta}\bigg\vert_{\lambda_1,T} - \frac{1}{\lambda_3}\frac{\partial n_e}{\partial\theta}\bigg\vert_{\lambda_3,T}\right)^{-1}$
$e \leftrightarrow e + e$ QPM	$\Delta\theta = \pm\frac{0.443}{L}\left(\frac{1}{\lambda_1}\frac{\partial n_e}{\partial\theta}\bigg\vert_{\lambda_1,T} - \frac{1}{\lambda_2}\frac{\partial n_e}{\partial\theta}\bigg\vert_{\lambda_2,T} - \frac{1}{\lambda_3}\frac{\partial n_e}{\partial\theta}\bigg\vert_{\lambda_3,T}\right)^{-1}$

where $\frac{\partial n_e}{\partial\theta}\bigg\vert_{\lambda,T} = \frac{\sin 2\theta}{2} n_e^3(\theta,\lambda,T)\left[\frac{1}{n_o^2(\lambda,T)} - \frac{1}{n_Z^2(\lambda,T)}\right]$

Phase-matching bandwidth (λ_1 monochromatic):

$$\Delta\lambda_3 = \frac{\lambda_3^2}{\lambda_2^2}|\Delta\lambda_2|,\ |\Delta\omega_2| = |\Delta\omega_3| = \frac{2\pi c}{\lambda_2^2}|\Delta\lambda_2|$$

$o \leftrightarrow o + o$ $e \leftrightarrow o + o$	$\Delta\lambda_2 = \pm\frac{0.443}{L}\frac{\lambda_2^2}{\left(n_o\big\vert_{\lambda_2} - \lambda_2\frac{\partial n_o}{\partial\lambda}\big\vert_{\lambda_2} - n_o\big\vert_{\lambda_3} + \lambda_3\frac{\partial n_o}{\partial\lambda}\big\vert_{\lambda_3}\right)}$
$o \leftrightarrow o + e$ $e \leftrightarrow o + e$	$\Delta\lambda_2 = \pm\frac{0.443}{L}\frac{\lambda_2^2}{\left(n_o\big\vert_{\lambda_2} - \lambda_2\frac{\partial n_{o2}}{\partial\lambda_2}\big\vert_{\lambda_2} - n_e\big\vert_{\lambda_3} + \lambda_3\frac{\partial n_e}{\partial\lambda}\big\vert_{\lambda_3}\right)}$
$o \leftrightarrow e + o$ $e \leftrightarrow e + o$	$\Delta\lambda_2 = \pm\frac{0.443}{L}\frac{\lambda_2^2}{\left(n_e\big\vert_{\lambda_2} - \lambda_2\frac{\partial n_{e2}}{\partial\lambda_2}\big\vert_{\lambda_2} - n_o\big\vert_{\lambda_3} + \lambda_3\frac{\partial n_o}{\partial\lambda}\big\vert_{\lambda_3}\right)}$
$o \leftrightarrow e + e$ $e \leftrightarrow e + e$	$\Delta\lambda_2 = \pm\frac{0.443}{L}\frac{\lambda_2^2}{\left(n_e\big\vert_{\lambda_2} - \lambda_2\frac{\partial n_e}{\partial\lambda_2}\big\vert_{\lambda_2} - n_e\big\vert_{\lambda_3} + \lambda_3\frac{\partial n_e}{\partial\lambda}\big\vert_{\lambda_3}\right)}$

SFG and DFG Bandwidth Formulae (cont.)

Phase-matching bandwidth (λ_2 monochromatic):

$$\Delta\lambda_3 = \frac{\lambda_3^2}{\lambda_1^2}|\Delta\lambda_1|, |\Delta\omega_1| = |\Delta\omega_3| = \frac{2\pi c}{\lambda_1^2}|\Delta\lambda_1|$$

$o \leftrightarrow o + o$ $o \leftrightarrow e + o$	$\Delta\lambda_1 = \pm\frac{0.443}{L}\frac{\lambda_1^2}{\left(n_o\Big\vert_{\lambda_1} - \lambda_1\frac{\partial n_o}{\partial\lambda}\Big\vert_{\lambda_1} - n_o\Big\vert_{\lambda_3} + \lambda_3\frac{\partial n_o}{\partial\lambda}\Big\vert_{\lambda_3}\right)}$
$o \leftrightarrow o + e$ $o \leftrightarrow e + e$	$\Delta\lambda_1 = \pm\frac{0.443}{L}\frac{\lambda_1^2}{\left(n_o\Big\vert_{\lambda_1} - \lambda_1\frac{\partial n_o}{\partial\lambda}\Big\vert_{\lambda_1} - n_e\Big\vert_{\lambda_3} + \lambda_3\frac{\partial n_e}{\partial\lambda}\Big\vert_{\lambda_3}\right)}$
$e \leftrightarrow o + o$ $e \leftrightarrow e + o$	$\Delta\lambda_1 = \pm\frac{0.443}{L}\frac{\lambda_1^2}{\left(n_e\Big\vert_{\lambda_1} - \lambda_1\frac{\partial n_e}{\partial\lambda}\Big\vert_{\lambda_1} - n_o\Big\vert_{\lambda_3} + \lambda_3\frac{\partial n_o}{\partial\lambda}\Big\vert_{\lambda_3}\right)}$
$e \leftrightarrow o + e$ $e \leftrightarrow e + e$	$\Delta\lambda_1 = \pm\frac{0.443}{L}\frac{\lambda_1^2}{\left(n_e\Big\vert_{\lambda_1} - \lambda_1\frac{\partial n_e}{\partial\lambda}\Big\vert_{\lambda_1} - n_e\Big\vert_{\lambda_3} + \lambda_3\frac{\partial n_e}{\partial\lambda}\Big\vert_{\lambda_3}\right)}$

where $$\frac{\partial n_e}{\partial\lambda} = n_e^3\left(\frac{\cos^2\theta}{n_o^3}\frac{\partial n_o}{\partial\lambda} + \frac{\sin^2\theta}{n_Z^3}\frac{\partial n_Z}{\partial\lambda}\right)$$

Phase-matching bandwidth may also be written in terms of **group velocity**. For example, the phase-matching bandwidth $\Delta\omega_2$ when ω_1 is monochromatic is

$$\frac{\partial\Delta k}{\partial\omega_2} = -\frac{\partial k_2}{\partial\omega_2} + \frac{\partial k_3}{\partial\omega_3} = v_{g3}^{-1} - v_{g2}^{-1}$$

where v_g^{-1} is the inverse group velocity, which is related to the **group delay** $d\phi/d\omega$. The bandwidth is

$$\Delta\omega_2 = \pm\frac{0.886\pi v_{g2}v_{g3}}{L|v_{g2} - v_{g3}|}$$

> Large bandwidths occur when the group velocities match. A determination of the bandwidth in these cases is made by plotting $\mathrm{sinc}^2(\Delta kL/2)$ versus frequency, or by going to a higher order in the Taylor series expansion for the analytic expression.

SHG Bandwidth Formulae

For **SHG** interactions where the fundamental frequency shifts, the second harmonic must also shift, leading to different expressions for bandwidth than the SFG case where one of the frequencies is assumed to be fixed. For example, the relationship between wavelengths and *e* and *o* polarizations is

$$\begin{matrix} e & + & o & \rightarrow & o \\ \lambda_F & & \lambda_F & & \lambda_{SHG} \end{matrix}$$

where λ_F is the fundamental wavelength. The notation for partial derivatives is the same as with SFG and DFG.

Phase-matching bandwidth:

$o + o \rightarrow e$	$\Delta\lambda_F = \pm\frac{0.443}{L}\lambda_F\left(\frac{\partial n_e}{\partial\lambda}\Big\|_{\lambda_{SHG},\theta_{PM}} - 2\frac{\partial n_o}{\partial\lambda}\Big\|_{\lambda_F}\right)^{-1}$
$e + e \rightarrow o$	$\Delta\lambda_F = \pm\frac{0.443}{L}\lambda_F\left(\frac{\partial n_o}{\partial\lambda}\Big\|_{\lambda_{SHG},\theta_{PM}} - 2\frac{\partial n_e}{\partial\lambda}\Big\|_{\lambda_F}\right)^{-1}$
$o + o \rightarrow o$ *QPM*	$\Delta\lambda_F = \pm\frac{0.443}{L}\lambda_F\left(\frac{\partial n_o}{\partial\lambda}\Big\|_{\lambda_{SHG},\theta_{PM}} - 2\frac{\partial n_o}{\partial\lambda}\Big\|_{\lambda_F}\right)^{-1}$
$e + e \rightarrow e$ *QPM*	$\Delta\lambda_F = \pm\frac{0.443}{L}\lambda_F\left(\frac{\partial n_e}{\partial\lambda}\Big\|_{\lambda_{SHG},\theta_{PM}} - 2\frac{\partial n_e}{\partial\lambda}\Big\|_{\lambda_F}\right)^{-1}$
$o + e \rightarrow e$ $e + o \rightarrow e$	$\Delta\lambda_F = \pm\frac{0.443}{L}\lambda_F\left(\frac{\partial n_e}{\partial\lambda}\Big\|_{\lambda_{SHG},\theta_{PM}} - \frac{\partial n_o}{\partial\lambda}\Big\|_{\lambda_F} - \frac{\partial n_e}{\partial\lambda}\Big\|_{\lambda_F,\theta_{PM}}\right)^{-1}$
$o + e \rightarrow o$ $e + o \rightarrow o$	$\Delta\lambda_F = \pm\frac{0.443}{L}\lambda_F\left(\frac{\partial n_o}{\partial\lambda}\Big\|_{\lambda_{SHG}} - \frac{\partial n_o}{\partial\lambda}\Big\|_{\lambda_F} - \frac{\partial n_e}{\partial\lambda}\Big\|_{\lambda_F,\theta_{PM}}\right)^{-1}$

where $\frac{\partial n_e}{\partial\lambda} = n_e^3\left(\frac{\cos^2\theta}{n_o^3}\frac{\partial n_o}{\partial\lambda} + \frac{\sin^2\theta}{n_Z^3}\frac{\partial n_Z}{\partial\lambda}\right)$

Other bandwidths: $\Delta\lambda_{SHG} = \frac{1}{2}\Delta\lambda_F$; $\Delta\omega_{SHG} = \frac{2\pi c}{\lambda_F^2}\Delta\lambda_F$

SHG Bandwidth Formulae (cont.)

Temperature bandwidth:

$o + o \to e$	$\Delta T = \pm \frac{0.222}{L}\lambda_F \left(\frac{\partial n_e}{\partial T}\Big\vert_{\lambda_{SHG},\theta_{PM}} - \frac{\partial n_o}{\partial T}\Big\vert_{\lambda_F} \right)^{-1}$
$e + e \to o$	$\Delta T = \pm \frac{0.222}{L}\lambda_F \left(\frac{\partial n_o}{\partial T}\Big\vert_{\lambda_{SHG}} - \frac{\partial n_e}{\partial T}\Big\vert_{\lambda_F,\theta_{PM}} \right)^{-1}$
$e + e \to e$ *QPM*	$\Delta T = \pm \frac{0.222}{L}\lambda_F \left(\frac{\partial n_e}{\partial T}\Big\vert_{\lambda_{SHG},\theta_{PM}} - \frac{\partial n_e}{\partial T}\Big\vert_{\lambda_F,\theta_{PM}} \right)^{-1}$
$o + o \to o$ *QPM*	$\Delta T = \pm \frac{0.222}{L}\lambda_F \left(\frac{\partial n_o}{\partial T}\Big\vert_{\lambda_{SHG}} - \frac{\partial n_o}{\partial T}\Big\vert_{\lambda_F} \right)^{-1}$
$o + e \to e$ $e + o \to e$	$\Delta T = \pm \frac{0.443}{L}\lambda_F \left(2\frac{\partial n_e}{\partial T}\Big\vert_{\lambda_{SHG},\theta_{PM}} - \frac{\partial n_o}{\partial T}\Big\vert_{\lambda_F} - \frac{\partial n_e}{\partial T}\Big\vert_{\lambda_F,\theta_{PM}} \right)^{-1}$
$o + e \to o$ $e + o \to o$	$\Delta T = \pm \frac{0.443}{L}\lambda_F \left(2\frac{\partial n_o}{\partial T}\Big\vert_{\lambda_{SHG}} - \frac{\partial n_o}{\partial T}\Big\vert_{\lambda_F} - \frac{\partial n_e}{\partial T}\Big\vert_{\lambda_F,\theta_{PM}} \right)^{-1}$

where $\frac{\partial n_e(\lambda,\theta,T)}{\partial T}\Big\vert_{\lambda,\theta} = n_e^3(\lambda,\theta,T)\left(\frac{\cos^2\theta}{n_o^3}\frac{\partial n_o}{\partial T} + \frac{\sin^2\theta}{n_Z^3}\frac{\partial n_Z}{\partial T} \right)$

Angular acceptance (internal to the crystal):

$o + o \to e$	$\Delta\theta = \pm \frac{0.222}{L}\lambda_F \left(\frac{\partial n_e}{\partial \theta}\Big\vert_{\lambda_{SHG},\theta_{PM}} \right)^{-1}$
$e + e \to o$	$\Delta\theta = \pm \frac{0.222}{L}\lambda_F \left(\frac{\partial n_e}{\partial \theta}\Big\vert_{\lambda_F,\theta_{PM}} \right)^{-1}$
$e + e \to e$ QPM	$\Delta\theta = \pm \frac{0.222}{L}\lambda_F \left(\frac{\partial n_e}{\partial \theta}\Big\vert_{\lambda_{SHG},\theta_{PM}} - \frac{\partial n_e}{\partial \theta}\Big\vert_{\lambda_F,\theta_{PM}} \right)^{-1}$
$o + e \to e$ $e + o \to e$	$\Delta\theta = \pm \frac{0.443}{L}\lambda_F \left(2\frac{\partial n_e}{\partial \theta}\Big\vert_{\lambda_{SHG},\theta_{PM}} - \frac{\partial n_e}{\partial \theta}\Big\vert_{\lambda_F,\theta_{PM}} \right)^{-1}$
$o + e \to o$ $e + o \to o$	$\Delta\theta = \pm \frac{0.443}{L}\lambda_F \left(\frac{\partial n_e}{\partial \theta}\Big\vert_{\lambda_F,\theta_{PM}} \right)^{-1}$

where $\frac{\partial n_e(\theta,\lambda,T)}{\partial \theta} = \frac{\sin 2\theta}{2} n_e^3(\theta,\lambda,T)\left[\frac{1}{n_o^2(\lambda,T)} - \frac{1}{n_Z^2(\lambda,T)} \right]$

Graphical Approach for Bandwidths

Bandwidths may be obtained by plotting sinc^2 $(\Delta kL/2)$ as a function of a particular parameter while holding all of the others constant. Δk is given by

$$\Delta k = 2\pi\left[\frac{n(\lambda_1,T,\theta,\hat{\mathbf{p}})}{\lambda_1} - \frac{n(\lambda_2,T,\theta,\hat{\mathbf{p}})}{\lambda_2} - \frac{n(\lambda_3,T,\theta,\hat{\mathbf{p}})}{\lambda_3}\right]$$

where $\hat{\mathbf{p}}$ is the polarization type e or o.

For o-waves

$$n(\lambda,T,\theta) = n_o(\lambda,T)$$

and for e-waves in a uniaxial crystal

$$\frac{1}{n_e^2(\theta,\lambda,T)} = \frac{\cos^2\theta}{n_o^2(\lambda,T)} + \frac{\sin^2\theta}{n_z^2(\lambda,T)}$$

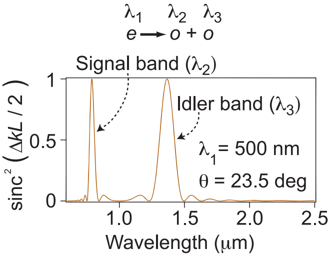

A plot of sinc$^2(\Delta kL/2)$ is made for a given crystal using the Sellmeier equations along with the wavelengths, angles, and temperatures involved.

To visualize bandwidth with an intensity image, make a 2D plot where each point is assigned the value of sinc$^2(\Delta kL/2)$ as a function of two parameters, while holding all of the other parameters fixed. A horizontal or vertical slice gives a bandwidth curve. Below is the same BBO example as above.

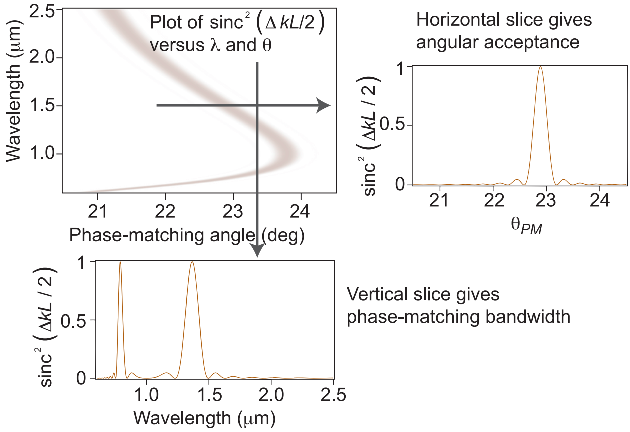

Noncollinear Bandwidth

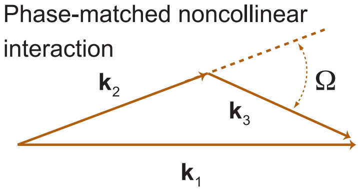

Bandwidths for noncollinearly phase-matched DFG interactions are found by plotting

$$\mathrm{sinc}^2\left(\frac{L}{2}\Delta\mathbf{k}\cdot\hat{\mathbf{k}}_3\right)$$

versus a parameter of interest, where $\hat{\mathbf{k}}_3$ is a unit vector in the direction of the generated DFG beam. The DFG interaction is defined by $\omega_1 = \omega_2 + \omega_3$. For a monochromatic pump at ω_1, an approximate expression for the DFG **phase-matching bandwidth** is

$$\Delta\omega_2 = \pm\frac{0.886\pi v_{g2}v_{g3}}{L(v_{g2} - v_{g3}\cos\Omega)}$$

where v_{g2} and v_{g3} are the group velocity at ω_2 and ω_3, respectively, and Ω is the angle between $\mathbf{k}_3$ and $\mathbf{k}_2$.

Large bandwidth occurs when the components of the group velocities match in the v_{g2} direction. Note that the k-vector direction and group-velocity directions may not be collinear due to Poynting vector walk-off.

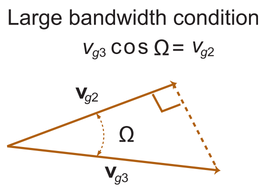

Also note that satisfying $\Delta\mathbf{k} = 0$ does not simultaneously guarantee group velocity matching. Only for special conditions will both conditions be satisfied.

Noncollinear SFG bandwidths are obtained by plotting $\mathrm{sinc}^2\left(\frac{L}{2}\Delta\mathbf{k}\cdot\hat{\mathbf{k}}_1\right)$ versus a parameter of interest, where $\hat{\mathbf{k}}_1$ is a unit vector in the direction of the SFG beam.

$\chi^{(2)}$ Waveguide Interactions

The electric field for a **mode** *m* of a **waveguide** is written as

$$\mathbf{E}_m = \frac{1}{2}A_m(z)f_m(x,y)e^{i(\beta_m z - \omega t)}\hat{\mathbf{e}} + c.c.$$

where A_m is the mode field amplitude, f_m is the transverse **normalized mode profile**, and β is longitudinal component of the *k* vector. Propagation of the mode is in the *z* direction. Normalization of the modes are such that $|A_m|^2$ gives the power in the mode and

$$\frac{\beta}{2\mu_0\omega}\int |f(x,y)|^2 dxdy = 1$$

For nonlinear calculations, the waveguide modes are determined using the linear properties of the waveguide. For many structures, such as slab and rectangular waveguides, these properties and modes are well known.

For **TE waves**, **E** is transverse to *z*, and for **TM waves** we assume, for nonlinear calculations, that the longitudinal component of the electric field is small. For a three-wave interaction defined by $\omega_1 = \omega_2 + \omega_3$, the coupled amplitude equations for lossless media are

$$\frac{dA_1}{dz} = i\kappa_1 A_2 A_3 e^{-i\Delta\beta z}, \quad \kappa_1 = \frac{\varepsilon_0\omega_1}{2}\iint f_1^* f_2 f_3\, d_{eff}\, dxdy$$

$$\frac{dA_2}{dz} = i\kappa_2 A_1 A_3^* e^{i\Delta\beta z}, \quad \kappa_2 = \frac{\varepsilon_0\omega_2}{2}\iint f_1 f_2^* f_3^*\, d_{eff}\, dxdy$$

$$\frac{dA_3}{dz} = i\kappa_3 A_1 A_2^* e^{i\Delta\beta z}, \quad \kappa_3 = \frac{\varepsilon_0\omega_3}{2}\iint f_1 f_2^* f_3^*\, d_{eff}\, dxdy$$

where κ_1, κ_2, and κ_3 are **overlap integrals** of the field modes with each other and with $d_{eff}(x,y)$, and $\Delta\beta = \beta_1 - \beta_2 - \beta_3 - 2\pi/\Lambda$ for a QPM interaction (one may omit the $2\pi/\Lambda$ if no QPM structure is present). The coupled amplitude equations for SHG are

$$\frac{dA_F}{dz} = i\kappa_F A_F^2 e^{i\Delta\beta z}, \quad \kappa_F = \frac{\varepsilon_0\omega_F}{2}\iint (f_F^*)^2 f_{SHG} d_{eff}\, dxdy$$

$$\frac{dA_{SHG}}{dz} = i\kappa_{SHG} A_F^2 e^{-i\Delta\beta z}, \quad \kappa_{SHG} = \frac{\varepsilon_0\omega_{SHG}}{4}\iint f_F^2 f_{SHG}^* d_{eff}\, dxdy$$

where $\Delta\beta = \beta_{SHG} - 2\beta_F - 2\pi/\Lambda$ for a QPM interaction.

$\chi^{(2)}$ Waveguide Devices

In the small-signal regime, expressions for SFG, DFG, and OPA for a lossless **waveguide** of length L are

$$P_{SFG} = P_1(L) = P_{20} P_{30} \kappa_1^2 L^2 \operatorname{sinc}^2\left[L\sqrt{(\lambda_1/\lambda_3)\kappa_1^2 P_{20} + \Delta\beta^2/4}\right]$$

$$P_{DFG} = P_3(L) = P_{10} P_{20} \kappa_3^2 L^2 \left|\frac{\sinh\left[L\sqrt{\lambda_3/\lambda_2|\kappa_3|^2 P_{10} - \Delta\beta^2/4}\right]}{\sqrt{\lambda_3/\lambda_2|\kappa_3|^2 P_{10} - \Delta\beta^2/4}}\right|^2$$

$$P_2(L) = P_{20} + \frac{\lambda_3}{\lambda_2} P_{DFG}$$

where P_{10}, P_{20}, and P_{30} are the input powers at λ_1, λ_2, and λ_3, respectively, $\omega_1 = \omega_2 + \omega_3$ ($1/\lambda_1 = 1/\lambda_2 + 1/\lambda_3$), and all λ's are vacuum wavelengths.

In the case of high conversion efficiency, and for $\Delta\beta = 0$

$$P_{SFG}(L) = \frac{\lambda_2}{\lambda_1} P_{20} \operatorname{sn}^2\left(\kappa_1 L\sqrt{\frac{\lambda_1}{\lambda_2} P_{30}}; \gamma\right), \ \gamma = \sqrt{\frac{P_{20}\lambda_2}{P_{30}\lambda_3}}$$

$$P_{DFG}(L) = -\frac{\lambda_2}{\lambda_3} P_{30} \operatorname{sn}^2\left(i\kappa_1 L\sqrt{\frac{\lambda_3}{\lambda_2} P_{10}}; \gamma\right), \ \gamma = i\sqrt{\frac{P_{20}\lambda_2}{P_{10}\lambda_1}}$$

$$P_2(L) = P_{20} + \frac{\lambda_3}{\lambda_2} P_{DFG}$$

where sn is a Jacobian elliptic function.

SHG power in the small signal regime is given by

$$P_{SHG} = \kappa_{SHG} \mathrm{P}_{F0}^2 L^2 \operatorname{sinc}^2(\Delta\beta L/2)$$

In the depleted pump regime, with $\Delta\beta = 0$,

$$P_{SHG} = P_{F0} \tanh^2(\kappa_{SHG} L\sqrt{P_{F0}})$$

A singly resonant OPO, with low losses for the pump and idler, has a threshold given by

$$P_{TH} = \frac{1}{\kappa_I \kappa_S L}[\alpha - \ln(R_L R_R)]$$

where R_L and R_R are the left- and right-end facet reflectivities, and α is the waveguide loss for the signal wavelength. Note that $\kappa_S = \kappa_2$ and $\kappa_I = \kappa_3$.

Waveguide Phase Matching

The phase-matching condition in a **waveguide** for a process defined by $\omega_1 = \omega_2 + \omega_3$ is

$$\Delta\beta = \beta_1 - \beta_2 - \beta_3 \quad \text{or} \quad \Delta\beta = \beta_1 - \beta_2 - \beta_3 - 2\pi/\Lambda$$

where β is the longitudinal component of the k vector in the waveguide, dependent on the TE or TM polarization. The second expression is appropriate for QPM interactions with a periodicity of Λ. A phase-matched interaction occurs for $\Delta\beta = 0$. We note that $\Delta k = 0$ in a bulk media does not correspond to $\Delta\beta = 0$ due to the differences between bulk and waveguide dispersion. β is sometimes written in terms of a mode index N as

$$\beta = 2\pi N/\lambda_{vacuum}$$

β is calculated from the linear properties of the waveguide. A general expression for β does not exist, as it depends on the specific geometry of the waveguide and on the specific indices of refraction. A large number of approaches to finding β for arbitrary structures are available in waveguide literature. A special case is a planar waveguide with indices as shown in the figure at the right. For this structure, it is possible to obtain the following transcendental equations for β:

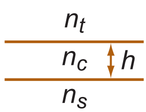

TE	TM
$\tan(h\kappa_c) = \dfrac{\gamma_s + \gamma_t}{\kappa_c\left(1 - \dfrac{\gamma_t\gamma_s}{\kappa_c^2}\right)}$	$\tan(h\kappa_c) = \dfrac{\kappa_c\left(\dfrac{n_c^2}{n_s^2}\gamma_s + \dfrac{n_c^2}{n_t^2}\gamma_t\right)}{\kappa_c^2 - \dfrac{n_c^4}{n_t^2 n_s^2}\gamma_t\gamma_s}$

where

$$\gamma_s = \sqrt{\beta^2 - k_o^2 n_s^2}, \quad \gamma_t = \sqrt{\beta^2 - k_o^2 n_t^2}, \quad \kappa_c = \sqrt{k_o^2 n_s^2 - \beta^2}, \quad k_o = 2\pi/\lambda_{vacuum}$$

and where k_o is the longitudinal k-vector magnitude. The solution β is found using numerical or graphical techniques.

Cerenkov phase matching is possible for SHG interactions when the mode index of the core at ω is less than that for the normal index in the cladding at 2ω. When this condition is satisfied, SHG is phase matched for an emitted angle given by $\cos\theta = N_\omega/n_{2\omega}$.

Four-Wave Mixing

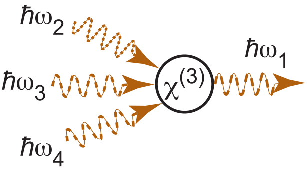

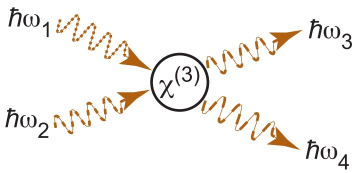

Four-wave mixing is a third-order nonlinear process that generally mixes four frequencies. When all four frequencies are distinct, the types of processes are described by $\hbar\omega_1 = \hbar\omega_2 + \hbar\omega_3 + \hbar\omega_4$, $\hbar\omega_1 + \hbar\omega_2 = \hbar\omega_3 + \hbar\omega_4$, or a rearrangement of one of these expressions. When ω_2, ω_3, and ω_4 are incident on a medium, the nonlinear polarization is given by

$$P_i^{(3)} = \frac{\varepsilon_0}{4}\sum_{j,k,\ell} D\chi^{(3)}_{ijk\ell}(\pm\omega_2 \pm\omega_3 \pm\omega_4; \omega_2, \pm\omega_3, \pm\omega_4) \times A_j(\pm\omega_2)A_k(\pm\omega_3)A_\ell(\pm\omega_4)e^{i(k_2+k_3+k_4)z}$$

where D is a multiplicity factor given in the table. The $\pm$ allows for sum- and difference-frequency combinations. Note that $A^*(\omega) = A(-\omega)$.

$$D = \begin{cases} 1 & \text{All fields same} \\ 3 & \text{Two fields same} \\ 6 & \text{All fields distinct} \end{cases}$$

When three of the inputs remain essentially constant throughout the interaction, one may use the following to determine the generated field:

$$2ik_{out}\frac{dA_{out}}{dz}e^{ik_{out}z} = -\mu_0\omega^2 P^{(3)}$$

where A_{out} and k_{out} are the amplitude and k vector magnitude of the generated wave, respectively. $P^{(3)}$ is found from the equation above. For example, a sum-frequency process defined by $\omega_1 = \omega_2 + \omega_3 + \omega_4$, and where $\chi^{(3)}$ has no dispersion, has a nonlinear polarization at ω_1:

$$P^{(3)}(\omega_1) = \frac{\varepsilon_o\chi^{(3)}}{4}\left[\begin{array}{l}(3|A_1|^2 + 6|A_2|^2 + 6|A_3|^2 + 6|A_4|^2)A_1e^{ik_1z} \\ +6A_2A_3A_4e^{i(k_2+k_3+k_4)z}\end{array}\right]$$

where all contributions such as $\omega_1=\omega_2-\omega_2+\omega_1$ are included in the expression for $P^{(3)}(\omega_1)$. The numerical factors inside the brackets give D for each contribution to $P^{(3)}(\omega_1)$.

Degenerate Four-Wave Mixing

A four-wave mixing process, defined by the energy conservation statement $\hbar\omega_{P1} + \hbar\omega_{P2} = \hbar\omega_S + \hbar\omega_{Pr}$, is called **degenerate four-wave mixing** when all four frequencies in the process are the same. This process can be envisioned as two pump beams $P1$ and $P2$, and a probe beam Pr, incident on a medium, all at frequency ω. A nonlinear polarization is induced at ω by these inputs:

$$P^{(3)}(\omega = \omega + \omega - \omega) = \frac{3\varepsilon_0\chi^{(3)}}{2} A_{P1}A_{P2}A^*_{Pr}e^{i(\mathbf{k}_{P1}+\mathbf{k}_{P2}-\mathbf{k}_{Pr})\cdot\mathbf{r}}$$

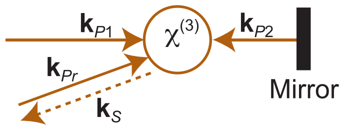

When the two pump beams counter-propagate along a given direction, the nonlinear polarization wave counter-propagates with respect to the probe beam. Hence, the generated signal counter-propagates with respect to the probe, as shown above. Also shown above is a method of generating counter-propagating pumps by retroreflecting the incident pump. Furthermore, phase matching, given by $\Delta\mathbf{k} = \mathbf{k}_{P1} + \mathbf{k}_{P2} - \mathbf{k}_{Pr} - \mathbf{k}_S = 0$, is automatically satisfied. When the pumps are undepleted, the output signal field is

$$A_S = -iA^*_{Pr}(0)\tan(\eta - L)$$

where $A_{Pr}(0)$ is the probe field's complex amplitude at the input to the $\chi^{(3)}$ medium, L is the medium length, and $\eta = 3\omega\chi^{(3)}\sqrt{I_{P1}I_{P2}}/(2\varepsilon_0 n^2 c^2)$. Because the signal counter-propagates with respect to the probe and has an amplitude that is proportional to the conjugated probe field, it is called a **phase-conjugate mirror (PCM)**. One application of an idealized PCM is image restoration, as shown in the figure below.

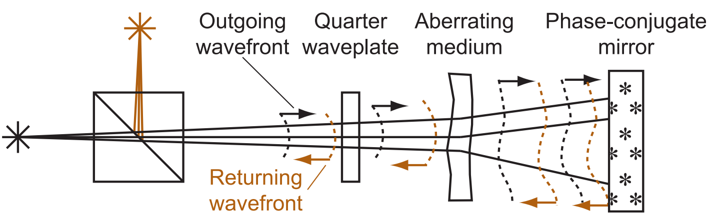

Third-Harmonic Generation

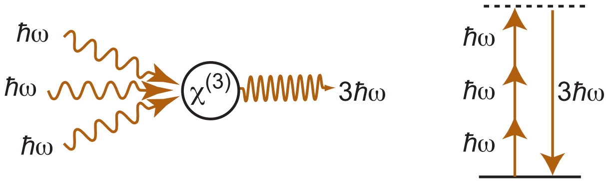

Third-harmonic generation (THG) is a $\chi^{(3)}$ process where three incident photons at ω_F are destroyed while a photon at $\omega_{THG} = 3\omega_F$ is created and is defined by the energy conservation statement $\hbar\omega_{THG} = \hbar\omega_F + \hbar\omega_F + \hbar\omega_F$. Equivalently, the third-harmonic-output wavelength is $\lambda_F/3$. For Gaussian beams, the THG output is

$$P_{THG} = \frac{3\omega_F^2}{4\pi^2\varepsilon_0^2 c^4 n_{THG} n_F^3 w_{oF}^4} (\chi^{(3)})^2 P_F^3 |J|^2$$

where P_F and w_{oF} are the power and beam waist ($1/e$ field radius) of the fundamental beam at ω, respectively.

$$|J|^2 = L^2 \text{sinc}^2(\Delta kL/2) \quad \text{loose focusing } (L \gg z_R)$$

$$|J|^2 = \begin{cases} 0 & \Delta k \leq 0 \\ (\pi b^2 \Delta k e^{-b\Delta k/2})/2 & \Delta k > 0 \end{cases} \quad \text{tight focusing } (L \ll z_R)$$

where $\Delta k = k_{THG} - k_F$ and $b = 2z_R$. In the tightly focusing case, $\Delta k = 0$ leads to a null output. This case is attributable to the π phase shift when going through a focus, known as the **Guoy phase shift**.

In most cases, frequency converting a laser to the third harmonic is accomplished in a two-stage cascaded $\chi^{(2)}$ process. The first stage is SHG, and its output is mixed with the fundamental in a second SFG stage, resulting in a third-harmonic output. This approach is much more efficient than using the $\chi^{(3)}$ approach.

THG has an I_F^3 dependence that, when coupled with a tight focus, leads to a 3D localization of the THG signal. This localization has important applications in microscopy.

$\chi^{(3)}$ Parametric Amplifier

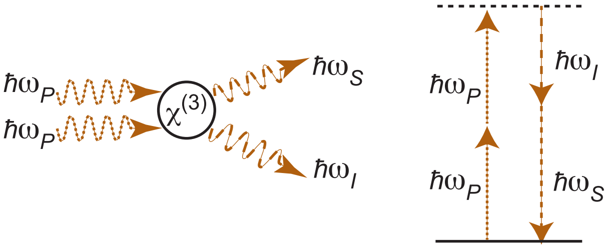

In a **parametric amplifier**, the energy from two incident pump photons (ω_P) goes to a signal (ω_S) and idler (ω_I) photon—that is, $2\omega_P = \omega_S + \omega_I$. Parametric amplifiers may be used to amplify the signal or to generate a new frequency at the idler. Typically, parametric amplification occurs in optical fibers where long interaction lengths can compensate for the low parametric gain. For a plane-wave interaction, the equations governing a parametric amplifier are

$$\frac{dA_P}{dz} = i\frac{3\omega_P\chi^{(3)}}{8nc}\left[\left(|A_P|^2 + 2|A_S|^2 + 2|A_I|^2\right)A_P + 2A_SA_IA_P^*e^{-i\Delta kz}\right]$$

$$\frac{dA_S}{dz} = i\frac{3\omega_S\chi^{(3)}}{8nc}\left[\left(|A_S|^2 + 2|A_I|^2 + 2|A_P|^2\right)A_S + A_P^2A_I^*e^{i\Delta kz}\right]$$

$$\frac{dA_I}{dz} = i\frac{3\omega_I\chi^{(3)}}{8nc}\left[\left(|A_I|^2 + 2|A_S|^2 + 2|A_P|^2\right)A_I + A_P^2A_S^*e^{i\Delta kz}\right]$$

where $\Delta k = 2k_P - k_S - k_I$. When the pump is undepleted (I_P constant), and when $I_I(0) = 0$, $I_S(0) = I_{S0}$, and $I_{S0} \ll I_P$,

$$I_S = \left[1 + \frac{\gamma^2\omega_S\omega_I}{g^2}\sinh^2(gz)\right]I_{S0}, \quad I_I = \frac{\gamma^2\omega_I^2}{g^2}I_{S0}\sinh^2(gz)$$

where

$$g^2 = \gamma^2\omega_S\omega_I - \left(\frac{\kappa}{2}\right)^2, \quad \kappa = \Delta k - 2\gamma\omega_P, \quad \text{and } \gamma = \frac{3\chi^{(3)}}{4\varepsilon_0 n^2c^2}I_P$$

Parametric amplifiers require phase matching that includes a nonlinear phase-shift term that subtracts from Δk. Typically, the signal and idler are close to the pump frequency, and the nonlinear phase term becomes appreciable for a high-peak-power pump laser.

Noncollinear Phase Matching for $\chi^{(3)}$ Processes

$\chi^{(3)}$ phase matching is, in many cases, more flexible than $\chi^{(2)}$ processes, especially when noncollinear processes are considered. For interactions defined by $\hbar\omega_1 + \hbar\omega_2 = \hbar\omega_3 + \hbar\omega_4$, the phase-matching parameter is given by $\mathbf{\Delta k} = \mathbf{k}_1 + \mathbf{k}_2 - \mathbf{k}_3 - \mathbf{k}_4$. For this type of process, it is always possible to find a **noncollinear phase matching geometry** where $\mathbf{\Delta k} = 0$, as shown in the figures below. The price we pay for noncollinear geometries is a reduced interaction length when working with finite-sized beams.

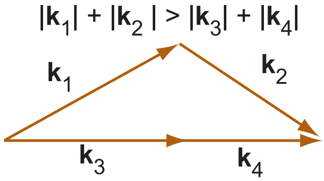

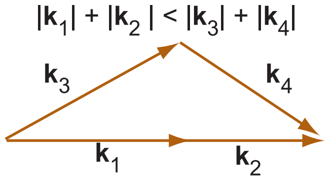

In an isotropic medium, and for a parametric amplifier where $\omega_1 = \omega_2$, we define $\Delta k_{collinear} = 2|\mathbf{k}_P| - |\mathbf{k}_S| - |\mathbf{k}_I|$. When the signal and idler are close to the pump frequency

$$\Delta k_{collinear} \approx \frac{1}{v_g^2}\frac{\partial v_g}{\partial \omega}\Delta\omega^2$$

where v_g is the group velocity of the pump, and $\Delta\omega = \omega_P - \omega_I = \omega_S - \omega_S$. From this expression, we can see that the group velocity dispersion determines the sign of $\Delta k_{collinear}$, and therefore, which noncollinear geometry to use for the parametric amplifier.

Another possible scenario for $\chi^{(3)}$ processes is a **backward geometry**, where one or more of the beams counter-propagates. Shown below is a backward parametric amplifier where the idler counter-propagates with respect to the pump and signal.

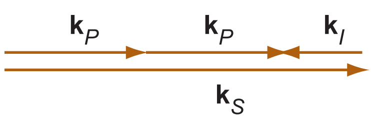

Nonlinear Refractive Index

Material index of refraction is a function of incident field intensity. This is a $\chi^{(3)}$ effect where nonlinear polarization is induced at the same frequency as the incident field. This polarization gives rise to a nonlinear phase shift and hence a change in the index of refraction. The nonlinear polarization for a plane wave propagating in the z direction in an isotropic medium is given by

$$P^{(3)}(\omega) = \frac{3\varepsilon_0}{4}\chi^{(3)}|A(\omega)|^2 A(\omega)e^{ikz}$$

The nonlinear polarization wave has the same spatial wavelength as the input field, and hence, is automatically phase matched. The solution to the wave equation with this nonlinear polarization yields

$$n = n_o + n_2^I I$$

where n_2^I is the **nonlinear index intensity coefficient**. This intensity-dependent index is called the **Kerr effect**. Other conventions for the nonlinear index are used—in particular, ones written in terms of $|A|^2$. One must use each convention consistently because the field amplitude does not have a universal definition (conventions differ by a factor of 2).

The nonlinear index gives rise to **self-focusing**: a beam with a nonuniform intensity will focus or defocus, since regions of high intensity experience a different index than regions of low intensity.

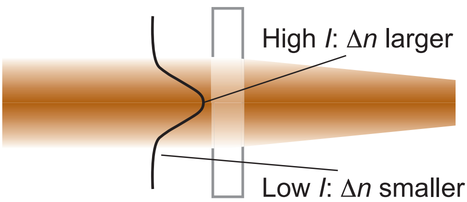

For a Gaussian beam, the effective focal length f induced by a thin slab of material of length L is given by

$$f \approx \frac{n_o w_o^2}{4 n_2^I I_o L}$$

where w_o is the beam radius on the sample, and I_o is the on-axis intensity. Note that the lens may be positive or negative depending on the sign of the nonlinear index.

Nonlinear Absorption

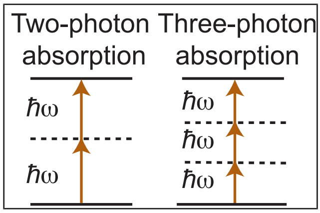

A beam traversing a transparent medium may experience an intensity-dependent **nonlinear absorption (NLA)** due to the simultaneous absorption of two or more photons. In a transparent medium, a single photon does not have sufficient energy to reach an excited state from the ground state. When the energy of the gap is equivalent to that of two photons, **two-photon absorption (TPA)** occurs. Similarly, **multi-photon absorption (MPA)** occurs when the gap and energy are equivalent to more than two photons. Although TPA and MPA are inherently quantum mechanical processes, they may be modeled as a $\chi^{(3)}$ process (TPA) or higher (MPA) when the photon flux is large. Using this model, a nonlinear polarization at the same frequency as the incident laser is induced 90 deg out of phase with the field driving it, leading to attenuation. The differential equations for TPA and **three-photon absorption (3PA)** resulting from this nonlinearity are

$$\text{TPA}: \frac{dI}{dz} = -\alpha I - \beta I^2 \qquad \text{3PA}: \frac{dI}{dz} = -\alpha I - \beta I^3$$

where α is the linear loss, β is the two-photon coefficient, and γ is the three-photon coefficient. β and γ are given by

$$\beta = \frac{3\pi}{\varepsilon_0 n_o^2 c\lambda} \mathrm{Im}\left(\chi^{(3)}\right) \qquad \gamma = \frac{5\pi}{\varepsilon_0^2 n_o^3 c^2 \lambda} \mathrm{Im}\left(\chi^{(5)}\right)$$

The transmission of a temporal Gaussian pulse with a Gaussian cross-section is given by

$$T_{TPA} = \frac{(1-R)^2 e^{-\alpha L}}{\sqrt{\pi} q_o} \int_{-\infty}^{\infty} \ln\left(1 + q_o e^{-x^2}\right) dx \quad q_o = \frac{\beta}{\alpha} I_o (1-R)\left(1 - e^{-\alpha L}\right)$$

$$T_{3PA} = \frac{(1-R)^2 e^{-\alpha L}}{\sqrt{\pi} p_o} \int_{-\infty}^{\infty} \ln\left(p_o e^{-x^2} + \sqrt{1 + p_o^2 e^{-2x^2}}\right) dx$$

$$p_o = (1-R) I_o \sqrt{\frac{\gamma}{\alpha}\left(1 - e^{-2\alpha L}\right)}$$

R is the surface reflection and I_o is the on-axis intensity.

Calculations of Nonlinear Index

To estimate Δn, we consider pulsed laser sources operating with an average power of P and a repetition rate of R. Hence, the average energy-per-pulse is

$$U_{Pulse} = \frac{P_{ave}}{R}$$

We assume that the pulses have a Gaussian envelope of the form $I(r,t) = I_{peak} e^{-2r^2/w_o^2} e^{-t^2/\tau^2}$, so the relationship between the peak intensity I_{peak}, pulse duration τ, and beam radius w_o, is

$$I_{peak} = \frac{2P_{ave}}{\pi\sqrt{\pi} w_o^2 \tau R}$$

1-W average power, w_o = 250 μm, $n_2 = 2.5\times10^{-20}$ m²/W			
Laser type	U_{pulse}	I_{peak}	Δn_{peak}
86-MHz mode-locked Ti:sapphire τ = 100 fsec	11.6 nJ	67 MW/cm²	1.7×10^{-8}
86-MHz mode-locked Nd:YAG τ = 10 psec	11.6 nJ	0.67 MW/cm²	1.7×10^{-10}
1-kHz amplified Ti: sapphire τ = 100 fsec	1 mJ	5.7 TW/cm²	1.4×10^{-3}
10-Hz Nd:YAG τ = 5 nsec	100 mJ	12 GW/cm²	2.9×10^{-6}

Typical values of n_2^I are ~10^{-20} m²/W. For example, n_2^I for fused silica measured at 1.55 μm is $n_2^I = 2.5\times\ 10^{-20}\mathrm{m}^2/\mathrm{W}$. When converting to n_2^I from n_2 in units of m²/V², we use

$$n_2^I(\mathrm{m}^2/\mathrm{W}) = \frac{n_2(\mathrm{m}^2/\mathrm{V}^2)}{n_o\varepsilon_0 c} = 376.6\frac{n_2(\mathrm{m}^2/\mathrm{V}^2)}{n_o}$$

To convert the **nonlinear index** from cgs units to SI units, use the following:

$$n_2(\mathrm{m}^2/\mathrm{V}^2) = \frac{10^8}{c^2} n_2(\mathrm{cm}^2/\mathrm{statV}^2)$$

$$n_2^I(\mathrm{m}^2/\mathrm{W}) = \frac{10^8}{n_o\varepsilon_0 c^3} n_2(\mathrm{cm}^2/\mathrm{statV}) = 4.18\times10^{-7} n_2(\mathrm{cm}^2/\mathrm{statV})$$

Self-Phase Modulation

When a pulse of light passes through a medium, its intensity induces a change in the index of refraction through the nonlinear index $\Delta n = n_2^I I(t)$, where n_2^I is the nonlinear index intensity coefficient. For a slowly varying envelope with a carrier frequency ω_o, the phase of the field traveling through a thin slab Δz is given by $n\omega_o\Delta z/c$. The nonlinear index leads to an intensity-dependent phase shift known as **self-phase modulation (SPM)**:

$$\Delta\phi = n_2^I I \omega_o \Delta z/c$$

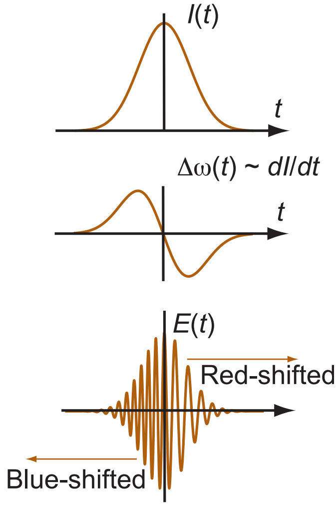

SPM can also be thought of in terms of an instantaneous frequency, $d\phi/dt$:

$$\omega_{inst} = \frac{n_2^I \omega_o}{c} \Delta z \frac{\partial I(t)}{\partial t}$$

For a Gaussian temporal profile given by $I(t) = I_o e^{-2(t/T_o)^2}$, the maximum frequency shift is

$$\omega_{inst,\max} = \frac{2|n_2^I|\omega_o}{cT_o\sqrt{e}} \Delta z I_o$$

Thus, the bandwidth added to the pulse is $\pm\omega_{inst,\max}$. The high intensities and short pulse durations of femtosecond and picosecond lasers make SPM a significant effect for ultrashort pulses traveling through nonlinear media. The accumulated excess bandwidth may be used to further compress ultrashort pulses. As seen in the figure above, the front and back end of the pulse see opposite frequency shifts, with the direction of the shift being dependent on the sign of n_2^I. This phenomena is known as a **frequency chirp**. By using a setup where the optical path lengths for the red- and blue-shifted frequency components are different, it is possible to compress the pulse.

z Scan

***z* scan** is a technique that scans a nonlinear sample in the z direction through the waist of a laser beam, while measuring the on-axis intensity and/or the integrated transmission. In the **closed-aperture *z* scan** shown below, as the sample is translated, the transmission through the pinhole changes as a function of z due to intensity-dependent self-focusing in the sample. An **open-aperture *z* scan** uses the same setup but with the pinhole removed. In this mode, nonlinear absorption leads to a change in the overall transmission as the sample translates through ranges of intensities. These measurements allow for measurement of the real and imaginary parts of $\chi^{(3)}$. Femtosecond lasers are typically used for the experiment because of their enhanced nonlinear signals due to the laser's high intensity.

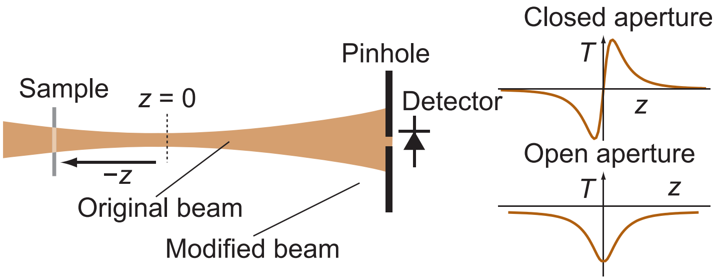

For a thin sample ($L \ll z_R$) with no nonlinear absorption, the closed-aperture transmitted signal is given by

$$T(z,\Delta\Phi_o) \approx 1 - \frac{4\Delta\Phi_o x}{(x^2+9)(x^2+1)}, \quad \Delta\Phi_o = 2\pi n_2^I I_o L_{eff}/\lambda$$

$$L_{eff} = (1 - e^{-\alpha L})/\alpha, \quad x \equiv z/z_R$$

where I_o is the on-axis intensity at $z = 0$, and α is the linear absorption coefficient. When the pinhole is removed, the entire beam power is measured using

$$T(z,\Delta\Phi_o) = \frac{e^{-\alpha L}}{\beta I_o L_{eff}}(1+x^2)\ln\left(1 + \frac{\beta I_o L_{eff}}{1+x^2}\right)$$

where β is the two-photon absorption coefficient. By fitting these functional forms to measured data, it is possible to extract n_2^I and β.

Optical Bistability

The intensity-dependent nonlinear index leads to interesting behavior when these materials are coupled with feedback. **Optical bistability** is one such behavior that enables the system to be in one of two states depending on its past history. An example of a system that can exhibit optical bistability is the Fabry–Pérot etalon with a nonlinear material between the mirrors. A Fabry–Pérot etalon has high transmission when the optical path length is an integer number of half-wavelengths. On resonance, the field amplitude inside the resonator becomes large, thus changing the index and the etalon resonance condition. This nonlinear coupling with feedback leads to the following relationship between incident I_o and transmitted I_{trans} intensities:

$$I_o = \left\{ 1 + \frac{4R}{(1-R)^2} \sin^2 \left[2\pi \left(n_o + \frac{n_2^I I_{trans}}{1-R} \right) \frac{L}{\lambda} \right] \right\} I_{trans}$$

Inverting the equation to write I_{trans} as a function of I_o is not possible; however, it is possible to plot I_o as a function of I_{trans} and then swap axes to achieve the same result. An optical bistable plot of I_{trans}/I_{int} as a function of the fractional change in index is shown below, where I_{int} refers to the intensity internal to the etalon.

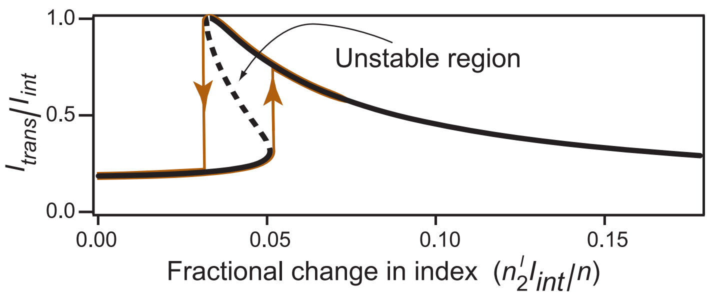

The unstable region in the figure indicates where two output states are possible for the same I_{int}, and the highlighted curve shows the hysteresis curve that the system would follow as the intensity is increased or decreased.

Spontaneous Raman Scattering

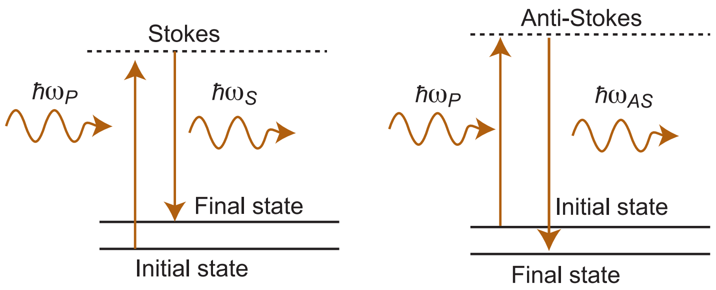

A small portion of light scattered from an object is inelastically scattered. **Spontaneous Raman scattering** is a process where inelastic scattering occurs due to the excitation or de-excitation of the material, such as occurs with a molecular vibrational or rotational mode. A **Stokes shift** occurs when an incident photon loses energy, leaving the medium in an excited state. An **anti-Stokes shift** occurs when the photon gains energy from an excited state of the medium. Spontaneous Raman scattering is characterized by a scattering cross-section through the relationship

$$P_{scatter} = \sigma_R I_o$$

where σ_R is the **Raman scattering cross-section** and I_o is the incident intensity. σ_R may be calculated for single molecules, but is typically determined empirically.

A **Raman spectrum** contains features corresponding to each vibrational or rotational state. Because these states are unique to a given molecule or material, a Raman spectrum can act as a means to identify, or "finger print," constituents in a sample. The key characteristic for identification is the energy difference between incident and scattered photons.

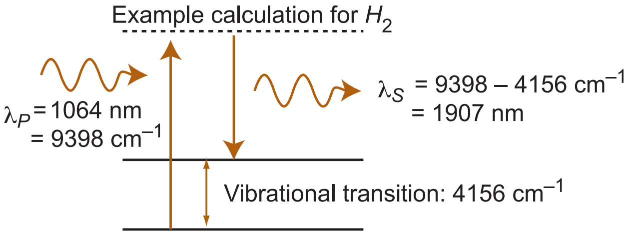

Stimulated Raman Scattering

When two lasers are present at the input of a sample with a frequency separation corresponding to a Raman transition, **stimulated Raman Scattering** occurs. The incident beams drive a Raman excitation that then mixes with the incident fields. Stimulated Raman processes are typically treated as effective $\chi^{(3)}$ interactions. For a plane-wave interaction, when the pump at ω_P and the Stokes at ω_S have a frequency separation given by the Raman transition, the nonlinear polarization at ω_S for the stimulated process is

$$P^{(NL)}(\omega_S) = -i\frac{3}{2}\varepsilon_0\left|\chi_R^{(3)}\right|\left|A_P\right|^2 A_S e^{ik_S z}$$

where A_P and A_S are the complex amplitudes for the pump and Stokes fields, respectively, and $\chi_R^{(3)}$ is the Raman susceptibility. The phasing of the nonlinear polarization leads to amplification of the Stokes field and is the basis for **Raman amplifiers**. Moreover, since the nonlinear polarization has the same k vector as the field it drives, the stimulated Raman scattering process is automatically phase matched. This feature is significant in optical fibers where stimulated Raman scattering can have long interaction lengths. In the undepleted pump approximation

$$I_S(z) = I_S(0)e^{g_R I_P z} \quad \text{where} \quad g_R = \frac{3\omega_S}{n_S n_P \varepsilon_0 c^2}\left|\mathrm{Im}(\chi_R^{(3)})\right|$$

The **Raman gain intensity factor** g_R is often tabulated for a given material. For example, in silica glass (for fiber optics) the peak Raman shift occurs at approximately 400 cm^{-1} with $g \sim 5\times10^{-13}$ W/m. Although this number is small, when coupled with long fiber lengths (on the order of 100 m) and small mode sizes (~3-μm radius), the exponential $e^{gI_P L}$ can be appreciable. When the pump depletes, the following expressions are used:

$$I_S(L) = \frac{(I_{S0}/\omega_S + I_{P0}/\omega_P)I_{S0}e^{C\gamma L}}{I_{P0}/\omega_P + I_{S0}e^{C\gamma L}/\omega_S}, \quad \gamma \equiv \frac{3\omega_S\omega_P}{4n_S n_P \varepsilon_0 c^2}\left|\mathrm{Im}(\chi_R^{(3)})\right|$$

$$I_P(L) = \frac{(I_{S0}/\omega_S + I_{P0}/\omega_P)I_{P0}}{I_{P0}/\omega_P + I_{S0}e^{C\gamma L}/\omega_S}, \quad C = I_P(0)/\omega_P + I_S(0)/\omega_S$$

Anti-Stokes Raman Scattering

Raman-enhanced four-wave mixing, or **coherent anti-Stokes Raman spectroscopy (CARS)**, gives rise to an appreciable **anti-Stokes** signal. A significant advantage of this approach for microscopy is that the anti-Stokes has a higher frequency than the inputs and is spectrally isolated from any fluorescence. The four-wave mixing-phase matching condition is

$$\Delta \mathbf{k} = 2\mathbf{k}_P - \mathbf{k}_{AS} - \mathbf{k}_S$$

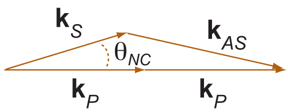

In an isotropic material, collinear phase matching is not possible; however, noncollinear phase matching is. The noncollinear angle is given by

$$\cos\theta_{NC} = \frac{k_{AS}^2 + 4k_P^2 - k_S^2}{4k_P k_S}$$

In gases, the noncollinear angle is small (less than 1 deg) because of low dispersion. In liquids and solids, the angle is on the order of a few degrees.

For a weak interaction, the anti-Stokes signal is given by

$$I_{AS} = \frac{\omega_{AS}^2 \left|\chi_R^{(3)}\right|^2}{16 n_{AS} n_S n_P^2 \varepsilon_0^2 c^4} I_P^2 I_{S0} L^2 \,\mathrm{sinc}^2(\Delta k L/2)$$

Because $\chi_R^{(3)}$ is small, picosecond pulse durations or shorter should be used to obtain an appreciable signal. The noncollinear geometry is chosen so that $\Delta k = 0$, and ω_s is then detuned over a small range to measure properties of $\chi^{(3)}$, such as its magnitude, linewidth, and scattering cross-section. Over this relatively small tuning range, $\Delta k \approx 0$. In a **CARS microscope**, the focal region is less than a coherence length so that a collinear interaction is possible, which makes for efficient signal collection geometry.

Raman Microscopy

A **Raman microscope** uses the large numerical aperture of a microscope to tightly focus the excitation laser, thus localizing and enhancing the Raman signal. It also allows for efficient collection of the scattered signal. Coupled with a microscope, a spectrometer enables species identification by means of spectroscopic line assignments. Typically, the microscope uses a common path for both viewing the sample optically and illuminating the central region with a laser.

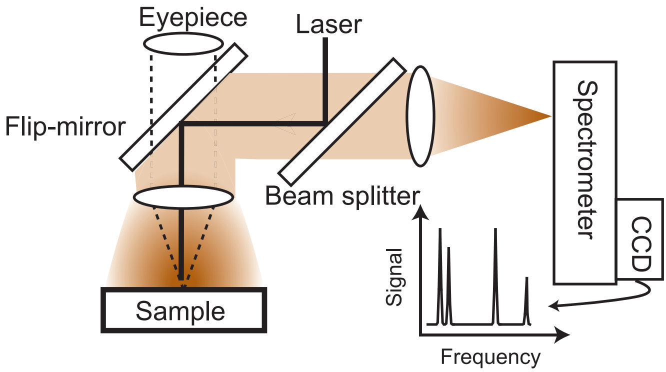

Raman microscopes do more than identify constituents in a given sample. In solid samples, stresses and strains of the material can be mapped by looking at shifts in the Raman lines. In some samples (notably biological ones), the Raman signal is accompanied by background fluorescence. Fluorescence can be mitigated using an excitation laser with a low frequency that does not excite the fluorescent transitions. The problem with this approach is that the Raman-shifted lines are located in the infrared, making detection more difficult. Another approach is to use UV excitation such that the Raman-shifted signal is well separated in frequency from the fluorescent signal, enabling filtering to separate the signals. This approach has the advantage of enhanced Raman scattering because the Raman cross-section is proportional to ω^4. A disadvantage of this approach is that the UV excitation may damage the sample.

Photo-acoustic Interactions

An acoustic wave in a material results in a density wave. Because the index of refraction depends on density, the acoustic wave creates a refractive-index grating, and **photo-acoustic** diffraction may occur where light diffracts from the acoustic wave. **Raman–Nath diffraction** occurs when the acoustic medium is thin. In this regime, the total output field is given by

$$\mathbf{E}(\mathbf{r},t) = \frac{\mathbf{A}_o}{2}\sum_{m=-\infty}^{\infty} J_m(\delta)\exp\left\{i[(\mathbf{k}_{opt} + m\mathbf{K}_{ac})\cdot\mathbf{r} - (\omega_{opt} + m\Omega)t]\right\} + c.c.$$

$$\delta = \frac{\Delta n_o L}{\cos\theta_{int}}\frac{\omega_{opt}}{c}$$

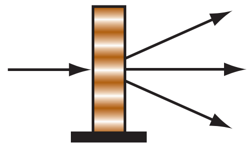

where $\mathbf{A}_o$ is the incident-field complex amplitude, $J_m(\delta)$ is a Bessel function of order m, $\mathbf{k}_{opt}$ and $\mathbf{K}_{ac}$ are the optical and acoustic k vectors, respectively, and ω_{opt} and Ω are the optical and acoustic angular frequencies, respectively. Δn_o is the modulation in the index of refraction, L is the thickness, and θ_{int} is the angle between $\mathbf{k}_{opt}$ and $\mathbf{K}_{ac}$ in the medium. This field shows that several diffracted orders are present with an angular separation of $\Delta\theta = K_{ac}/k_{opt}$. A given diffracted order m is frequency shifted according to $\omega_m = \omega_{opt} + m\Omega$. The frequency shifts may be thought of in terms of Doppler up and down shifts, depending on the relationship between the acoustic wave and diffracted beam.

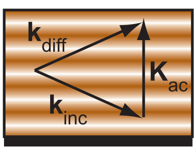

Bragg scattering occurs when the medium thickness is large. Only one diffracted order that satisfies the **Bragg condition** is present. The diffraction efficiency is

$$\frac{I_{diff}}{I_o} = \sin^2\left(\frac{\pi L}{\sqrt{2}\lambda_{opt}}\sqrt{MI_{ac}}\right)$$

where L is the interaction length, I_{ac} is the acoustic intensity, and M is a diffraction figure of merit (looked up for a given material). This expression shows that the diffraction efficiency can be 100%.

Stimulated Brillouin Scattering

In **spontaneous Brillouin scattering**, refractive index variations brought about by density fluctuations in a material cause light to scatter. The scattered light is shifted by the **Brillouin frequency** Ω_B:

$$\Omega_B = (4\pi n v_{ac}/\lambda)\sin(\theta/2)$$

where v_{ac} is the speed of sound in medium, λ is the optical wavelength in vacuum, and θ is the scattering angle.

Stimulated Brillouin scattering in an optical fiber occurs when two beams are present, one propagating in the forward direction at the pump frequency ω_P, and a second backward-propagating with a frequency at ω_B. When ω_B is offset from ω_P by Ω_B, the two beams drive an acoustic wave that reinforces the scattering of the pump wave into the Brillioun wave. In an optical fiber, the Brillouin wave is initiated by spontaneous Brillioun scattering. In the undepleted pump regime,

$$I_B = I_B(L)\exp[g_B I_P(L - z)]$$

$$g_B = \frac{(n^2-1)^2(n^2+2)^2\omega_P^2}{9n\rho_o v_{ac} c^3 \Gamma_B}\left\{\frac{(\Gamma_B/2)^2}{[\Omega_B - (\omega_P - \omega_B)]^2 + (\Gamma_B/2)^2}\right\}$$

where g_B is the **Brillouin intensity gain factor**, ρ_o is the density, and Γ_B is the gain-line width (FWHM). Note that I_B is maximum at $z = 0$ since it is a backwards-traveling wave. Stimulated Brillouin scattering is a serious problem for fiber laser systems because it takes energy away from the desired forward-propagating beam and because the backward-propagating Brillouin wave can damage the source laser. Brillouin mitigation strategies are outlined in the table below.

Reduce Brillouin gain $g_B I_P L$	Disrupt acoustic wave
• Large mode-area fiber • Short fiber length	• Change longitudinal properties ○ Differential doping ○ Temperature profile ○ Distributed stress • Modulate laser ~1 GHz • Acoustic anti-guiding structure

Saturable Absorption

Linear absorption in materials is characterized by an absorption coefficient α_o with a transmission through a length L given by $T = \exp(-\alpha_o L)$. This form of dependence is called **Beer's law**. Absorption occurs when electrons are excited from a ground state to an excited state. When the incident intensity becomes high, it is possible to begin depleting the ground state so that transmission increases. This effect is called **saturable absorption**. The absorption coefficient in this situation is given by

$$\alpha = \frac{\alpha_o}{1 + I/I_S}$$

where I is the intensity, and I_S is the **saturation intensity**. The change in intensity of a beam passing through such a material is characterized by $dI/dz = -\alpha I$, with a transcendental solution:

$$T = T_o \exp\left[\frac{I_o}{I_S}(1 - T)\right]$$

where $T_o = \exp(-\alpha_o L)$, and $T = I/I_o$. Saturable absorbers are critical to ultrashort-pulse formation, where they play a central role in mode-locking. Engineered materials such as a **semiconductor saturable absorber mirror (SESAM)** have an absorption that saturates with increasing intensity so that the reflectivity increases.

Transcendental equations, such as the one above, may be solved using the **method of contours**. In this example, the equation is rewritten as $T_o(T,\eta) = Te^{-\eta(1-T)}$ (where $\eta = I_o/I_S$), and contours of constant T_o are plotted on a grid scaled to T and η. Note that most mathematical packages will plot contours automatically. In this example, the contours show T as a function of I_o/I_S for materials with different T_o's.

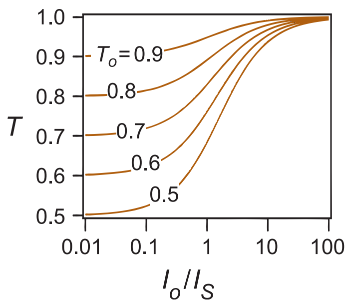

Temporal Solitons

Temporal solitons occur in nonlinear media where dispersion is balanced by the material's nonlinearity. As a pulse propagates in a linear medium, its frequency components travel at different group velocities, leading to a chirped pulse. In a nonlinear medium, **self-phase modulation (SPM)** due to the Kerr effect also chirps the pulse, and if it has the opposite sign from material dispersion, then a soliton can form. The scalar electric field is written in terms of an envelope $A(z,\tau)$:

$$E = \frac{1}{2}A(z,\tau)\exp\left\{i\left[(k_o - \omega_o/v_g)z - \omega_o\tau\right]\right\} + c.c.$$

where v_g is the group velocity, $\tau = t - z/v_g$, ω_o is the carrier frequency, and k_o is the beam's longitudinal k vector. In this form, $A(z,\tau)$ is written in a coordinate system that moves with the pulse. In a medium with a nonlinear index, the wave equation (under the slowly varying envelope approximation) yields the **pulse propagation equation**:

$$\frac{\partial A}{\partial z} + i\frac{k_2}{2}\frac{\partial^2}{\partial\tau^2}A = i\gamma\left|A(\tau)\right|^2 A(\tau)$$

$$k_2 \equiv -\frac{1}{v_g^2}\frac{\partial v_g}{\partial\omega}\bigg|_{\omega_o} \quad \text{and} \quad \gamma \equiv \frac{1}{2}n_o\varepsilon_0\omega_o n_2^I$$

where $\partial v_g/\partial\omega$ is the **group velocity dispersion (GVD)**.

When the sign of k_2 and γ are opposite, a soliton solution, where GVD balances dispersion, is given by

$$A(z,\tau) = A_o\text{sech}(\tau/\tau_o)\exp(i\kappa z)$$

where

$$\tau_o = \sqrt{\frac{k_2 c}{n_2^I I_o\omega_o}}, \quad \kappa = \frac{n_2^I I_o\omega_o}{2c}$$

and I_o is the peak intensity. A restriction to the solution is that the pulse width and peak intensity are not independent, as shown in the expression above for τ_o. Therefore, the amplitude of the soliton is also restricted, and, in terms of the pulse width, is given by

$$\left|A_o\right|^2 = -\frac{k_2}{\gamma\tau_o^2}$$

Spatial Solitons

Spatial solitons occur in nonlinear media where diffraction is balanced by self-focusing due to the Kerr effect. This balancing occurs provided that the sign of n_2^I leads to focusing (positive n_2^I) instead of defocusing (negative n_2^I). Consider a planar-waveguide situation where the mode is free to spread out in one dimension (x), but is confined in the other (y), and the wave propagates in the z direction. In this situation, and for a $\chi^{(3)}$ Kerr nonlinearity, the wave equation gives the following envelope amplitude equation:

$$\frac{\partial A}{\partial z} = i\frac{1}{2k_o}\frac{\partial^2 A}{\partial x^2} + i\frac{n_o\varepsilon_0\omega_o}{2}n_2^I\left|A\right|^2 A$$

where ω_o is the center frequency, and k_o is the z component of the k vector evaluated at ω_o. This equation can be written in a dimensionless form by making the following variable substitutions:

$$Z = \kappa z, \quad X = x/W, \quad U = A/|A_o|$$

$$\kappa \equiv \frac{\omega_o}{c}\left|n_2^I\right| I_o \quad \text{and} \quad \frac{1}{W^2} \equiv k_o\kappa$$

where I_o is the peak intensity, and $I_o = n_o\varepsilon_0 c\left|A_o\right|^2/2$. We further assume that n_2^I is positive (leads to self-focusing), so that the amplitude equation becomes

$$\frac{\partial U}{\partial Z} - \frac{i}{2}\frac{\partial^2 U}{\partial X^2} = i\left|U\right|^2 U$$

This dimensionless equation is in the form of a **nonlinear Schrödinger equation (NLSE)**. Note that the pulse propagation equation for temporal solitons is also in the form of an NLSE. The fundamental soliton solution is

$$U = \text{sech}(X)e^{iZ/2} \Rightarrow A(x,z) = A_o\text{sech}(x/W)\exp(i\kappa z)$$

Note that the beam width W and peak intensity are not independent for the soliton solution. The relationship between A_o and W is given by

$$\left|A_o\right|^2 = \frac{2c}{\varepsilon_0 n_2^I n_o^2 \omega_o^2 W^2}$$

High Harmonic Generation

High-energy ultrashort-pulse lasers have extremely high intensities and, when focused into a gas, can result in **high harmonic generation (HHG)**, where harmonics are generated to well over 100 times those of the fundamental laser frequency. Because the gas is centrosymmetric, only odd harmonics are generated. HHG is understood in terms of a three-step process:

1. Ionization via tunneling,
2. Classical motion of the electron in the laser's electric field,
3. Radiative recombination.

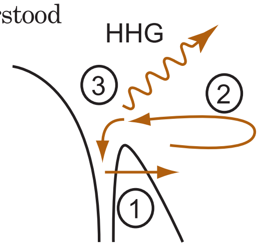

In the first step, the laser's electric field distorts the atomic potential, making tunnel ionization possible. Once the electron is free, its motion in the continuum is treated as an electron moving under the influence of the laser's electric field. The maximum kinetic energy combined with recombination gives the maximum photon energy:

$$E_{cutoff} = I_p + 3.17U_p$$

where I_p is the ionization energy. U_p is the **ponderomotive energy** that corresponds to the time-averaged energy of an electron oscillating in an electric field and is given by

$$U_p = \frac{e^2}{2m\varepsilon_0 c}\frac{I}{\omega_o^2}$$

where ω_o is the carrier frequency, and I is the intensity. These relationships show that ultrashort pulses with a lower carrier frequency have the potential to generate higher harmonics.

Example calculation
$I = 10^{15}$ W/cm^2
$\lambda = 800$ nm (1.55 eV)
$I_p = 24.6$ eV (Helium)
$E_{cutoff} = 214$ eV
$E_{cutoff}/E_{photon} = 138$
137$^{\text{th}}$ HHG possible

HHG is a coherent process, requiring phasing of the radiated harmonics with the driving field. Longer-wavelength pump lasers, pressure tuning, and quasi-phase-matching are employed to improve the phase-matching efficiency.

Ultrashort-Pulse Measurement

The measurement of **ultrashort pulses** relies on nonlinear techniques that mix the pulses with themselves. An **auto-correlator (AC)** splits a laser pulse train into two beams that are then recombined in a nonlinear medium with a variable time delay.

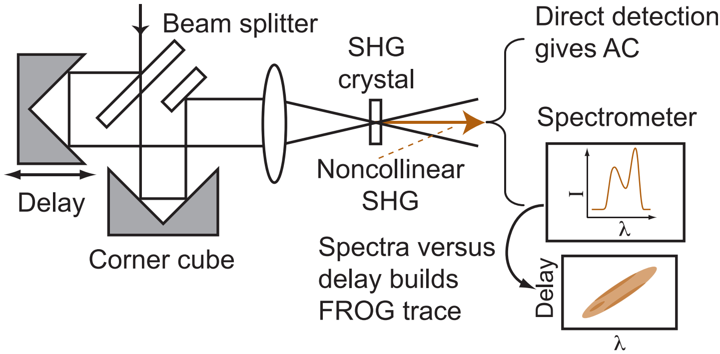

Spectrally resolving the output of an AC is called **frequency-resolved optical gating (FROG)**. The record of the spectrum as a function of delay is called a **FROG trace**. This trace is analogous to a musical score, showing the acoustic frequency as a function of time. The FROG trace may be thought of as a set of overdetermined equations for the intensity and phase. A 2D phase-retrieval algorithm then inverts the FROG trace to yield amplitude and phase in both the time and frequency domains, giving an accurate description of the pulse shape.

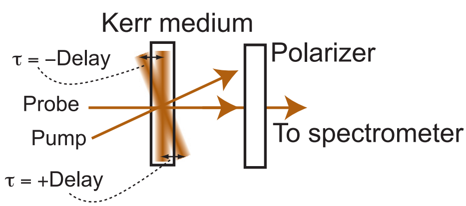

A single-shot FROG based on the Kerr nonlinearity is shown above. The probe-beam polarization is rotated via the optical Kerr effect. The amount of rotation depends on the intensity of the pump beam and, therefore, on the relative delay. A camera on the output of the spectrometer records a single-shot FROG trace.

Gaussian Beams

Lasers and resonator cavities with high-quality beams are characterized by a **Gaussian beam** profile. The envelope of this profile is given by

$$E(r,z) = E_o \frac{w_o}{w(z)} \exp\left[\frac{-r^2}{w^2(z)}\right] \exp\left[-ik\frac{r^2}{2R(z)} + i\zeta(z)\right]$$

where

$$w(z) = w_o\sqrt{1+\left(\frac{z}{z_R}\right)^2},\ R(z) = z\left[1+\left(\frac{z_R}{z}\right)^2\right],\ \zeta(z) = \tan^{-1}\left(\frac{z}{z_R}\right)$$

$$z_R = \frac{\pi n w_o^2}{\lambda}$$

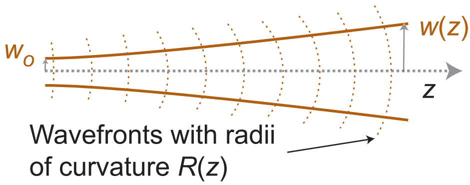

$w(z)$ is the **beam radius** defined as the $1/e$ field radius, and w_o is the radius at the **beam waist**.

The **Rayleigh range** z_R is the distance over which the beam radius increases by a factor of $\sqrt{2}$. Near-optimum focusing occurs for many nonlinear interactions when the interaction length is $2z_R$.

The propagation of Gaussian beams through a chain of optical elements is characterized by the transformation of the **Gaussian beam parameter** q:

$$\frac{1}{q(z)} = \frac{1}{R(z)} - i\frac{\lambda}{\pi n w^2(z)}$$

The q parameter transforms according to

$$q' = (Aq+B)/(Cq+D) \text{ with } \begin{pmatrix} A & B \\ C & D \end{pmatrix} =$$

$\begin{pmatrix} 1 & d \\ 0 & 1 \end{pmatrix}$	$\begin{pmatrix} 1 & 0 \\ -1/f & 1 \end{pmatrix}$	$\begin{pmatrix} 1 & 0 \\ 0 & n_1/n_2 \end{pmatrix}$
Free space length, d	Lens focal length, f	Index change from n_1 to n_2

Matrices appear in reverse order when cascaded. For example, $M_{total} = M_3\, M_2\, M_1$ for three optical elements and where M_1 is the first optical element encountered.

Sellmeier Equations for Selected $\chi^{(2)}$ Crystals

λ entered in microns:

BBO, β-BaB_2O_4, β-barium borate[1]

$$n_o^2 = 2.7359 + \frac{0.01878}{\lambda^2 - 0.01822} - 0.01354\lambda^2$$

$$n_z^2 = 2.3753 + \frac{0.01224}{\lambda^2 - 0.01677} - 0.01516\lambda^2$$

BIBO, BiB_3O_6, bismuth triborate[2]

$$n_x^2 = 3.07403 + \frac{0.03231}{\lambda^2 - 0.03163} - 0.013376\lambda^2$$

$$n_y^2 = 3.16940 + \frac{0.03717}{\lambda^2 - 0.03483} - 0.01827\lambda^2$$

$$n_z^2 = 3.6545 + \frac{0.05112}{\lambda^2 - 0.03713} - 0.02261\lambda^2$$

GaAs, gallium arsenide[3]

$$n^2 = 5.372514 + \frac{27.83972}{1/\lambda_1^2 - 1/\lambda^2} + \frac{0.031764 + F}{1/\lambda_2^2 - 1/\lambda^2} + \frac{0.00143636}{1/\lambda_3^2 - 1/\lambda^2}$$

$$F = 4.350 \times 10^{-5}\Delta T + 4.664 \times 10^{-7}\Delta T^2$$

$$\lambda_1 = 0.44313071 + 5.0564 \times 10^{-5}\Delta T$$

$$\lambda_2 = 0.8746453 + 1.913 \times 10^{-4}\Delta T - 4.8821 \times 10^{-8}\Delta T^2$$

$$\lambda_3 = 36.9166 - 0.011622\,\Delta T; \Delta T = T - 22, \text{and } T \text{ is in } ^\circ\text{C}$$

GaP, gallium phosphide[4]

$$n^2 = 4.1705 + \frac{4.9113}{1 - (0.1174/\lambda^2)} + \frac{1.9928}{1 - (756.46/\lambda^2)}$$

KDP, KH_2PO_4, potassium dihydrogen phosphate[5]

$$n_o^2 = 2.259276 + \frac{10.089562 \times 10^{-3}}{\lambda^2 - 1.2942625 \times 10^{-2}} + \frac{13.00522\lambda^2}{\lambda^2 - 400}$$

$$n_z^2 = 2.132668 + \frac{8.637494 \times 10^{-3}}{\lambda^2 - 1.2281043 \times 10^{-2}} + \frac{3.2279924\lambda^2}{\lambda^2 - 400}$$

DKDP (KD*P), KD_2PO_4, deuterated potassium dihydrogen phosphate[5]

$$n_o^2 = 2.240921 + \frac{9.676393 \times 10^{-3}}{\lambda^2 - 1.5620153 \times 10^{-2}} + \frac{2.2469564\lambda^2}{\lambda^2 - 126.920659}$$

$$n_e^2 = 2.126019 + \frac{8.578409 \times 10^{-3}}{\lambda^2 - 1.1991324 \times 10^{-2}} + \frac{0.7844043\lambda^2}{\lambda^2 - 123.403407}$$

Sellmeier Equations for Selected $\chi^{(2)}$ Crystals (cont.)

LBO, LiB_3O_5, lithium triborate[1]

$$n_x^2 = 2.4542 + \frac{0.01125}{\lambda^2 - 0.01135} - 0.01388\lambda^2$$

$$n_y^2 = 2.5390 + \frac{0.01277}{\lambda^2 - 0.01189} - 0.01848\lambda^2$$

$$n_z^2 = 2.5865 + \frac{0.01310}{\lambda^2 - 0.01223} - 0.01861\lambda^2$$

$LiNbO_3$, lithium niobate (congruent)[6]

$$n_o^2 = 4.9048 + \frac{0.11775 + 2.2314 \times 10^{-8}F}{\lambda^2 - (0.21802 - 2.9671 \times 10^{-8}F)^2} + 2.1429 \times 10^{-8}F - 0.027153\lambda^2$$

$$n_z^2 = 4.5820 + \frac{0.09921 + 5.2716 \times 10^{-8}F}{\lambda^2 - (0.21090 - 4.9143 \times 10^{-8}F)^2} + 2.2971 \times 10^{-7}F - 0.021940\lambda^2$$

For QPM calculations use[7]

$$n_z^2 = 5.35583 + 4.629 \times 10^{-7}F + \frac{0.100473 + 3.862 \times 10^{-8}F}{\lambda^2 - (0.20692 - 0.89 \times 10^{-8}F)^2} + \frac{100 + 2.657 \times 10^{-5}F}{\lambda^2 - 128.806} - 1.5334 \times 10^{-2}\lambda^2$$

$F = (T - T_o)(T + T_o + 546)$; $T_o = 24.5$ °C, T is entered in °C.

$LiTaO_3$, lithium tantalate[8]

$$n_e^2 = 1 + \frac{2.97584\lambda^2}{\lambda^2 - 0.138^2} + \frac{0.54622\lambda^2}{\lambda^2 - 0.24028^2} - 0.023497\lambda^2$$

ZGP, $ZnGeP_2$, zinc germanium phosphide[9]

$$n_o^2 = 4.47330 + \frac{5.26576\lambda^2}{\lambda^2 - 0.13381} + \frac{1.49085\lambda^2}{\lambda^2 - 662.55}$$

$$n_e^2 = 4.63318 + \frac{5.34215\lambda^2}{\lambda^2 - 0.14255} + \frac{1.45795\lambda^2}{\lambda^2 - 662.55}$$

ZnTe, zinc telluride[10]

$$n^2 = 9.92 + \frac{0.42530}{\lambda^2 - 0.14263} + \frac{2.63580}{\lambda^2/3192.3 - 1}$$

Properties of Selected $\chi^{(2)}$ Crystals

Common name	Point group & type	Transparency range (nm)	Nonlinear coefficients (pm/V)
BBO[11,12]	3m Negative uniaxial	185–2600	$d_{22} = -2.2$ $d_{31} = 0.08$ $r_{22} = -2.41$
BIBO[13]	2 Biaxial	286–2500	$d_{14} = 2.4$ $d_{16} = 2.8$ $d_{21} = 2.3$ $d_{22} = 2.5$ $d_{23} = -1.3$ $d_{25} = 2.4$ $d_{34} = -0.9$ $d_{36} = 2.4$
GaAs[12,14]	$\bar{4}3m$ Isotropic	1000–17,000	$d_{36} = 94$ $r_{41} = 1.24$
GaP[12,15]	Isotropic	570–11,000	$d_{14} = 70.6$ $r_{41} = 0.8$
KDP[12,16]	$\bar{4}2m$ Negative uniaxial	180–1500	$d_{36} = 0.39$ $r_{41} = 8.6$ $r_{63} = 9.4$
KTP[17,18]	mm2 Biaxial	350–4500	$d_{15} = 2.0$ $d_{24} = 3.9$ $d_{31} = 2.1$ $d_{32} = 3.8$ $d_{33} = 15$ $r_{13} = 9.5$ $r_{23} = 16$ $r_{33} = 36$ $r_{42} = 9.3$ $r_{51} = 7.3$
LBO[9]	mm2 Biaxial	160–2600	$d_{31} = -0.67$ $d_{32} = 0.85$ $d_{33} = 0.04$
$LiNbO_3$, Lithium niobate[9,12]	3m Negative uniaxial	400–5500	$d_{22} = 2.1$ $d_{31} = -4.35$ $d_{33} = -27.2$ $r_{13} = 10$ $r_{22} = 6.8$ $r_{33} = 32.2$ $r_{51} = 32$
$LiTaO_3$, Lithium tantalate[12,15]	3m Positive uniaxial	280–5500	$d_{31} = 0.85$ $d_{33} = -13.8$ $r_{13} = 8.4$ $r_{33} = 30.5$
ZGP[9,12]	Class $\bar{4}2m$ Positive uniaxial	740–12,000	$d_{14} = 75$ $r_{41} = 1.6$ $r_{63} = -0.8$
ZnTe[12]	$\bar{4}3m$ Isotropic	600–20,000	$r_{41} = 4.45–3.95$

References for Selected $\chi^{(2)}$ Crystals Tables

1. Kato, K., "Temperature-tuned 90° phase-matching properties of LiB_3O_5," *IEEE Journal of Quantum Electronics* **30**, p. 2950 (1994).
2. Umemura, N., K. Miyata, and K. Kato, "New data on the optical properties of BiB_3O_6," *Optical Materials* **30**(4), p. 532 (2007).
3. Skauli, T. et al., "Improved dispersion relations for GaAs and applications to nonlinear optics," *Journal of Applied Physics* **94**(10), p. 6447 (2003).
4. Madarasz, F. L. et al., "Sellmeier parameters for $ZnGaP_2$ and GaP," *Journal of Applied Physics* **87**(3), p. 1564 (2000).
5. Lozhkarev, V. V. et al., "Study of broadband optical parametric chirped pulse amplification in a DKDP crystal pumped by the second harmonic of a NdYLF laser," *Laser Physics* **15**(9), p. 1319 (2005).
6. Edwards, G. J. and M. Lawrence, "A temperature-dependent dispersion equation for congruently grown lithium niobate," *Optical and Quantum Electronics* **16**(4), p. 373 (1984).
7. Jundt, D. H., "Temperature-dependent Sellmeier equation for the index of refraction, n_e, in congruent lithium niobate," *Optics Letters* **22**(20), p. 1553 (1997).
8. Barboza, N. A. and R. S. Cudney, "Improved Sellmeier equation for congruently grown lithium tantalite," *Applied Physics B* **95**, p. 453 (2009).
9. Dmitriev, V. G. et al., *Handbook of Nonlinear Optical Crystals*, Springer, New York, p. 136 (1997).
10. Li, H. H., "Refractive index of ZnS, ZnSe, and ZnTe and its wavelength and temperature derivatives," *Journal of Chem. Ref. Data* **13**(1), p. 103 (1984).

References for Selected $\chi^{(2)}$ Crystals Tables (cont.)

11. Eckardt, R. C. et al., "Absolute and relative nonlinear optical coefficients of KDP, KD*P, BaB_2O_4, $LiIO_3$, MgO:$LiNbO_3$, and KTP measured by phase-matched second-harmonic generation," *IEEE Journal of Quantum Electronics* **26**, p. 922 (1990).

12. Weber, M. J., *Handbook of Optical Materials*, CRC, Boca Raton, p. 148 (2003).

13. Hellwig, H., J. Liebertz, and L. Bohaty, "Exceptional large nonlinear optical coefficients in the monoclinic bismuth borate BiB_3O_6 (BIBO)," *Solid State Communications* **109**(4), p. 249 (1999).

14. Skauli, T. et al., "Measurement of the nonlinear coefficient of orientation-patterned GaAs and demonstration of highly efficient second-harmonic generation," *Optics Letters* **27**(8), p. 628 (2002).

15. Shoji, I. et al., "Absolute scale of second-order nonlinear-optical coefficients," *Journal of the Optical Society of America B* **14**(9), 2268 (1997).

16. Eimerl, D., "Electro-optic, linear, and nonlinear optical properties of KDP and its isomorphs," *Ferroelectrics* **72**(1), pp. 95–139 (1987).

17. Pack, M. V., D. J. Armstrong, and A. V. Smith, "Measurement of the $\chi^{(2)}$ tensors of $KTiOPO_4$, KTiOAsO4, $RbTiOPO_4$, and $RbTiOAsO_4$ crystals," *Applied Optics* **43**(16), pp. 3319–3323 (2004).

18. Bierlein, J. D. and C. B. Arweiler, "Electro-optic and dielectric properties of $KTiOPO_4$," *Applied Physics Letters* **49**(15), p. 917 (1986).

Equation Summary

Maxwell's equations:

$$\nabla \cdot \mathbf{D} = \rho_f \qquad \nabla \times \mathbf{E} = -\frac{\partial \mathbf{B}}{\partial t} \qquad \mathbf{D} = \varepsilon_0 \mathbf{E} + \mathbf{P}$$

$$\nabla \cdot \mathbf{B} = 0 \qquad \nabla \times \mathbf{H} = \mathbf{j}_f + \frac{\partial \mathbf{D}}{\partial t} \qquad \mathbf{H} = \frac{\mathbf{B}}{\mu_0} - \mathbf{M}$$

Scalar plane wave in complex notation:

$$E = \frac{1}{2} A e^{i(kz - \omega t)} + c.c.$$

k vector magnitude:

$$k = \frac{n\omega}{c} = \frac{2\pi n}{\lambda_{vacuum}}$$

Wave equation in the slowly varying envelope approximation:

$$\frac{dA(\omega)}{dz} = i \frac{\omega}{2n\varepsilon_0 c} P^{NL}(\omega) e^{-ikz}$$

Intensity:

$$I = \frac{1}{2} n \varepsilon_0 c |A|^2$$

Coupled amplitude equations—three-wave process:

$$\frac{dA_1}{dz} + \frac{\alpha_1}{2} A_1 = i \frac{\omega_1}{n_1 c} d_{eff} A_3 A_2 e^{-i\Delta kz}$$

$$\frac{dA_2}{dz} + \frac{\alpha_2}{2} A_2 = i \frac{\omega_2}{n_2 c} d_{eff} A_1 A_3^* e^{i\Delta kz}$$

$$\frac{dA_3}{dz} + \frac{\alpha_3}{2} A_3 = i \frac{\omega_3}{n_3 c} d_{eff} A_1 A_2^* e^{i\Delta kz}$$

Field for Gaussian beam:

$$E(r,z) = E_o \frac{w_o}{w(z)} \exp\left[\frac{-r^2}{w^2(z)}\right] \exp\left[-ik \frac{r^2}{2R(z)} + i\zeta(z)\right]$$

Equation Summary

Gaussian beam parameters:

$$w(z) = w_o\sqrt{1+\left(\frac{z}{z_R}\right)^2},\ R(z) = z\left[1+\left(\frac{z_R}{z}\right)^2\right],\ \zeta(z) = \tan^{-1}\left(\frac{z}{z_R}\right)$$

$$z_R = \frac{\pi n w_o^2}{\lambda}, \quad \frac{1}{q(z)} = \frac{1}{R(z)} - i\frac{\lambda}{\pi n w^2(z)}$$

Focused Gaussian beam gain reduction factors:

$$g_1 = \frac{2\overline{w}_1^2}{\overline{w}_1^2 + w_1^2} \qquad g_2 = \frac{2\overline{w}_2^2}{\overline{w}_2^2 + w_2^2} \qquad g_3 = \frac{2\overline{w}_3^2}{\overline{w}_3^2 + w_3^2}$$

$$\frac{1}{\overline{w}_3^2} \equiv \frac{1}{w_1^2} + \frac{1}{w_2^2} \qquad \frac{1}{\overline{w}_2^2} \equiv \frac{1}{w_1^2} + \frac{1}{w_3^2} \qquad \frac{1}{\overline{w}_1^2} \equiv \frac{1}{w_2^2} + \frac{1}{w_3^2}$$

Intensity for confocally focused Gaussian beam:

$$I_o = \frac{4n}{\lambda L}P$$

Crystal optics—uniaxial crystals:

$$\frac{1}{n_e^2(\theta)} = \frac{\cos^2\theta}{n_o^2} + \frac{\sin^2\theta}{n_Z^2} \quad \text{or} \quad n_e(\theta) = n_o\sqrt{\frac{1+\tan^2\theta}{1+\frac{n_o^2}{n_Z^2}\tan^2\theta}}$$

Crystal optics—Poynting vector walk-off angle in uniaxial crystals:

$$\rho = \tan^{-1}\left(\frac{n_o^2}{n_z^2}\tan\theta\right) - \theta$$

Crystal optics—biaxial crystals:

XY plane $$\frac{1}{n_e^2(\phi)} = \frac{\cos^2\phi}{n_Y^2} + \frac{\sin^2\phi}{n_X^2} \qquad n_o = n_Z$$

YZ plane $$\frac{1}{n_e^2(\theta)} = \frac{\cos^2\theta}{n_Y^2} + \frac{\sin^2\theta}{n_Z^2} \qquad n_o = n_X$$

XZ plane $$\frac{1}{n_e^2(\theta)} = \frac{\cos^2\theta}{n_X^2} + \frac{\sin^2\theta}{n_Z^2} \qquad n_o = n_Y$$

$$\tan V_z = \pm(n_Z/n_X)\sqrt{\left|n_X^2 - n_Y^2\right| / \left|n_Y^2 - n_Z^2\right|}$$

Equation Summary

Nonlinear polarization:

$$P = \varepsilon_0 \chi^{(1)} E + \varepsilon_0 \chi^{(2)} E^2 + \varepsilon_0 \chi^{(3)} E^3 + \cdots \quad d_{ijk} \equiv \frac{1}{2} \chi^{(2)}_{ijk}$$

Miller's rule:

$$\begin{aligned} \chi^{(2)}(\omega_1; \omega_2, \omega_3) &= \chi^{(1)}(\omega_1)\chi^{(1)}(\omega_2)\chi^{(1)}(\omega_3)\Delta \\ &= [n^2(\omega_1) - 1][n^2(\omega_2) - 1][n^2(\omega_3) - 1]\Delta \end{aligned}$$

Nonlinear polarization for DFG:

$$\mathbf{P}^{(2)}(\omega_1 - \omega_2) = 2\varepsilon_0 \times$$

$$\begin{pmatrix} d_{11} & d_{12} & d_{13} & d_{14} & d_{15} & d_{16} \\ d_{21} & d_{22} & d_{23} & d_{24} & d_{25} & d_{26} \\ d_{31} & d_{32} & d_{33} & d_{34} & d_{35} & d_{36} \end{pmatrix} \begin{pmatrix} A_x(\omega_1)A_x^*(\omega_2) \\ A_y(\omega_1)A_y^*(\omega_2) \\ A_z(\omega_1)A_z^*(\omega_2) \\ A_y(\omega_1)A_z^*(\omega_2) + A_z(\omega_1)A_y^*(\omega_2) \\ A_x(\omega_1)A_z^*(\omega_2) + A_z(\omega_1)A_x^*(\omega_2) \\ A_x(\omega_1)A_y^*(\omega_2) + A_y(\omega_1)A_x^*(\omega_2) \end{pmatrix}$$

Nonlinear polarization for SFG:

$$\mathbf{P}^{(2)}(\omega_1 + \omega_2) = 2\varepsilon_0 \times$$

$$\begin{pmatrix} d_{11} & d_{12} & d_{13} & d_{14} & d_{15} & d_{16} \\ d_{21} & d_{22} & d_{23} & d_{24} & d_{25} & d_{26} \\ d_{31} & d_{32} & d_{33} & d_{34} & d_{35} & d_{36} \end{pmatrix} \begin{pmatrix} A_x(\omega_1)A_x(\omega_2) \\ A_y(\omega_1)A_y(\omega_2) \\ A_z(\omega_1)A_z(\omega_2) \\ A_y(\omega_1)A_z(\omega_2) + A_z(\omega_1)A_y(\omega_2) \\ A_x(\omega_1)A_z(\omega_2) + A_z(\omega_1)A_x(\omega_2) \\ A_x(\omega_1)A_y(\omega_2) + A_y(\omega_1)A_x(\omega_2) \end{pmatrix}$$

Nonlinear polarization for SHG:

$$\mathbf{P}^{(2)}(2\omega) = \varepsilon_0 \begin{pmatrix} d_{11} & d_{12} & d_{13} & d_{14} & d_{15} & d_{16} \\ d_{21} & d_{22} & d_{23} & d_{24} & d_{25} & d_{26} \\ d_{31} & d_{32} & d_{33} & d_{34} & d_{35} & d_{36} \end{pmatrix} \begin{pmatrix} A_x^2(\omega) \\ A_y^2(\omega) \\ A_z^2(\omega) \\ 2A_y(\omega)A_z(\omega) \\ 2A_x(\omega)A_z(\omega) \\ 2A_x(\omega)A_y(\omega) \end{pmatrix}$$

Equation Summary

Electro-optic effect:

$$B' = \begin{pmatrix} 1/n_x^2 & 0 & 0 \\ 0 & 1/n_y^2 & 0 \\ 0 & 0 & 1/n_z^2 \end{pmatrix} + \begin{pmatrix} \Delta B_1 & \Delta B_6 & \Delta B_5 \\ \Delta B_6 & \Delta B_2 & \Delta B_4 \\ \Delta B_5 & \Delta B_4 & \Delta B_3 \end{pmatrix}$$

$$\begin{pmatrix} \Delta B_1 \\ \Delta B_2 \\ \Delta B_3 \\ \Delta B_4 \\ \Delta B_5 \\ \Delta B_6 \end{pmatrix} = \begin{pmatrix} r_{11} & r_{12} & r_{13} \\ r_{21} & r_{22} & r_{23} \\ r_{31} & r_{32} & r_{33} \\ r_{41} & r_{42} & r_{43} \\ r_{51} & r_{52} & r_{53} \\ r_{61} & r_{62} & r_{63} \end{pmatrix} \begin{pmatrix} E_x \\ E_y \\ E_z \end{pmatrix}$$

Electric field for phase-modulated beam:

$$E_{out} = E_o J_0(\delta)\cos(\omega_o t)$$
$$+ E_o \sum_{k=1}^{\infty} \left\{ J_k(\delta) \left[\cos(\omega_o - k\Omega_m)t + (-1)^k \cos(\omega_o + k\Omega_m)t \right] \right\}$$

Energy conservation for three-wave process:

$$\omega_1 = \omega_2 + \omega_3$$

$$1/\lambda_1 = 1/\lambda_2 + 1/\lambda_3 \text{ (vacuum wavelengths)}$$

Difference-frequency generation for plane waves:

$$I_3 = \frac{8\pi^2 L^2}{n_1 n_2 n_3 \varepsilon_0 c \lambda_3^2} d_{eff}^2 I_1 I_2 \mathrm{sinc}^2(\Delta k L/2) \quad \mathrm{sinc}(x) \equiv \frac{\sin(x)}{x}$$

Confocally focused Gaussian beam DFG:

$$\mathrm{P}_3(L) = \frac{32\pi^2 d^2 L}{n_3 \varepsilon_0 c \lambda_3^2 (n_2\lambda_1 + n_1\lambda_2)} P_1(0) P_2(0)$$

Optical parametric amplification:

$$P_{OPA}(L) = P_{OPA}(0) + \frac{\lambda_{DFG}}{\lambda_{OPA}} P_{DFG}(L)$$

Equation Summary

Sum-frequency generation for plane waves:

$$I_1 = \frac{8\pi^2 L^2}{\varepsilon_0 c n_1 n_2 n_3 \lambda_1^2} d_{eff}^2 I_2 I_3 \ \mathrm{sinc}^2(\Delta k L/2)$$

Confocally focused Gaussian beam SFG:

$$P_{SFG} = \frac{32\pi^2 L}{n_1 \varepsilon_0 \lambda_1^2 c(n_2\lambda_3 + n_3\lambda_2)} d^2 P_2 P_3$$

Second-harmonic generation for plane waves:

$$I_{SHG} = \frac{8\pi^2 L^2}{n_{SHG} n_F^2 \varepsilon_0 c \lambda_F^2} d_{eff}^2 I_F^2 \ \mathrm{sinc}^2(\Delta k L/2)$$

Confocally focused Gaussian beam SHG:

$$P_{SHG} = \frac{16\pi^2 d^2 L}{\varepsilon_0 c n_F^2 \lambda_F^3} P_F^2$$

Optical parametric generation:

$$dP_s(z) = \frac{\hbar n_S \omega_S^4 \omega_I d_{eff}^2}{2\pi^2 \varepsilon_0 c^5 n_p n_i} \frac{\sinh^2(gz)}{g^2} P_p \theta d\theta d\omega_s$$

OPO threshold for plane waves:

$$P_{TH} = A \frac{n_p n_S n_I \varepsilon_0 c \lambda_S \lambda_I}{4\pi^2 d_{eff}^2 L^2} \frac{(1-\rho_S)(1-\rho_I)}{\rho_S + \rho_I}$$

OPO threshold (Gaussian beams):

$$P_{TH} = \frac{n_P n_S n_I \varepsilon_0 c \lambda_S \lambda_I W^2}{32\pi L^2 d_{eff}^2} \frac{(1-\rho_S)(1-\rho_I)}{\rho_S + \rho_I}$$

$$\frac{1}{W^2} = \left(\frac{w_P w_S w_I}{w_P^2 w_S^2 + w_P^2 w_I^2 + w_S^2 w_I^2} \right)^2$$

$$\rho_S = \sqrt{R_{aS} R_{bS}} e^{-2\alpha_S L} \quad \text{and} \quad \rho_I = \sqrt{R_{aI} R_{bI}} e^{-2\alpha_I L}$$

Equation Summary

Phase matching:

Birefringent: $\Delta\mathbf{k} = \mathbf{k}_1 - \mathbf{k}_2 - \mathbf{k}_3 = 0$

QPM $$\Delta k_m = k_1 - k_2 - k_3 - \frac{2\pi}{\Lambda} m = 0$$

Waveguide $$\Delta\beta = \beta_1 - \beta_2 - \beta_3$$

Waveguide with QPM $$\Delta\beta = \beta_1 - \beta_2 - \beta_3 - \frac{2\pi}{\Lambda}$$

Quasi-phase-matching:

$$d_{eff} = \frac{2}{m\pi} d_o \sin\left(m\pi \frac{W}{\Lambda}\right)$$

$$\Lambda_m = \frac{2\pi}{\Delta k} m$$

Bandwidth for three-wave interactions:

$$\Delta\theta = \pm \frac{0.886\pi}{L|\partial \Delta k/\partial\theta|} \qquad \Delta T = \pm \frac{0.886\pi}{L|\partial \Delta k/\partial T|}$$

$$\Delta\omega = \pm \frac{0.886\pi}{L|\partial \Delta k/\partial\omega|}$$

DFG bandwidth when ω_1 monochromatic:

$$\Delta\omega_2 = \pm \frac{0.886\pi v_{g2} v_{g3}}{L|v_{g2} - v_{g3}|}$$ collinear DFG

$$\Delta\omega_2 = \pm \frac{0.886\pi v_{g2} v_{g3}}{L(v_{g2} - v_{g3}\cos\Omega)}$$ noncollinear DFG

Third-harmonic generation:

$$P_{THG} = \frac{3\omega^2}{4\pi^2 \varepsilon_0^2 c^4 n_{3\omega} n_F^3 w_{oF}^4} \left(\chi^{(3)}\right)^2 P_F^3 \left|J\right|^2$$

$\chi^{(3)}$ parametric amplifier:

$$I_S = \left[1 + \frac{\gamma^2 \omega_S \omega_I}{g^2} \sinh^2(gz)\right] I_{S0}, \quad I_I = \frac{\gamma^2 \omega_I^2}{g^2} I_{S0} \sinh^2(gz)$$

Equation Summary

Nonlinear index:

$$n = n_o + n_2^I I$$

Two-photon absorption transmission:

$$T_{TPA} = \frac{(1-R)^2 e^{-\alpha L}}{\sqrt{\pi} q_o} \int_{-\infty}^{\infty} \ln\left(1 + q_o e^{-x^2}\right) dx$$

$$q_o = \frac{\beta}{\alpha} I_o (1-R)\left(1 - e^{-\alpha L}\right)$$

***z* scan transmission for a closed aperture:**

$$T(z, \Delta\Phi_o) \approx 1 - \frac{4\Delta\Phi_o x}{(x^2+9)(x^2+1)}, \quad \Delta\Phi_o = 2\pi n_2^I I_o L_{eff}/\lambda$$

$$L_{eff} = \left(1 - e^{-\alpha L}\right)/\alpha, \quad x \equiv z/z_R$$

***z* scan transmission for an open aperture:**

$$T(z, \Delta\Phi_o) = \frac{e^{-\alpha \Delta z}}{\beta I_o L_{eff}} \left(1 + x^2\right) \ln\left(1 + \frac{\beta I_o L_{eff}}{1 + x^2}\right)$$

Spontaneous Raman processes:

$$P_{scatter} = \sigma_R I_o$$

Undepleted pump regime for stimulated Raman:

$$I_S(z) = I_S(0) e^{g I_P z}, \quad g = \frac{3\omega_S}{n_S n_P \varepsilon_0 c^2} \left|\mathrm{Im}\left(\chi_R^{(3)}\right)\right|$$

Depleted pump regime for stimulated Raman:

$$I_S(L) = \frac{(I_{S0}/\omega_S + I_{P0}/\omega_P) I_{S0} e^{C\gamma L}}{I_{P0}/\omega_P + I_{S0} e^{C\gamma L}/\omega_S}, \quad \gamma \equiv \frac{3\omega_S \omega_P}{4 n_S n_P \varepsilon_0 c^2} \left|\mathrm{Im}\left(\chi_R^{(3)}\right)\right|$$

$$I_P(L) = \frac{(I_{S0}/\omega_S + I_{P0}/\omega_P) I_{P0}}{I_{P0}/\omega_P + I_{S0} e^{C\gamma L}/\omega_S},$$

$$C = I_P(0)/\omega_P + I_S(0)/\omega_S$$

Equation Summary

Anti-Stokes phase matching condition:

$$\Delta\mathbf{k} = 2\mathbf{k}_P - \mathbf{k}_{AS} - \mathbf{k}_S, \quad \cos\theta_{NC} = \frac{k_{AS}^2 + 4k_P^2 - k_S^2}{4k_P k_{AS}}$$

Undepleted pump and Stokes fields for anti-Stokes:

$$I_{AS} = \frac{\omega_{AS}^2 \left|\chi_R^{(3)}\right|^2}{16\varepsilon_0^2 n_P^2 n_S n_{AS} c^4} I_P^2 I_S L^2 \operatorname{sinc}^2(\Delta k L/2)$$

Raman–Nath diffracted field:

$$\mathbf{E}(\mathbf{r},t) = \frac{\mathbf{A}_o}{2}\sum_{m=-\infty}^{\infty} J_m(\delta)\exp\left\{i\left[(\mathbf{k}_{opt} + m\mathbf{K}_{ac})\cdot\mathbf{r} - (\omega_{opt} + m\Omega)t\right]\right\} + c.c.$$

Bragg scattering diffraction efficiency:

$$\frac{I_{diff}}{I_o} = \sin^2\left(\frac{\pi L}{\sqrt{2}\lambda_{opt}}\sqrt{MI_{ac}}\right)$$

Stimulated Brillouin scattering:

$$I_B = I_B(L)\exp[g_B I_P(L-z)]$$

$$g_B = \frac{(n^2-1)^2(n^2+2)^2\omega_P^2}{9n\rho_o v_{ac} c^3 \Gamma_B}\left\{\frac{(\Gamma_B/2)^2}{[\Omega_B - (\omega_P - \omega_B)]^2 + (\Gamma_B/2)^2}\right\}$$

Saturable absorption:

$$\alpha = \frac{\alpha_o}{1 + I/I_S} \qquad T = T_o\exp\left[\frac{I_o}{I_S}(1-T)\right]$$

Co-directional two-beam coupling:

$$I_1(L) = I_{10}\frac{I_{10}+I_{20}}{I_{10}+I_{20}e^{\gamma L}}, \qquad I_2(L) = I_{20}\frac{I_{10}+I_{20}}{I_{20}+I_{10}e^{-\gamma L}},$$

$$\gamma = \frac{2\pi}{\lambda} n^3 r_{eff} E_{SC}$$

Equation Summary

Contra-directional two-beam coupling:

$$I_1(L) = I_{10}\frac{I_{10}+I_{2L}}{I_{10}+I_{2L}e^{\gamma L}} \quad I_2(0) = I_{2L}\frac{I_{10}+I_{2L}}{I_{2L}+I_{10}e^{-\gamma L}}$$

Pulse propagation equation:

$$\frac{\partial A}{\partial z} + i\frac{k_2}{2}\frac{\partial^2}{\partial \tau^2}A = i\gamma|A(\tau)|^2 A(\tau)$$

$$k_2 \equiv -\frac{1}{v_g^2}\frac{\partial v_g}{\partial \omega}\bigg|_{\omega_o} \quad \text{and} \quad \gamma \equiv \frac{1}{2}n_o\varepsilon_0 c n_2^I$$

Soliton solution:

$$A(z,\tau) = A_o \operatorname{sech}(\tau/\tau_o)\exp(i\kappa z)$$

$$\tau_o = \sqrt{\frac{k_2 c}{n_2^I I_o \omega_o}} \quad \text{and} \quad \kappa = \frac{n_2^I I_o \omega_o}{c}$$

Nonlinear Schrödinger equation:

$$\frac{\partial U}{\partial Z} - \frac{i}{2}\frac{\partial^2 U}{\partial X^2} = i\left|U\right|^2 U$$

Soliton solution:

$$U = \operatorname{sech}(X)e^{iZ/2}$$

High harmonic generation:

$$E_{cutoff} = I_p + 3.17U_p$$

$$U_p = \frac{e^2}{2m\varepsilon_0 c}\frac{I}{\omega_o^2}$$

Bibliography

Agrawal, G. P., *Nonlinear Fiber Optics*, 5th ed., Academic Press, Waltham, MA (2012).

Akhmanov, S. A. and R. V. Khokhlov, *Problems of Nonlinear Optics: Electromagnetic Waves in Nonlinear Dispersive Media*, Gordon and Breach Science Publishers, New York (1972).

Banerjee, P. P., *Nonlinear Optics: Theory, Numerical Modeling, and Applications*, Marcel Dekker, New York (2004).

Bloembergen, N., *Nonlinear Optics*, 4th ed., World Scientific, River Edge, NJ (1996).

Born, M. and E. Wolf, *Principles of Optics: Electromagnetic Theory of Propagation, Interference and Diffraction of Light*, 7th ed., Cambridge University Press, New York (1999).

Boyd, R. W., *Nonlinear Optics*, 3rd ed. Academic Press, Burlington, MA (2008).

Butcher, P. N. and D. Cotter, *The Elements of Nonlinear Optics*. (Cambridge Studies in Modern Optics), Cambridge University Press, New York (1991).

Demtröder, W., *Laser Spectroscopy*, 4th ed., Springer, Berlin (2008).

Gurzadyan, G. G., V. G. Dmitriev, and D. N. Nikogosyan, *Handbook of Nonlinear Optical Crystals* (Springer Series in Optical Sciences), 3rd ed., Springer, New York (1999).

He, G. and S. H. Liu, *Physics of Nonlinear Optics*, World Scientific, River Edge, NJ (1999).

Mandel, P., *Nonlinear Optics: An Analytical Approach*, Wiley-VCH, Weinheim (2010).

Martienssen, W. and H. Warlimont, *Springer Handbook of Condensed Matter and Materials Data*, Springer, New York (2005).

Bibliography

Mertz, J., *Introduction to Optical Microscopy*, Roberts and Company, Greenwood Village, CO (2010).

Moloney, J. V. and A. C. Newell, *Nonlinear Optics*, Westview Press, Boulder, CO (2004).

Mukamel, S., *Principles of Nonlinear Optics and Spectroscopy*, Oxford University Press, New York (1995).

New, G. H. C., *Introduction to Nonlinear Optics*, Cambridge University Press, New York (2011).

Pedrotti, F. L., L. S. Pedrotti, and L. M. Pedrotti, *Introduction to Optics*, 3rd ed., Addison-Wesley, Upper Saddle River, NJ (2007).

Powers, P. E., *Fundamentals of Nonlinear Optics*, CRC Press, Boca Raton (2011).

Sauter, E. G., *Nonlinear Optics* (Wiley Series in Microwave and Optical Engineering), Wiley, New York (1996).

Shen, Y. R., *The Principles of Nonlinear Optics*, Wiley, New York (2003).

Smith, A. V., SNLO nonlinear optics code, AS-Photonics, Albuquerque, NM (2010).

Stegeman, G. I., *Nonlinear Optics: Phenomena, Materials, and Devices* (Wiley Series in Pure and Applied Optics), Wiley, Hoboken, NJ (2012).

Sutherland, R. L., D. G. McLean, and S. Kirkpatrick, *Handbook of Nonlinear Optics*, 2nd ed., Marcel Dekker, New York (2003).

Tang, C. L., *Quantum Electronics* (Methods of Experimental Physics), Vol. 15A, Academic Press, New York (1979).

Träger, F., *Springer Handbook of Lasers and Optics*, 2nd ed., Springer, New York (2012).

Trebino, R., *Frequency-Resolved Optical Gating: The Measurement of Ultrashort Laser Pulses*, Kluwer Academic, Boston (2000).

Bibliography

Weber, M. J., *CRC Handbook of Laser Science and Technology—Supplement 2: Optical Materials*, CRC Press, Cleveland (1994).

Weiner, A. M., *Ultrafast Optics*, Wiley, Hoboken, NJ (2009).

Yariv, A., *Quantum Electronics*, 3rd ed., Wiley, New York (1989).

Zernike, F. and J. E. Midwinter, *Applied Nonlinear Optics*, Wiley, New York (1973).

Index

Index

Index

Index

Peter E. Powers is professor of Physics and Electro-optics at the University of Dayton where he has held the position of Mann Chair of Sciences since 2010. Previous to joining the faculty at the University of Dayton in 1997, he spent three years at Sandia National Laboratories developing infrared nonlinear frequency-converted sources for remote sensing and trace species detection. In 1995, he received a Ph.D. in Applied and Engineering Physics at Cornell University where he developed femtosecond optical parametric oscillators. Dr. Powers has published widely in nonlinear optics and has presented his results at numerous conferences. From 2004–2010, he chaired the SPIE "Nonlinear Frequency Generation and Conversion: Materials, Devices, and Applications" conference. He currently holds five patents related to nonlinear frequency-converted devices. He is author of *Fundamentals of Nonlinear Optics* published in 2011 by CRC Press. Dr. Powers is a fellow of SPIE and a member of the Optical Society of America as well as the American Physical Society.

Nonlinear Optics

Peter E. Powers

This Field Guide is designed for those looking for a condensed and concise source of key concepts, equations, and techniques for nonlinear optics. Examples throughout this Field Guide illustrate fundamental concepts while demonstrating the application of key equations. Topics covered include technologically important effects, recent developments in nonlinear optics, and linear optical properties central to nonlinear phenomena, with a focus on real-world applicability in the field of nonlinear optics.

SPIE Field Guides

The aim of each *SPIE Field Guide* is to distill a major field of optical science or technology into a handy desk or briefcase reference that provides basic, essential information about optical principles, techniques, or phenomena.

Written for you—the practicing engineer or scientist—each field guide includes the key definitions, equations, illustrations, application examples, design considerations, methods, and tips that you need in the lab and in the field.

John E. Greivenkamp
Series Editor

SPIE

P.O. Box 10
Bellingham, WA 98227-0010
ISBN: 978081949635-5
SPIE Vol. No.: FG29

ISBN 978-0-8194-9635-5
90000
9 780819 496355

SPIE PRESS

www.spie.org/press/fieldguides